Radical Initiation in the Class I Ribonucleotide Reductase: Long-Range Proton-Coupled Electron Transfer?

JoAnne Stubbe,* Daniel G. Nocera,* Cyril S. Yee, and Michelle C. Y. Chang

Department of Chemistry, 77 Massachusetts Avenue, Massachusetts Institute of Technology, Cambridge, Massachusetts 02139-4307

Received January 16, 2003

Contents

* To whom correspondence should be addressed. E-mail: stubbe@mit.edu, nocera@mit.edu.

I. Introduction

Ribonucleotide reductases (RNRs) catalyze the conversion of nucleotides to deoxynucleotides in all organisms (eq 1).[1−3] These enzymes play an essential role in DNA replication and repair by providing all of the monomeric precursors (deoxynucleotides) required for these processes.[4] RNRs have been divided into three classes, based on the metallo-cofactor required for the radical initiation process (Figure 1).[1,5] Many excellent reviews have recently been published on the mechanism of the nucleotide reduction

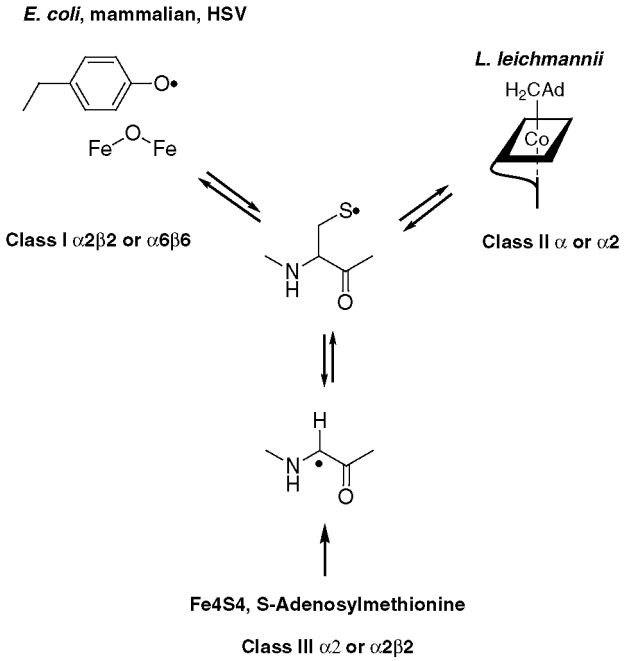

Figure 1. Cofactors required for the class I, class II, and class III RNRs. In the class I RNR, a diiron−Y• located on β2 is essential for generation of a putative S• on α2. In the class II enzymes, adenosylcobalamin (in schematic form with the corrin ring represented as a parallelogram and the dimethylbenzimidazole axial ligand indicated by a vertical bar) binds to α or α2 and generates a S•. In the class III RNR, a 4Fe4S cluster and *S*-adenosylmethionine located on an activating protein β, generates a G• on α2 that generates a S• also on α2.

10.1021/cr020421u CCC: $44.00
Published on Web 05/24/2003

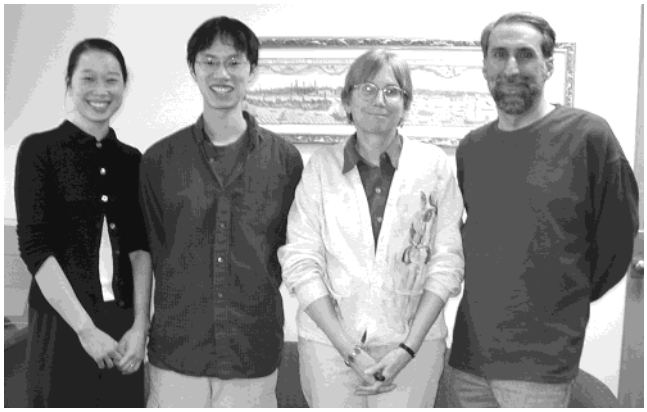

JoAnne Stubbe (second from right) has two cats, fatty Matty and flabby Abbey. She loves cats, chemistry, and biology. Daniel G. Nocera (right) is the W.M. Keck Professor of Energy and Professor of Chemistry. From the wonderful palette of experiences at MIT, he most likes collaborating with JoAnne on the PCET of RNR. Cyril S. Yee (second from left) graduated with a B.A. from Swarthmore College in 1997 and is currently a graduate student in JoAnne's laboratory at MIT. Michelle C. Y. Chang (left) graduated from the University of California–San Diego in 1997 and is currently a graduate student in Dan's laboratory at MIT.

of all classes of RNRs[6,7] and the similarities and differences in their regulation.[3,8,9]

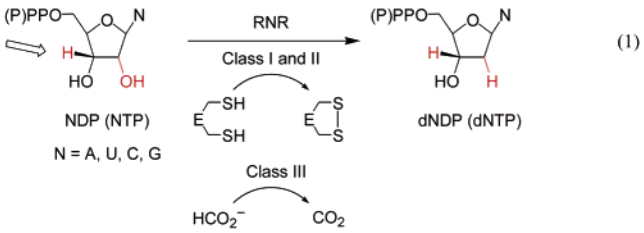

(1)

RNRs have provided a paradigm for thinking about the role of amino acid radicals and substrate-derived radicals in biological catalysis,[5] assembly of metal clusters required for generation of amino acid radical cofactors,[10] and for identification of protein and substrate radical intermediates using time-resolved and high field EPR methods.[11−13] A major unresolved issue in the study of the class I RNRs is the mechanism of radical initiation. How does a stable tyrosyl radical (Y•) on one subunit generate a putative transient thiyl radical (S•) on a second subunit located 35 Å away?[1,14,15] Radical transport in biology involves electron transfer (ET) or proton-coupled electron transfer (PCET), for which the transport of a hydrogen atom is a reaction subset. This review will present our understanding of the mechanism of long-range ET and PCET in biology, using the radical initiation process of class I RNRs as a focal point.

An introduction to the class I RNRs will first be presented. This background section will be followed by a presentation of the theoretical framework for ET and PCET. Charge transport within small, model proteins provides test cases of this theory and provides the framework to think about the more complex biological systems. The focus will then shift to several extensively investigated biological systems: hole migration in DNA, PCET in photolyases, and ET and PCET in the photosynthetic reaction center. Insight from these systems as it pertains to the RNR radical initiation process will then be presented. Finally, postulated mechanisms for the radical initiation process for RNR will be outlined. Methods will be presented that can distinguish between different mechanistic options.

II. Background and Scope of the Problem

All class I RNRs are composed of two types of homodimeric subunits: R1 (α2) and R2 (β2). R1s are composed of two 85-kDa monomers that bind the substrate nucleotides (NDPs or NTPs) and the allosteric effectors (dNTPs and ATP). The effectors have multiple binding sites and control the specificity of nucleotide reduction and the rate of reduction. R1s contain five cysteines that are essential for catalysis. Three cysteines are in the active site of R1: C439 in the *Escherichia coli* R1 (Figure 2) becomes the

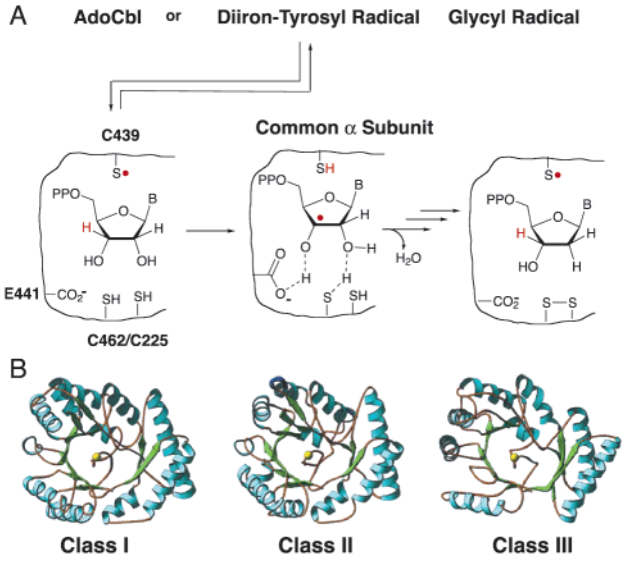

Figure 2. (A) Each class of RNR generates a S• on α2 or α using a different metallo-cofactor. The mechanism described, in which two cysteines (*E. coli* numbering) are oxidized to a disulfide, providing the reducing equivalents to generate deoxynucleotide, is pertinent to the class I and II RNRs. In addition, a conserved glutamate is also known to be essential for substrate reduction. The class III RNR uses a single cysteine (equivalent to C225) and formate as reductant. (B) The structures of the active sites for nucleotide reduction located on α2 or α are homologous in all three classes of RNRs.[235] Shown are the conserved 10-stranded α,β barrel with a finger loop whose tip houses the putative S•. The helices are shown in blue and the strands in green. The SH of the cysteine is shown in yellow.

putative S•, and C225 and C462 are oxidized concomitant with substrate reduction.[16−19] In addition, there are two cysteines in the C-terminus of R1 that re-reduce the active-site disulfide and are subsequently re-reduced by an external protein reducing system such as thioredoxin or glutathione and glutaredoxin. R2s are composed of two 43.5-kDa monomers. Each monomer contains a diferric cluster, and there are 1.2 stable Y•s per dimer. The diiron−Y• cofactor is the essential radical initiator of nucleotide reduction.[20]

The *E. coli*, calf thymus, and mouse enzymes[21−23] have been the most extensively studied of the class I

RNRs. The active *E. coli* RNR is thought to be a 1:1 complex of R1 and R2 ($\alpha 2\beta 2$). The active complex of the mouse RNR has been reported to have both an $\alpha 2\beta 2$ and an $\alpha 6\beta 6$ composition.[24] Structures at atomic resolution of *E. coli* R1[15,25] and *E. coli* (classes Ia and Ib),[26−29] mouse,[30] and yeast R2s[31] have been reported, though an active complex of R1 and R2 has yet to be crystallographically characterized. The structure of each subunit and the absolute conservation of amino acid residues from 40 sequences of RNRs have provided a docking model for the R1−R2 complex and a pathway model for communication between Y122 on R2 and C439 on R1 (Figure 3). The distances

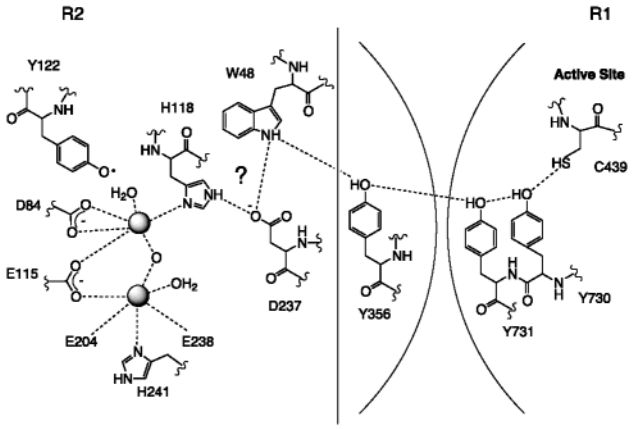

Figure 3. Using a docking model of R1 and R2, the conserved residues proposed to be involved in the ET between R1 and R2 are shown. Shown in red is Y356 located at the C-terminus of R2. The last 30−40 amino acids of all R2s are thermally labile; therefore, no structural data for these amino acids are available.

between Y122 and W48 on R2 and Y731 and C439 on R1 are known. The distance between W48 and Y731 is estimated to be 25 Å on the basis of the docking model. Y356 (located on the C-terminus of R2) is an absolutely conserved residue, and it is thought to be positioned between W48 and Y731. The hole migration from Y122• to C439 and back, on each conversion of a nucleotide to a deoxynucleotide, is a major focus of this review. Before this issue of radical initiation in class I RNRs is directly addressed, a basic framework for ET and hole migration in biology will be presented.

III. Principles of Electron Transfer

A. Marcus Equation

Treatments of charge transport in biology have been largely confined to the transfer of an electron. The description of ET most commonly used began to emerge in the late 1950s, with activated complex theory as the starting point.[32] In standard form, the observed rate constant is related to the activation energy for ET, ΔG^*, as follows:

$$k_{ET} = A \exp\left[\frac{-\Delta G^*}{RT}\right] \qquad (2)$$

The prefactor A defines the limiting rate of reaction. In Marcus's fêted theory of ET,[33−37] ΔG^* is related to two experimental observables, $\Delta G°$, the free energy driving force for the charge-transfer reaction, and λ, the energy related to reorganization of the nuclei from the equilibrium positions of the reactants to the equilibrium position of the products:

$$k_{ET} = k_{ET}(0) \exp\left[\frac{-(\lambda + \Delta G°)^2}{4\lambda RT}\right] \qquad (3)$$

where A of eq 2 is replaced by $k_{ET}(0)$, the activationless ($\Delta G° = -\lambda$) ET rate constant.

Equation 3 results from the analysis of the nonequilibrium free energy changes associated with electron localization on the donor and acceptor. Treatment of the polarization response of the solvent by continuum electrostatics showed that the energy of the system displays a quadratic dependence on solvent polarization. This result may be understood by considering the harmonic parabolic surfaces shown in Figure 4. The parabolic surfaces are effectively harmonic potentials, $y = {}^1/_2\, kx^2$, where k is the

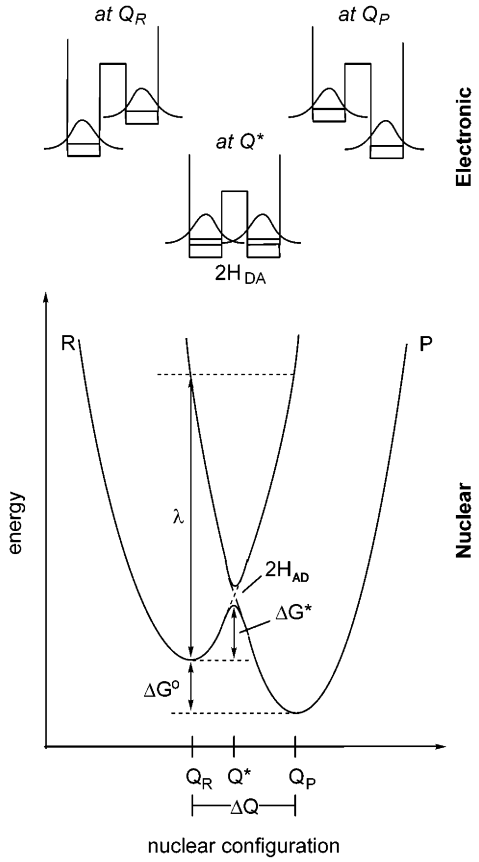

Figure 4. (Top) Electronic energy surfaces for an ET reaction. The three conditions correspond to nuclear configuration Q_R, where the electron is in its initial state on the acceptor (left), and nuclear configuration Q_P, where the electron is in its final state on the product (right). With the nuclear configuration for the transition state, Q^*, the resonance condition is met and the electron can tunnel from acceptor to donor, obeying the Franck−Condon condition. (Bottom) The harmonic potential energy of the reactants (R) and products (P) as a function of the nuclear configuration for an ET reaction. The variables are as follows: λ is the reorganization energy, $\Delta G°$ is the driving force of the ET reaction, ΔG^* is the activation energy, and H_{AD} is the electronic coupling. The coordinates Q_R, Q_P, and Q^* are defined above, and $\Delta Q = Q_P - Q_R$.

effective "force constant" of the harmonic potential arising from nuclear displacements along an x coordinate. The energy surface labeled R in Figure 4 describes the total energy of the system as a function of the positions of nuclei for the reacting redox cofactors and surrounding medium before ET has occurred; similarly, the product surface labeled P describes the total energy for products and surrounding medium at a given nuclear configuration after ET has occurred. In this coordinate system, Q defines this general nuclear coordinate for reactants, products, and the protein (or solvent) environment along which ET proceeds. As defined in Figure 4, the relations of $\Delta G°$ and λ in terms of the nuclear displacement coordinate are

$$\lambda = {}^1/_2\, k(\Delta Q)^2 \tag{4}$$

$$\Delta G^* = {}^1/_2\, k(Q^*)^2 \tag{5}$$

Relative to the product well, the free energy and activation energy are related to the nuclear displacements as follows:

$$\Delta G^* + (-\Delta G°) = {}^1/_2\, k(\Delta Q - Q^*)^2 \tag{6}$$

where Q_R has been set equal to 0. Expanding eq 6 and making the appropriate substitutions of eqs 4 and 5 yields

$$k(\Delta Q)(Q^*) = \lambda + \Delta G° \tag{7}$$

Squaring both sides of eq 7 and multiplying by $^1/_4$ yields the following,[38]

$$[{}^1/_2\, k(Q^*)^2][{}^1/_2\, k(\Delta Q)^2] = {}^1/_4\, (\lambda + \Delta G°)^2 \tag{8}$$

which can be rearranged to yield the Marcus activation energy for ET,

$$\Delta G^* = \frac{(\lambda + \Delta G°)^2}{4\lambda} \tag{9}$$

This derivation of the Marcus expression, though remarkably simple, shows that the overall form of the ET rate constant arises in a straightforward way from the application of activated complex theory to a single harmonic (i.e., parabolic) energy potential. The height of the activation barrier is determined by the vertical and horizontal displacements of the product well with respect to the reactant well. The driving force of the reaction, $-\Delta G°$, accounts for the vertical displacement of the potential energy surfaces, whereas the reorganization energy, λ, accounts for the horizontal displacement. Thus, a decrease in the driving force (for constant λ) will displace the product well upward, causing ΔG^* to increase and consequently the ET rate constant to decrease. Similarly, at constant $-\Delta G°$, an increase in λ will increase the horizontal displacement of the product well from the reactant well, imposing a higher activation barrier to ET.

B. Franck–Condon Principle and Electron Transfer

The Franck−Condon principle states that nuclear distances and velocities do not change during an electronic transition. In the case of an ET reaction, the electronic transition occurs from the reactant to product surfaces. The Franck−Condon principle, therefore, confines ET to occur at a constant nuclear configuration and energy. In classical treatments of ET, such as Marcus theory, the Franck−Condon condition is uniquely satisfied at the intersection of the reactant and product surfaces (at Q^* in Figure 4).[35] As represented at the top of Figure 4, the nuclear configuration of the transition state optimally supports the "instantaneous" tunneling of an electron. In the original Marcus formulation, electron transfer occurs every time the transition-state configuration is attained (i.e., the reaction is said to be adiabatic).

Within the context of Figure 4, λ is related to the energy needed to deform the nuclear configuration of the system from the equilibrium configuration of the reactant state to the transition state. In Marcus theory, λ is succinctly expressed in terms of a sum of energies required to reorganize the bond lengths and angles of the redox cofactor (the inner-sphere reorganization energy, λ_i) and the surrounding medium (outer-sphere reorganization energy, λ_o). Often the surrounding medium is solvent, and therefore λ_o accounts for changes in solvent position and orientation. For biological ET, however, λ_o will also include contributions arising from the protein matrix such as the repositioning of structured water and dipoles of the amino acids within the polypeptide, and reorientation at protein interfaces when reduction−oxidation occurs between cofactors of different subunits.

C. Bimolecular Electron Transfer

One of the most celebrated predictions of eq 3 is that the ET rate constant will decrease as the free energy of the reaction increases. ET in this "inverted" region will occur when the driving force for reaction is greater than the reorganization energy ($-\Delta G° > \lambda$). Consequently, inverted region effects are most easily discerned for those reactions with small reorganization energies and large driving forces. However, even when these criteria are present for a bimolecular ET reaction, diffusion of the reactants will conceal the inverted region and other ET parameters as well.

The observed reaction rate constant of a bimolecular reaction has the form of a consecutive reaction mechanism consisting of diffusion rate constant (k_d) and activated ET rate constant,

$$k_{obs} = \frac{k_{ET}k_d}{(k_{ET} + k_d)} \tag{10}$$

The above expression arises for the immediate reaction of two species upon contacting each other (the diffusion constant in this treatment is appropriately defined such that its units are $M^{-1}\ s^{-1}$). Because activated ET can be extremely fast when $-\Delta G° = \lambda$, the diffusion limit may impose an upper limit upon the observed reaction rate ($k_{obs} = k_d$ for $k_{ET} \gg k_d$). As shown in Figure 5, the parabolic dependence predicted by eq 3 is truncated by diffusion. Consequently, the observed rate constants of most bimolecular reactions display an increase with increasing

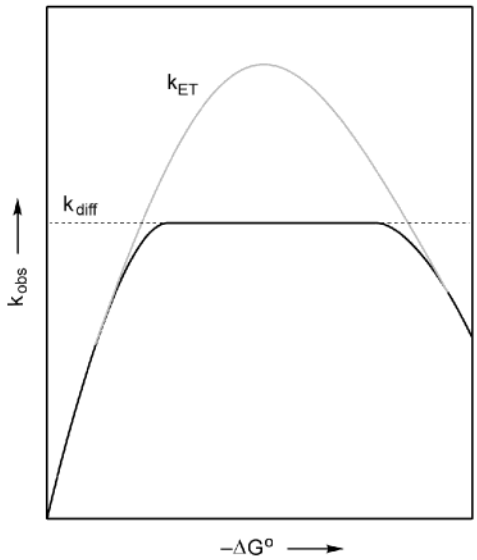

Figure 5. Parabolic dependence of the ET rate constant on the free energy driving force predicted by eq 3. The diffusion limit, signified by the horizontal solid line, truncates the parabola and thus can mask the Marcus inverted region.

free energy, followed by a leveling at the diffusion limit. The inverted region might be observed for bimolecular reactions, but such behavior is unusual.[39−44] For instance, by judiciously choosing redox cofactors such as cytochrome *c* and positively charged small-molecule donors, the Marcus curve can be displaced below the diffusion limit, enabling inverted ET to be observed at reasonable driving forces.[45]

If its impact was limited to the inverted region, the consequence of diffusion would be small since most proteins and enzymes operate at modest potentials. The inverted region, however, is not the only Marcus phenomenon that is difficult to quantify for a bimolecular reaction. Even if the ET is slow with respect to diffusion (i.e., a pre-equilibrium model as defined by Michaelis−Menton kinetics yields $k_{obs} = K_D k_{ET}$ for $k_{ET} \ll k_d$, where $K_D = k_d/k_{-d}$), work accompanies the congregation of charged reactants and/or separation of charged products. Work term contributions to k_{ET} can overwhelm the intrinsic factors that govern the ET event, making it difficult to extract reorganization energies and develop reliable driving force dependences. This is best seen from the large body of work in the 1970s on the *bimolecular* ET reactions between redox proteins (primarily cytochrome *c*) and untethered small-molecule reactants.[46−54] Redox cofactors in sites of high charge, such as the heme cofactor in the lysine pocket of cytochrome *c*, lead to very large work term contributions, thus obscuring the factors governing the ET event itself.

D. Electron Transfer in Biology

The problem presented by diffusion to the study of bimolecular ET in proteins is circumvented when the redox cofactors are held at fixed distances. By virtue of the secondary and tertiary structure of proteins and enzymes, redox cofactors can be positioned at fixed distances. The ET reaction is typically photoinitiated to provide a large time window for observation (microseconds to picoseconds). Three approaches have been pursued in biological ET studies:

Redox-Labeled Metalloproteins. This approach entails the covalent attachment of a small-molecule oxidant or reductant to a polypeptide side chain of a redox protein. The first such experiment involved the covalent attachment of a Ru(III) pentammine donor to histidine-33 of cytochrome *c*, $Ru^{III}(NH_3)_5$(His-33)−ferricytochrome *c* (Figure 6).[55,56] In this experiment,

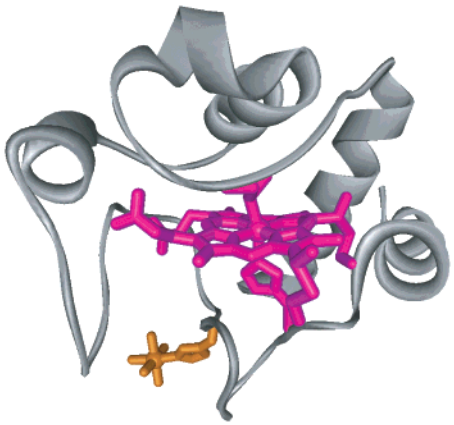

Figure 6. Model of the structure of cytochrome *c* modified with a Ru(II) pentammine redox cofactor at histidine-33. The heme and its axial ligands, methionine and histidine, are highlighted in purple, and the $Ru(NH_3)_5$(His-33) center is highlighted in orange. (Figure provided courtesy of Harry B. Gray and Jay R. Winkler.)

an electron was injected into the $Ru^{III}(NH_3)_5$(His-33)$^{3+}$ center from the excited state of a $Ru^{II}(bpy)_3^{2+}$, which was prepared by flash photolysis. The oxidized $Ru^{III}(bpy)_3^{2+}$ was irreversibly quenched with a sacrificial donor back to its Ru(II) resting state before back-ET from the photoreduced $Ru^{II}(NH_3)_5$(His-33)$^{2+}$ could occur. Electron transfer from the photoreduced $Ru^{II}(NH_3)_5$(His-33)$^{2+}$ to the Fe(III) center of ferricytochrome *c* was monitored by transient absorption spectroscopy. Since this initial report, many redox proteins have come under investigation, the most prominent of which are blue copper proteins[57−61] and cytochromes.[62−65] An important advance made since the initial experiment has been the development of the flash-quench method.[66] Here, a photoactive Ru(II) polypyridine center is attached to a specific amino acid residue of the protein. The excited state of the Ru(II) center, produced by laser excitation, is oxidized or reduced in a bimolecular reaction with a quencher added to solution. The bimolecular back-ET with the photogenerated hole (a Ru(III) center) or electron (a Ru(I)) trap state is generally slow with respect to intramolecular ET within the protein complex. Accordingly, long time windows for ET may be achieved; even longer time windows can be examined if irreversible quenchers are used. The flash-quench method has allowed very slow ET reactions to be examined.[67] Moreover, Ru(II) redox sites of varying potential have been attached to the surface of protein platforms at specific polypeptide sites, thus allowing the ET distance and driving force to be systematically varied. Electron transfer in other biological systems such as DNA loosely falls under this class of investigation. Here, the DNA chain is typically modified

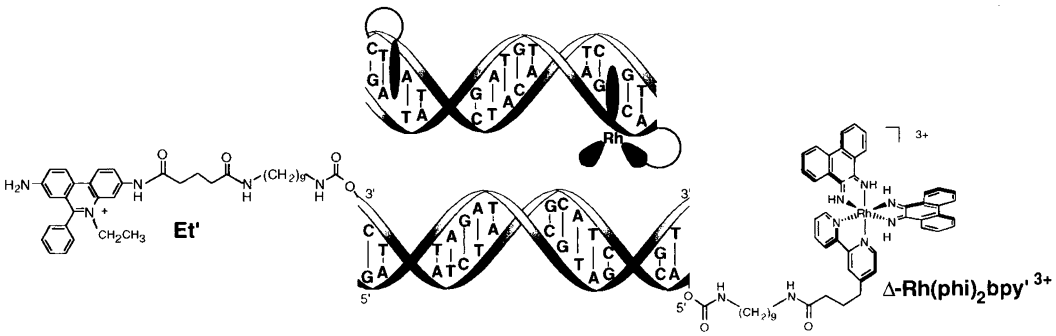

Figure 7. A Ru(II) bipyridine donor and ethidium acceptor covalently attached to duplex DNA at defined positions. The ET reaction, initiated by excitation of the Ru(II) complex, occurs between the intercalated donor and acceptor (top schematic).[337] The ET reaction was probed by fluorescence quenching.

with two cofactors (Figure 7) or, alternatively, a single cofactor with guanine (G_{DNA}) serving as the other redox counterpart (section III.D.3).

Protein−Protein ET. Fixed-distance ET between redox cofactors of protein pairs has also provided crucial insights into the factors governing the transfer of electrons across protein interfaces.[61,64,68−75] Many protein−protein systems include a heme cofactor. The advantage here is that Fe may be replaced with Zn, thus permitting the ET reaction to be photoinitiated by production of the excited state of Zn porphyrin of the modified cofactor. The rate constant for ET from the laser-excited Zn(II) porphyrin cofactor of one protein to the redox cofactor of its partner is usually determined by transient absorption spectroscopy. Melding protein−protein and redox-labeling constructs, interprotein ET has also been photoinitiated from small-molecule photoreagents appended to protein−protein complexes.[76] In some cases, the interprotein ET rates are slow enough (millisecond time scale) that photoinitiation of the charge-transfer event is not required; the kinetics may be obtained from rapid mixing experiments.[70]

Cofactor-Substituted Proteins. The final method to study fixed-distance ET in biology relies on the modification of a cofactor in a multicofactor protein or enzyme. The archetype here is the bacterial reaction center (RC) (Figure 8). The quinone cofactors, Q_A and Q_B, at the terminus of the charge-separating L branch of RC have been systematically replaced to provide a detailed analysis of ET in the RC.[77,78] This type of approach has been elaborated in several other multi-cofactor protein redox systems.

Two important paradigms of biological ET have emerged from these foregoing classes of ET studies: biological ET proceeds at a relatively constant λ, and electrons transfer over long distances in biology at appreciable rates.

1. Reorganization Energies in Biological Electron Transfer

The argument of the exponential of eq 3 is typically referred to as the Franck−Condon term of ET, and, as mentioned above, it is this term that embodies Marcus's theory of ET. The free energy reaction is well understood, defined by the reduction potential of the redox cofactors, though the issue of how proteins precisely modulate the redox potential is often not well understood. The reorganization energy for a biological ET reaction is more abstruse because

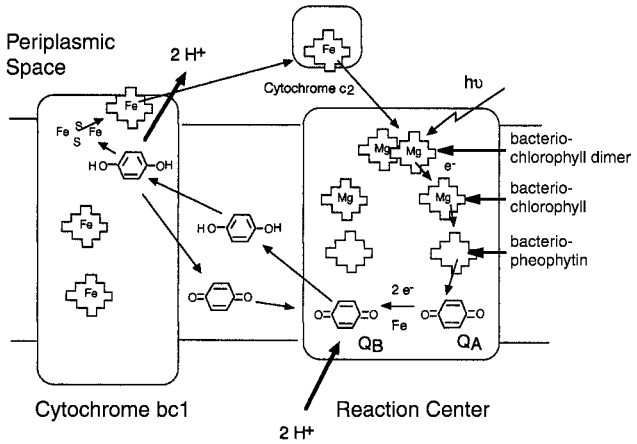

Figure 8. Simplified representation of proton transfer and ET in photosynthetic membranes. The bacterial RC containing L and M subunits couples light-induced electron-to-proton transfer by reducing the ubiquinone in the Q_B site. Members of the electron pathway are labeled in the schematic representation. In the accompanying text, SP is the special pair, BChl is bacteriochlorophyll, and BPh is bacteriopheophytin. (Adapted from ref 205 with permission from Elsevier.)

of difficulties intrinsic to its measurement. λ may be ascertained by two methods. Measurement of k_{ET} as a function of driving force permits a Marcus curve to be constructed, from which λ may be extracted. Alternatively, the temperature dependence of k_{ET} will afford λ, as long as the temperature dependence of $\Delta G°$ is defined. Most accurate measurements of λ have come from application of the former method to redox-labeled metalloproteins that are free from complex conformational changes (which can mask ET in many biological systems).[62,64] The work to obtain λ encompasses the synthesis of a protein family modified at a single site with redox labels of varying potentials (see Figure 6 above). From this self-consistent set of proteins, the ET rate constant is then measured and a Marcus curve constructed. The temperature dependence of k_{ET} is determined for the redox-modified protein of the set that exhibits the activationless ET.

As a result of these Herculean experimental efforts, a comprehensive picture for the reorganization energy of biological ET has begun to emerge. It has been long recognized that many proteins sequester cofactors in hydrophobic environments, away from the very polar environment of water. Within the context of Figure 4, bringing a redox cofactor from water into

a protein environment serves to attenuate the horizontal displacement of the ET potential energy surfaces, thereby lowering the activation barrier to ET and consequently accelerating the overall rate of ET. The striking feature of the data shown in Table 1,

Table 1. Reorganization Energy of Different Classes of Enzymes and Proteins

protein/enzyme	λ/mV	ref
cytochrome *c*	700	326
$Ru(LL)_2(im)$(His33)−cytochrome *c* (LL = polypyridine ligands)	740	67, 327
blue copper proteins		
$Ru(bpy)_2(im)$(His83)−azurin	700	328, 329
Ru(trpy)(LL)(His59)−plastocyanin	640−700	330
HiPIPs		
$Ru(LL)_2(im)$(HisX)−HiPIP	600−800	331
bacterial reaction center	700	99
cytochrome *c*/ cytochrome b_5	700	332

however, is the remarkable consistency in λ despite a significant variance in protein structure and function.

The data of Table 1 lead to significant insights into the structure/function relation of protein redox systems. Especially notable in this regard is the similarity of the ET reactions of azurin and cytochromes. The Fe(II)/Fe(III) redox change of heme model compounds typically displays small inner-sphere reorganization energies when the spin state is preserved; consequently, it is not surprising that the outer-sphere reorganization energy tends to dominate the ET reactions of heme proteins and enzymes. Conversely, large inner-sphere reorganization energies accompany the redox change of Cu(II)/Cu(I) model compounds owing to distinctly different preferred tetrahedral/trigonal planar ligand fields of Cu(I) centers vs the square planar ligand field of Cu(II).[36,79,80] Redox changes must therefore accommodate a large inner-sphere reorganization, which augments the outer-sphere contribution to the reorganization energy. For this reason, ET reactions involving Cu redox centers tend to be slow with respect to heme systems. Notwithstanding, numerous fixed-distance ET measurements of Cu proteins and enzymes show rates of ET that are fast and commensurate to those of heme proteins.[62] As shown in Table 1, measurements of λ for blue copper proteins are similar to those of proteins and enzymes that display little reorganization of the cofactor upon redox changes. These observations suggest that redox proteins of Cu have evolved to constrain the environment about the redox cofactor.[81] Specifically, numerous crystal structures show apo- and native-protein structures that are nearly similar. A heavily hydrogen-bonded network in the folded structure of copper proteins excludes water and strictly controls the positions of the ligands to copper, especially the axial ligand.[82,83] The ability of the protein to preserve a common structure in Cu(II) and Cu(I) redox states dramatically lowers the inner-sphere reorganization energy, thus bringing the overall reorganization energy (and consequently rates of ET) in line with that observed for heme proteins. This picture is consistent with Malmström's original "rack mechanism"[84] and Williams's "entactic state"[80] for copper proteins, in which it was proposed that the unusual redox and spectroscopic properties of copper were due to a ligand stereochemistry imposed by the protein environment rather than dictated by the ligand field of Cu(II) centers.

As noted by Williams,[85] the value of $\lambda = 750 \pm 100$ mV in Table 1 is similar to that observed for ET reactions between simple donor−acceptor pairs in rigid media ($\lambda = \sim$600 mV). Here, the dielectric contribution arising from the reorientation of the dipoles of the surrounding medium is suppressed, and λ is very nearly accounted for by only the contribution of the medium's optical dielectric response to the change in charge attendant to the ET reaction. The parallel between λ values for the ET reactions of cofactors in proteins and rigid media such as glasses highlights the importance of the biological milieu to provide a rigid "solvation" environment so that efficient electron flow may be sustained in proteins and enzymes confined to an aqueous existence.

The foregoing discussion emphasizes proteins whose primary function is ET. When catalysis is coupled to ET, a larger variance in λ has been reported. Reorganization energies in excess of 2 V have been calculated for interprotein ET reaction of methylamine dehydrogenase with amicyanin.[70,86] Interestingly, the partial exposure of cofactors in the active site to solvent in these enzymes may account for these larger λ values. Conversely, for the more isolated active site of flavoprotein glucose oxidase, a λ consistent with those listed in Table 1 has been observed.[87] However, we note that it is difficult to isolate the ET reaction (and therefore extract λ) when it is coupled to the multitude of other processes accompanying redox-driven catalytic conversions.

2. Long-Distance Electron Transfer

The distance dependence of ET was never treated in Marcus's original formalism of ET. In eq 3, ET proceeds with a maximal rate constant, $k_{ET}(0)$, for redox pairs at contact (i.e., the ET distance is the sum of the radii of the two redox cofactors). When electrons are required to move over long distances, they tunnel. A schematic for wave functions of two redox cofactors separated by a distance r_{DA} is shown in Figure 9A. The efficiency for the electron to tunnel directly from the donor to the acceptor depends on the extent of overlap of the decaying tails of the wave functions. Because wave functions decay exponentially with distance, it is logical that the ET rate constant decreases exponentially with increasing distance between redox cofactors.

The basic formalism for electron tunneling was in place before ET theory was developed. The textbook treatment for electron tunneling is through a square potential barrier,[88] which was adapted to the long-range ET in biology by Hopfield,[89] though Levich had incorporated tunneling into the ET problem several years earlier.[90] Figure 4 presents the electron-tunneling problem for nuclear configurations paramount to ET. The probability of tunneling is given by H_{AD}^2, which reflects the exponential distance dependence for electron tunneling,

$$H_{AD} = H_{AD}^{\circ}\, e^{-\beta(r_{DA}-r_o)} \qquad (11)$$

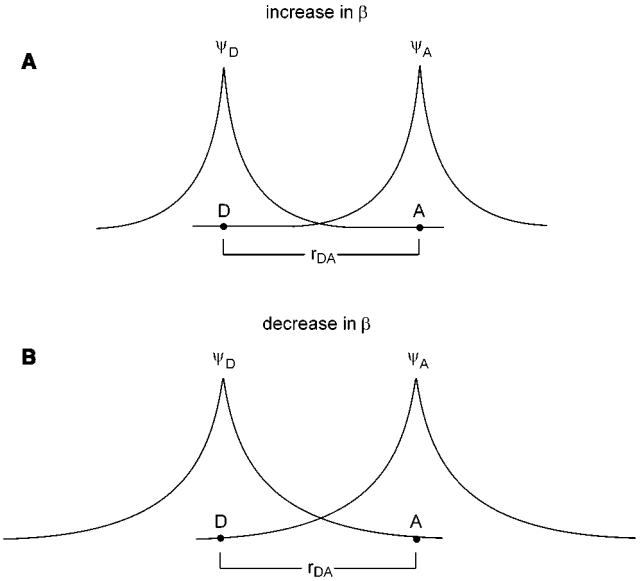

Figure 9. Wave functions for the electron on the donor and the acceptor at a well-separated distance *R*, with weakly overlapping, exponentially decaying tails. The rapidity of the falloff of the exponential decay is determined by β. At a given distance, (A) the wave function overlap is small for large β but (B) increases significantly as β decreases.

where r_o is the center-to-center distance of the donor−acceptor pair at contact and β is a constant, reflecting the alacrity at which the exponential wave function decays. The integration of electron tunneling with the classical treatment of ET via a Marcus formalism gives rise to the commonly used expression (sometimes referred to as the Marcus−Levich equation) for ET between two cofactors at fixed distance and orientation,

$$k_{ET} = \sqrt{\frac{4\pi^3}{h^2 \lambda k_B T}} H_{AD}{}^2 \exp\left[\frac{-(\lambda + \Delta G°)^2}{4\lambda RT}\right] \quad (12)$$

where the pre-exponential ($k_{ET}(0)$ in eq 3) is limited by the strength of electronic coupling. For this commonly adopted formalism, the description accounts for a weak electronic interaction between the different states. Under such circumstances, the transition state is formed many times before the electron is transferred from the donor cofactor to the acceptor cofactor. This process is said to be electronically nonadiabatic.

In the square-barrier (sometimes called the tunneling barrier) treatment, β is a measure of the height of the barrier through which the electron tunnels (which in turn determines the exponential fall of the wave function in square well tunneling problems).[88,89] β is estimated to be 3.4 Å^{-1} for ET in a vacuum, limiting ET to occur on only a 100-ms time scale at distances of ∼10 Å. Considering that the rates of ET over long distances (typically 10−15 Å) in proteins are appreciable, electron tunneling must be mediated by the protein milieu. Effectively, electron (and hole) states of the intervening protein medium serve to reduce the barrier height and consequently stretch out the wave function (Figure 9B). This phenomenon, known as superexchange coupling, was first developed by McConnell to treat hole transport among aromatic cations spaced by bridges composed of identical subunits.[91] Contrary to a common misconception of superexchange, the electron *directly* tunnels from the acceptor to donor; no intermediates are formed from electron or hole residency along the pathway from donor to acceptor.

The McConnell superexchange mechanism assumes a homologous bridge constructed of repetitive units between the donor and acceptor. In this case, a straightforward analytical expression can be obtained for electronic coupling, which falls off exponentially with the number of bonds in the bridge. In contrast, the intervening bridge between the cofactors and enzymes has a surfeit of interactions, bonds and nonbonds, in a variety of conformations. Tunneling-pathway models have been developed in an effort to accommodate such biological complexity.[92−95] For instance, the complex pathways of the protein matrix may be decomposed into bonding, nonbonding, and hydrogen-bonding contacts between atom pairs.[96−98] Each of these three contact types is assigned an effective value for the electronic coupling decay; the overall electronic coupling is determined by taking a product of the coupling decays normalized by the number of bonds along a specific pathway in the protein. Optimized pathways for ET through the protein may be determined by using a structure-dependent search algorithm[97] to identify the pathway with optimized electronic coupling between redox cofactors.

Theoretical treatments of β have been augmented by an expansive body of experimental work on long-distance ET in biology. Most investigations have focused on measurements of β and its correlation to protein structure. Controversy has developed, primarily surrounding the value of β in biology. At one extreme, Dutton has assigned a universal value of $\beta = 1.4$ Å^{-1} for all long-distance ET reactions in biology.[99] The imposition of a uniform barrier height implies that biological ET is independent of the nature and structure of the biological milieu.[100] The correlation works grossly over 14 orders of magnitude of ET rates for a variety of systems, but deviations from this correlation can be as great as 10^3−10^4, suggesting at a more detailed level a structural dependency on β. The aforementioned ET studies of numerous protein and enzymes support this contention.[64,101]

What, then, are the origins of the controversy in β? Some of it depends on an element of fidelity. A $\beta = 1.2 \pm 0.2$ Å^{-1} accounts for nearly all ET reactions in biology. For this reason, the application of a uniform β to ET rate constants spanning several decades loosely accounts for the rate constants for long-distance ET in biology. Under such criteria, the uniform-barrier model for ET holds. At a more detailed level of inspection, however, the range of ± 0.2 Å^{-1} in β gives rise to significant differences in ET rates, and, as predicted by tunneling-pathway models and corroborated by experiment,[64,101] structural dependences of β are clearly observed for different classes of proteins. Over time, the uniform-barrier and tunneling-pathway models of ET have been converging.[102] For tunneling-pathway models, the electronic coupling may be described as a weighted

average of pathways.[103] This has some leveling effect on β, though the exponential distance dependence of H_{AD} usually translates to a few key pathways of similar β or a "bundle" that dominates the ET reaction. More significantly, the uniform-barrier method has recently been modified to allow β to be adjusted for the packing density of polypeptide chains within the protein.[104] Though this modification does not explicitly consider the precise bond pathway, the packing density is another way to introduce a structure-dependent variation of β; to this end, the uniform-barrier method begins to take on basic elements of a tunneling-pathway-type treatment of long-distance ET.

Not all disagreements about β in biological ET, however, are due to the level of detail that one chooses to inspect ET. Interpretations of β by uniform-barrier and tunneling-pathway models are at odds for specific systems. In many of these cases, the controversy arises from the choice of edge-to-edge distance of the cofactors participating in ET.[105] In other cases, discrepancies arise from the method by which β was measured. Because there is a distance dependence to λ, measurements of β are best performed for ET reactions in the activationless regime (those at or near the top of the Marcus curve in Figure 4). Owing to the enormous amount of work involved in constructing a Marcus curve, the activationless regime is not always determined, and consequently β is extracted from ET reactions that are activated, making it difficult to disentangle the distance dependence of tunneling from that of the activated ET processes.

3. Electron Transfer in DNA: Hopping and Radicals

Long-distance charge transport in DNA (Figure 10A) has led to the most stimulating developments in the understanding of ET in recent years. For DNA, hole transfer rather than ET is the predominant mechanism for charge transport (vide infra). Three types of experiments, summarized in Figure 10, have been developed to monitor charge transport in DNA; all use light-mediated initiation. The approach pioneered by Barton[106−108] (Figures 7 and 10B) and emulated by others[109−111] involves the intercalation of a donor and an acceptor along the DNA chain. As for fixed-distance donor−acceptor studies of proteins and enzymes, ET may be investigated by varying the distance between the donor−acceptor pair along the DNA strand. It should be noted, however, that a lack of good structural insight and an understanding of dynamics generally complicate the interpretation of the distance dependence for DNA charge transport. A second approach, elaborated by Giese and co-workers,[112−114] extracts the ET rate constant from a photochemical competition experiment. In these studies, charge injection is prompted by the photogeneration of a C4′ DNA radical from 4′-*tert*-butyl ketones of deoxynucleotides. The radical rapidly loses phosphate to generate the ether cation radical (Figure 10C); this species is capable of oxidizing nearby guanines within the DNA duplex. In competition with this internal migration of a hole, the oxidized G_{DNA} can be irreversibly trapped by water to yield products

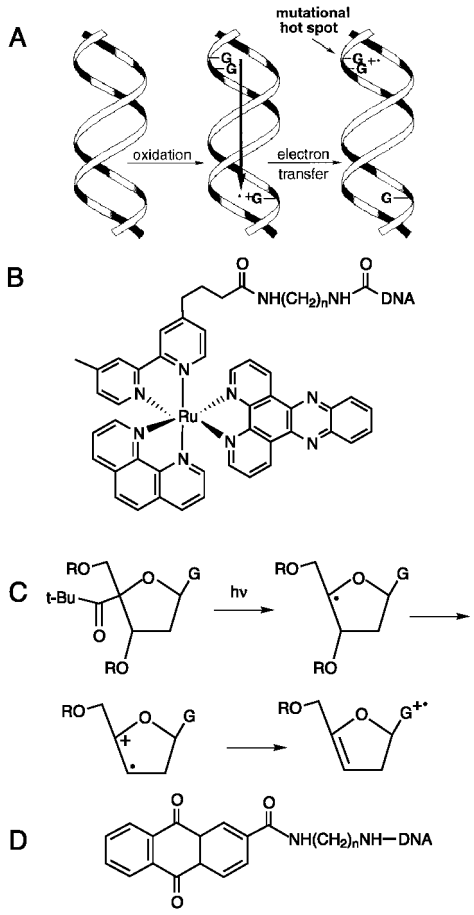

Figure 10. Three methods are indicated that have been used to study hole migration in DNA. (A) Hole migration in DNA initiated by light. (Reprinted with permission from ref 114. Copyright 2000 American Chemical Society.) (B) Use of tethered ruthenium phen-bpy-phi derivatives studied extensively by the Barton group.[156] (C) Photolysis of a *tert*-butyl ketone studied extensively by the Giese group.[114] (D) One of several anthraquinones studied by the Schuster group.[122]

that can undergo phosphodiester bond cleavage in the presence of base and are detected on DNA sequencing gels. The relative rate for ET along a DNA strand may be ascertained by measuring the product yield of these irreversible reactions as a function of the distance separating the G_{DNA} and the original ether radical cation. A third approach, developed by Lewis and Schuster and their co-workers,[115,116] uses the base pairs of DNA, typically G_{DNA}, as the electron donor to a photoexcited acceptor such as stilbene (two-point attachment, hairpin) or anthraquinone (one-point attachment, end-capped, Figure 10D) incorporated at the end of the DNA strand.

Hole migration in all three systems is monitored biochemically (for long- and short-range transport) by building in GG or GGG sequences that potentiate $G_{DNA}^{\bullet+}$ formation within this sequence relative to lone Gs because of facilitated oxidation (Figure 10A). The reduction potentials of any given nucleic acid base are modified by its neighbors. The depths of the GG and GGG traps (0.5 and 0.7 V, respectively) are based on measurements from single nucleotides; however, recent experiments and theory suggest that the relative depths of these hole traps (G_{DNA} vs GG vs

GGG)[117,118] are much shallower than the measurements on the single nucleotides would imply.[119] Because G_{DNA} dimers are more easily oxidized than G_{DNA} monomers,[118,120,121] ET in these systems is dominated by transport of a hole to GG and GGG base pairs, when they are present within the strand. A number of excellent reviews is available on these charge migration experiments in DNA; we will simply focus on the issues raised in these studies that are instructive in formulating the mechanism of radical initiation in the RNRs.[108,114,122]

Initial measurements on donor−acceptor complexes of DNA were provocative, showing charge transfer over very long distances (40−200 Å) at appreciable rates (picosecond time scales).[123−126] Adherence to a direct-tunneling (i.e., superexchange) mechanism requires that β approaches values as small as 0.1 $Å^{-1}$.[123,127] Such values of β are characteristic of electrons in conductors, leading to the proposition of DNA as a "pi-way" or "wire" for electrons.[128] This proposition prompted intense experimental scrutiny, which produced results in conflict with a "pi-way" tenet. First, the optical and electronic properties of DNA suggest that it is neither a metal nor a semiconductor.[129] Second, ET through π stacks is not especially efficient. Consider graphite, which is an extremely good conductor within the plane of graphitic sheets but not in a direction normal to the π stack (i.e., small β along the C−C σ bonds in the plane of graphite sheets and large β through π-stacked sheets). Finally, the photochemical trapping experiments reported by Giese and the photoinduced ET reactions of hairpin DNA yielded more normal β values of 0.6−1.2 $Å^{-1}$;[109,110,130,131] subsequent theory supported these experimental values of β for DNA.[132]

a. The Hopping Mechanism for Hole Transport. After several years of study by many groups, a unified picture involving β and, more generally, charge transport in DNA has emerged. First, the original proposal by Barton is irrefutable—charge efficiently transfers over extremely long distances of DNA—but not by a superexchange mechanism with an extraordinarily small β. DNA, like any other biological medium, exhibits normal to slightly accentuated values of β. Several studies show that the efficiency of charge transport in DNA directly scales with the number of G_{DNA} base pairs[114,133−135] and, to a lesser degree, adenines.[136] This observation has led to the proposition that charge transport of the hole is mediated by its hopping among intervening guanines and adenines (Schuster has modified this proposition by delocalizing the charge of the oxidizing hole over several adjacent base pairs, akin the existence of polarons in a single crystal).[122,137] Here, unlike a superexchange mechanism, the hole actually resides on the base pair, tunneling from G_{DNA} to G_{DNA} in its journey from donor to acceptor.

The consequences of multistep hopping versus direct tunneling (superexchange) to the overall rate of ET are profound. As discussed for the superexchange process, tunneling between donor and acceptor is inefficient at long distances because of the poor overlap of exponentially decaying wave functions. For a given β (i.e., exponential decay), an electron (or hole) hop to an intervening base pair significantly enhances the wave function overlap owing to the shorter distance over which the electron tunnels. In this manner, the apparent overall electronic coupling and, correspondingly, the rate of ET are markedly increased.

Jortner and Bixon have treated the hopping problem quantitatively.[138−140] The overall result is that the charge-transfer rate constant (k_{CT}) resulting from hopping scales algebraically with distance as opposed to the exponential distance dependence of a unistep tunneling process. Specifically, the overall rate constant follows a power law on distance,

$$\begin{array}{ccc} \text{direct tunneling} & \rightarrow & \text{multistep hopping} \\ k_{CT} \propto e^{-\beta(nR')} & \rightarrow & k_{CT} \propto k_{ib} n^{-\eta} \end{array} \qquad (13)$$

where the distance dependence of eq 11 has been reformulated as nR', with n equated to the number of intervening base pairs between donor and acceptor and R' equated to the distance between base pairs, $\eta = 1-2$, and k_{ib} is the rate for interbase charge transfer. The hopping process is treated kinetically as a series of sequential charge-transfer reactions. The model has been tested experimentally by controlling the composition of base pairs within a duplex strand.[141] As predicted by such a model, the longest hopping steps are found to be the crucial determinant of the efficiency of long-distance ET.[135] This hopping mechanism simply serves to reduce the distance over which the electron or hole needs to tunnel. Whether an electron or hole tunnels between donor and acceptor directly (unistep) or hops (multistep) depends simply on the thermodynamics of donor and acceptor and the intervening medium. Since the oxidation of the base pairs is energetically accessible, hopping is especially prevalent in charge transport along DNA duplexes.

It should be emphasized that the usual parameters governing an ET reaction are operative as the hole hops from base pair to base pair. In the formal hopping theory, the electronic coupling and Franck−Condon terms for charge transfer between bases are accounted for with k_{ib}. The relative contributions of each to k_{ib} remain an open question, though it should be noted that the movement of a positive hole is likely accompanied by the concomitant movement of anions along the DNA strand. Accordingly, large reorganization energies attendant to ion transport along the DNA duplex may be expected. This contention would explain why the temperature dependence for charge migration in DNA has been observed to be large.

b. Direct Detection of Radicals by Spectroscopic Methods. The concept of hopping in DNA has naturally led to a second major contribution to ET in biology. DNA has become a test bed for the detection of radical intermediates along ET pathways. Inasmuch as hopping predicts the presence of an authentic hole or electron on the base pair of the DNA duplex, several groups have sought to directly detect the radical by transient laser absorption methods.

Barton and Zewail have incorporated photoexcitable acceptors within DNA duplexes that can undergo

charge transfer with G_{DNA} or a modified base donor. Figure 11 shows one construct in which a photoexcitable acceptor, 2-aminopurine (Ap), is placed at a fixed distance from G_{DNA}.[142] The time evolution of optical signatures of the absorption spectrum of the laser-excited Ap is perturbed by charge transfer from the G_{DNA} donor within the DNA duplex according to the photophysics of Scheme 1 (k_o is the rate constant

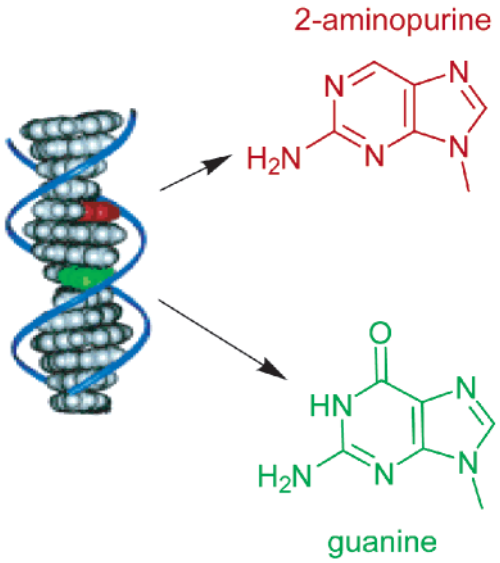

Figure 11. DNA duplexes containing photoexcitable acceptors, 2-aminopurine (red) and guanine (green), as the ET donor. (Reprinted with permission from ref 142. Copyright 2000 National Academy of Sciences, U.S.A.)

Scheme 1

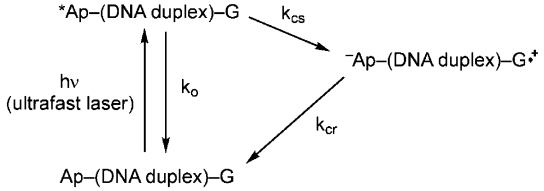

for the natural lifetime of the Ap*, and k_{cs} and k_{cr} are the charge separation and recombination rate constants, respectively). The charge-transfer rate constant may be deduced from the decay kinetics of the Ap* absorption spectrum in the absence of other competing decay pathways, such as energy transfer, which is not favored between Ap* and G_{DNA}. In a related experimental design, a photoexcitable acceptor, ethidium (E^+), has been tethered to a base of DNA, which has been further modified with the electron donor, 7-deazaguanine (Z).[143] The charge-transport cascade,

$$E^{+}*-(DNA, G_{DNA})-Z \rightarrow {}^{\bullet}E-(DNA, G_{DNA}^{\bullet+})-Z \rightarrow {}^{\bullet}E-(DNA, G_{DNA})-Z^{\bullet+} \quad (14)$$

is initiated by excitation of ethidium. A net driving force of ~0.2 V leads the hole to its final trap site on 7-deazaguanine. Charge transport is inferred from the decay of the transient absorption spectrum of the initially populated photoexcited acceptor, E^+*, at 400 nm. In one case, the radical of an externally tethered donor has been detected.[144] The system is similar to the one shown in Figure 7. A phenothiazine electron donor, PTZ, attached to the 5′ terminal of one oligodeoxynucleotide strand, undergoes ET with a ruthenium intercalator, $Ru(bpy)_2(4\text{-m-}4'\text{-pa-bpy})^{2+}$ chromophore [bpy = 2,2′-bipyridine and 4-m-4′-pa-bpy = 4-methyl-4′-carbonylpropargylamine], covalently linked to a uridine of the complementary strand. The transient absorption spectrum of the product of the forward electron-transfer reaction, $PTZ^{\bullet+}$, has been observed.

Lewis and Wasielewski have directly observed radicals in DNA structures in which a hairpin linker serves as the photoexcitable electron acceptor and a nucleobase serves as the electron donor (Figure 12).

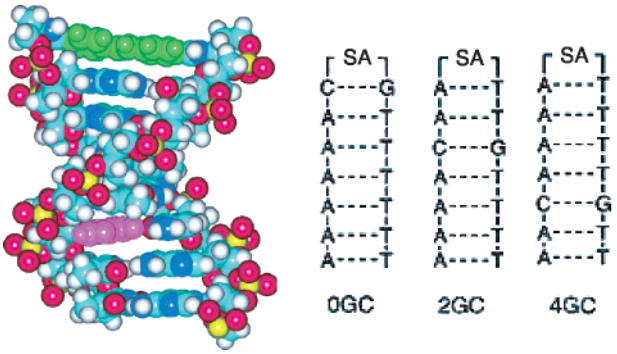

Figure 12. Hairpin DNA duplex used for the study of ET in DNA. The hairpin (green) is SA (see Chart 1), and the donor is guanine (pink). Charge migration may be examined by positioning the donor guanine along the DNA duplex. (Reprinted with permission from ref 145. Copyright 1997 American Association for the Advancement of Science.)

Chart 1 shows the various photoexcitable acceptors that have been used as hairpin linkers. The most

Chart 1

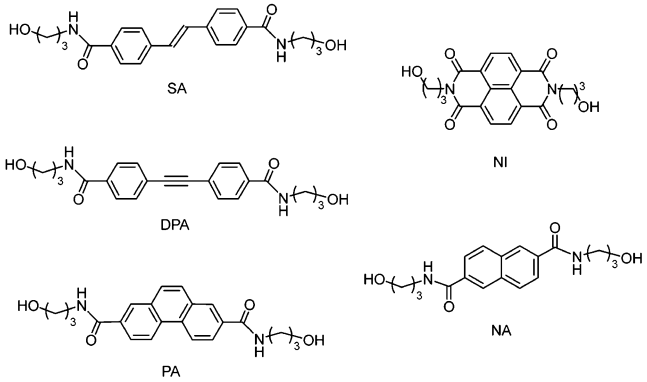

popular hairpin has been the stilbene-4,4′-dicarboxamide (SA) acceptor, which undergoes facile ET with G_{DNA},[131,145] GG, and GGG donor[117,146,147] nucleobases within the duplex or with modified bases such as 7-deazaguanine incorporated within the DNA strand.[148] The transient absorption spectrum is initially dominated by the SA excited state (SA*) and then evolves to the radical anion SA^- as the charge transfer proceeds; the charge recombination rate may be determined by the disappearance of the SA^- spectrum. Charge migration within the DNA strand and its dependence on the constitituency of the

intervening bases may be conveniently probed by walking the G_{DNA} (or GG and GGG) donor down the duplex chain, as schematically depicted in Figure 12.

The energetics of the ET process have been varied with the excited-state potential of the hairpin. Owing to the higher oxidation potential of the diphenylacetylene-4,4′-dicarboxamide (DPA) singlet excited state, substitution of the SA hairpin by DPA allows charge transport between adenine (as well as G_{DNA}) to be established.[149,150] More generally, the hairpins of Chart 1 have provided a sufficiently wide range of excited-state potentials to permit the determination of the driving force dependence for ET in DNA hairpins.[151] In all cases, the kinetics for the appearance and disappearance of the radical anion of the hairpin was identified.

Electron transfer to DNA base pairs (as opposed to hole transfer) may be established when the excited state of the hairpin is reducing. This is the case for the 2-(hydroxyalkyl)stilbene-4,4′-diether (SD) shown in Figure 13. Excitation of the hairpin with a femtosecond laser induces ET to cytosine or thymine base pairs within the DNA strand;[152] for either transfer, the SD cation radical has been observed in the transient absorption spectrum. The SD hairpin is further distinguished because it is the only system that has been structurally characterized by X-ray analysis,[153] confirming the hairpin motif (Figure 13). When SD and SA hairpins are contained in the same DNA strand, both the radical cation and anion products of photoinduced ET may be detected.[154] The absorption spectra of SA^- and SD^+ differ sufficiently to be distinguished by transient absorption spectroscopy.

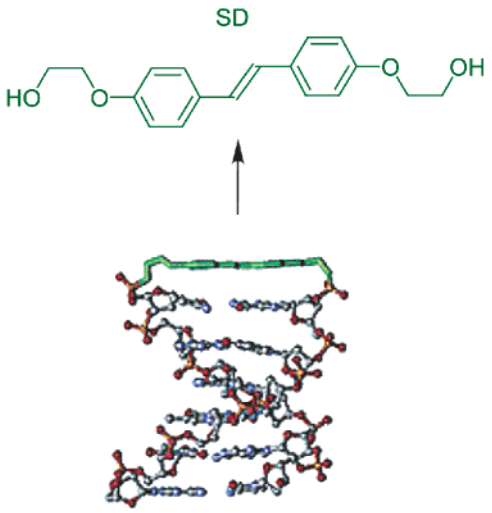

Figure 13. Crystal structure of a DNA duplex possessing a SD hairpin. Unlike most hairpins, charge transport occurs by ET as opposed to hole transfer. Electron injection to cytosines and thymines within the DNA duplex is initiated from the SD excited state. (Adapted from ref 153.)

The foregoing studies of DNA hairpins show that the observation of both the initially formed lowest excited singlet state of the acceptor and its anion radical provides a powerful method for investigating the dynamics of charge separation, charge recombination, and charge migration processes in DNA. However, it should be emphasized that in no case has the hopping intermediate, the $G_{DNA}^{\bullet+}$, been observed along the DNA chain. The inability to detect this radical cation highlights the difficulties attendant to detecting radicals along charge-transport chains. Generally, the molar absorptivities of natural radicals are too small to provide detectable optical signatures. Therefore, as exemplified in studies of DNA-mediated ET, the system under investigation must be modified by a chromophore that gives a sufficient change in optical density upon radical formation. Even if the base can be detected, transient absorption methods cannot distinguish similar radicals along a hopping chain. Consider the transport of the $G_{DNA}^{\bullet+}$ radical among different guanines of a DNA duplex. Once the radical is formed, its optical density will not change as the hole hops from G_{DNA} to G_{DNA}, and accordingly the kinetics of its transport cannot be ascertained.

These limitations of the transient absorption method suggest that other methods must be developed if the radicals responsible for hole migration are to be directly observed. Transient EPR methods should play an especially crucial role in future studies aimed at disentangling the role of radicals in the hopping kinetics of ET pathways. Indeed, EPR signals from radical base pairs within the DNA duplex have been observed under photolytic conditions. A steady-state EPR signal ($g = 2.0048$) for the $G_{DNA}^{\bullet+}$ is observed when the DNA duplex tethered with a ruthenium intercalator (Figure 10B) is photolyzed under flash-quench conditions.[155] The experiment has been further elaborated with the incorporation of 4-methylindole into known positions in the DNA duplex.[156] For this case, an EPR signal is observed at $g = 2.0065$, which is similar to an indole cation radical ($WH^{\bullet+}$). The absence of an EPR signal for $G_{DNA}^{\bullet+}$ is expected, given the lower oxidation potential of 4-methylindole (1.0 V versus NHE) relative to that of the nucleic acid base (1.3 V).[156] In both of these experiments, no hyperfine interactions were associated with $G_{DNA}^{\bullet+}$ or $WH^{\bullet+}$; this was attributed to π-stacking of the amino acids in the DNA duplex. The steady-state EPR experiments of the indole-modified DNA were complemented by transient absorption experiments, which show a transient signal for the appearance of a 4-methylindole cation radical that was identical to the rate of the excited-state ruthenium quenching to the Ru(III) oxidant. Unfortunately, the distance dependence on hole migration could not be measured because intra-DNA ET was not rate-limiting.

Whereas EPR experiments to date have established the production of radicals under photolytic conditions, time-resolved EPR methods will have to be applied to obtain direct kinetics for hole (or electron) hopping among the nucleobases of the DNA duplex.

4. Hopping Processes in Biology

The lesson learned from long-distance ET studies in DNA is that the constraint imposed by tunneling on the overall rate can be overcome when the ET distances are short. Transport of an electron over a long pathway in biology therefore necessarily demands that electrons hop if the ET rate is critical to biological function. Notwithstanding, this concept has

not been fully appreciated and, excepting DNA, more explicit treatments of hopping in biology have only recently appeared.[157] After years of controversy, consensus is emerging for electron transport by hopping in the reaction center of photosynthesis.[158] In bacterial RCs (Figure 8), electrons are ejected from the excited state of the special pair (SP) to bacteriochlorophyll *a* (BChl *a*) to form a $(SP)^+-(BChl\ a)^-$ charge-separated state. The electron is then transferred to a bacteriopheophytin (BPh) to produce a $(SP)^+-(BChl\ a)-(BPh)^-$ charge-separated state. Similarly, charge transport in Photosystem II (PSII) proceeds with an electron hopping from P680 to chlorophyll and subsequently to pheophytin; the electron is then conveyed to the quinone terminus of the electron transport chain in PSII.

In the foregoing examples of hopping, only an electron (or hole) is transferred among intervening redox cofactors or base pairs. In some cases, hopping necessarily requires the intervening medium to support the equivalent transfer of an *electron* and *proton* or hydrogen atom. For instance, hopping has been inextricably linked to the transfer of a proton and electron in studies of the quinone terminus of the RC and other biological systems, most notably, photolyase (see sections IV.B.1 and IV.B.2). The link between electrons and protons would also appear to be especially relevant to radical initiation by RNR. First, a hopping mechanism is implicated by the sheer 35-Å distance between Y122 neighboring the oxidizing diiron center (Figure 3) of the R2 subunit and the cysteine in the active site of the R1 subunit. Second, the radical initiation pathway of Figure 3 involves W and Y. The redox chemistry of latter amino acid entails the movement of a proton from the amino acid upon its oxidation, while that of tryptophan may or may not entail proton movement on oxidation. Finally, the chemistry of cysteine in the active site is most likely initiated by a hydrogen atom abstraction, which is initiated from the diiron−$Y^\bullet$ site of R2. In a limit, the hydrogen atom decomposes to an electron and proton transfer. Before the issue of PCET-assisted hopping in biology is discussed, mechanistic aspects of PCET will be presented.

IV. Proton-Coupled Electron Transfer

A. Mechanistic Considerations

The PCET problem steps beyond ET because both the electron *and* the proton affect H_{AD} and the FC term in eq 12. As mentioned in regard to Figure 4, the electron tunnels through the potential barrier from D to A when the medium fluctuates to a configuration where the energies of the electron donor and acceptor are equal at the surface crossing. For a PCET reaction, the problem is intrinsically more complicated because both the electron and proton tunnel. These tunneling events also are induced by fluctuations in the medium, but now the electron and proton influence each other thermodynamically and kinetically. As the electron moves, the pK_a of the oxidized cofactor will change, but to predict kinetics, the driving force of the reaction is not sufficient. The FC factors will be affected by the charge redistribution resulting from electron and proton motion. In addition, the electronic coupling will change parametrically with the proton coordinate. It should be emphasized that any motion of the proton from its initial position will perturb H_{AD} and FC and consequently the PCET kinetics; complete transfer of the proton is not required.

The need to account for both proton and electron motion in the PCET problem requires new experimental and theoretical design methods. To this end, PCET has emerged only recently as a field of study. PCET was launched at a mechanistic level with studies of the donor−acceptor redox pairs depicted in Scheme 2.[159,160] In this approach, the PCET reac-

Scheme 2

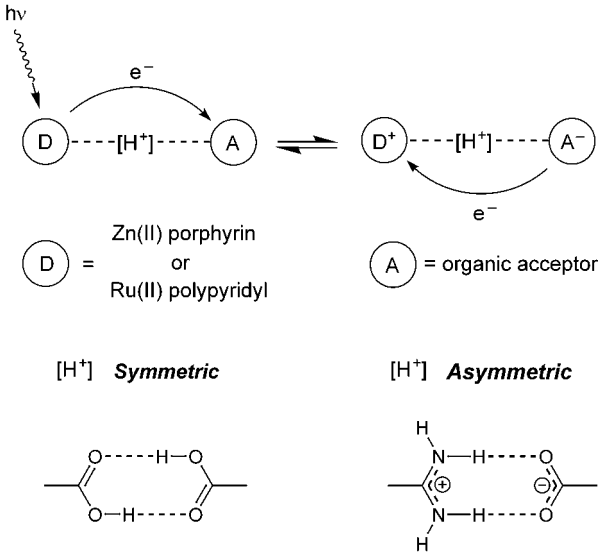

tion is initiated by photoexciting a donor or acceptor juxtaposed to each other by a hydrogen-bonding interface, D- - -$[H^+]$- - -A. The first D- - -$[H^+]$- - -A construct exploited the propensity of carboxylic acids to form cyclic dimers ($[H^+] = [(COOH)_2]$) in low-polarity, non-hydrogen-bonding solvents.[161] The D- - -$[(COOH)_2]$- - -A system provided the first direct experimental validation to the hypothesis that donor−acceptor coupling is affected by the presence and nature of the proton. Charge separation and recombination rate constants exhibit pronounced deuterium isotope effects. As was subsequently elaborated,[162] it is this observed deuterium isotope effect that reveals coupling between the electron and proton.

Within the - - -$[(COOH)_2]$- - - interface, proton displacement on one side of the dicarboxylic acid interface is compensated by the concomitant displacement of a proton from the other side. Because charge redistribution within this interface is negligible, the only mechanism available to engender PCET is the dependence of the electronic coupling on the position of the protons within the interface.[162,163] Similar results have been obtained for acceptor−donor pairs separated by guanine−cytosine base pairs[164−172] and related interfaces[173] where proton motion within the interface is minimized. These cases, however, are unusual in biology, where proton displacement typically accompanies the redox process.

In response to the issue of PCET in biology, mechanistic studies were extended to include salt-bridge interfaces such as that afforded from the association of an amidinium and carboxylate.[174−178] This salt-bridge interface combines the dipole of an electrostatic ion-pair interaction with a hydrogen-bonding scaffold. The effect of proton motion on ET in these systems has been demonstrated directly by a comparative kinetics study of a D- - -[amidinium-carboxylate]- - -A complex and its switched interface D- - -[carboxylate-amidinium]- - -A counterpart.[178,179] Differences between the rates of charge transport of 10^2-10^3 have been observed for the two congeners. A subsequent theoretical description of PCET[160,180−190] has evolved around these data to explain the pronounced rate effects.

To date, PCET has been treated as an analog of a pure ET reaction, where a four-state model is used to describe the electron in its initial (i) and final (f) states and the proton in its initial (a) and final (b) states,

$$\begin{aligned} &D_e{-}D_pH\text{- - -}A_p{-}A_e \quad \text{(ia)}\\ &D_e^{\oplus}{-}D_pH\text{- - -}A_p{-}A_e^{\ominus} \quad \text{(fa)}\\ &D_e{-}D_p^{\ominus}\text{- - -}HA_p^{\oplus}{-}A_e \quad \text{(ib)}\\ &D_e^{\oplus}{-}D_p^{\ominus}\text{- - -}HA_p^{\oplus}{-}A_e^{\ominus} \quad \text{(fb)} \end{aligned} \tag{15}$$

D_e is the electron donor, D_p is the proton donor, A_p is the proton acceptor, and A_e is the electron acceptor. In eq 15, the initial state is (ia) and the final PCET state is (fb). An ET with no proton transfer (PT) is described by (fa), and a PT with no ET is described by (ib). Schematics of the continuum of possible PCET reaction pathways are presented in Figure 14.

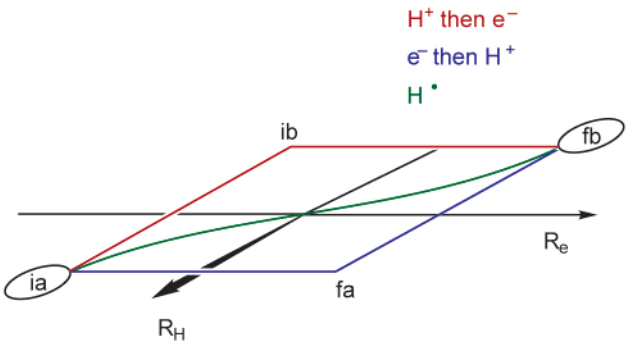

Figure 14. Schematic of the PCET pathways ia, ib and fa, fb, as given in eq 15. The blue pathway describes the transfer of the electron followed by the proton. The red pathway describes proton transfer followed by ET. All other possible PCET pathways are confined within the space of the red and blue paths. One especially important pathway is along the diagonal, shown in green. Here, the electron and proton transfers are concerted; this corresponds to hydrogen atom transfer.

The two zigzag ET/PT pathways describe a change of the proton coordinate to an appropriate configuration, after which ET occurs, or the prompt transfer of an electron, followed by the transfer of a proton. The diagonal pathway corresponds to the concerted PCET reaction; chemically, the path describes a hydrogen atom transfer.[191]

The putatively challenging aspect of developing a PCET theory is the disparate time scales for electron and proton motion. A proton is a much less quantum mechanical object than an electron due to its mass. Thus, the solvent fluctuations that drive ET can open up a number of channels for the PT. To date, the time scale (or mass) separation between the electron and the proton has been treated by a Born−Oppenheimer separation of the proton from the electron. Under these conditions, the PCET rate constant is given by[160,181,190,192]

$$k_{\mathrm{PCET}} = H_{\mathrm{AD}}{}^2\sqrt{\frac{4\pi^3}{h^2\lambda_{\mathrm{PCET}}k_{\mathrm{B}}T}}\sum_{n'}\rho_{in'}\sum_{n}|\langle\chi_{fn}|\chi_{in'}\rangle|^2 \times \exp\left[\frac{-(\lambda_{\mathrm{PCET}}+\Delta G_{\mathrm{PCET}}^{\circ})^2}{4\lambda_{\mathrm{PCET}}RT}\right] \tag{16}$$

where $\rho_{in'}$ is a normalized Boltzmann factor accounting for the equilibrium distribution of the proton in the reactant well, with the electron in its initial state, i. In eq 16, the electronic coupling of the ET problem (i.e., eq 12) is weighted by Franck−Condon factors connecting the proton in its initial and final states, $|\langle\chi_{fn}|\chi_{in'}\rangle|^2$. Moreover, the proton also contributes to both parts of the FC term. The driving force and reorganization energy depend on the charge distribution—from the electron and the proton—since the initial and final charge values are dependent on whether the process corresponds to ET, PT, or PCET. Therefore, the two ingredients that determine the rate of a charge-transfer reaction, the activation energy and the electronic coupling, depend on the reaction pathway. This coupling of the charge shift resulting from electron *and* proton motion to the polarization of the surrounding environment is the distinguishing characteristic of a PCET reaction. An understanding of how biology exploits this characteristic to control charge transport, especially by hopping, is one of the defining challenges in biophysics.

B. PCET in Biology

Many examples of PCET in biological transformations have been studied over the past decade. In addition, the first example of a proposed hopping mechanism over a long distance involving aromatic amino acids has recently been reported.[193] Information gleaned from two of these well-characterized systems, the photolyases and the photosynthetic reaction center, has been useful in constructing a framework for the radical initiation problem in class I RNRs.

1. Photolyase: PCET Hole Migration through Aromatic Amino Acids?

DNA photolyases catalyze the repair of cyclobutane pyrimidine dimers and 6-4 photoproducts with near-UV light.[194,195] The *E. coli* protein (55 kDa)[196] requires the anionic form of a reduced flavin ($FADH^-$) for activity. However, the protein as isolated is inactive and exists in the semiquinone form ($FADH^{\bullet}$).[197] The inactive form of the photolyase can be converted into the active form by reduction in a light-mediated ET

process. The photoactivation process has been studied in detail by the Sancar, Heelis, and Babcock groups.[198] Recently this process has been examined by transient absorption spectroscopy in the millisecond to picosecond time range,[193] allowing the disappearance of the photoexcited state of the flavin semiquinone radical ($FADH^{\bullet}$*), formation of a $WH^{\bullet+}$, and deprotonation of the $WH^{\bullet+}$ to a $W^{\bullet}$ to be monitored. The resulting model from these studies is shown in Figure 15. The $FADH^{\bullet}$* is lost within 30 ps, and the $WH^{\bullet+}$

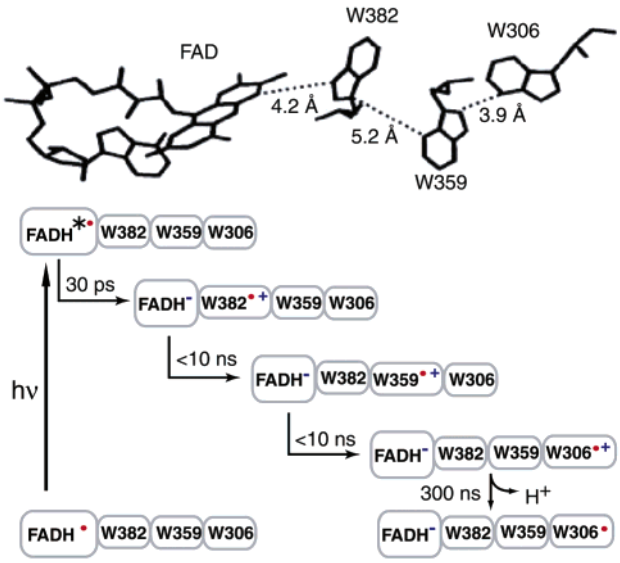

Figure 15. Proposed mechanism for photoreactivation of photolyase. (Reprinted with permission from *Nature* (http://www.nature.com), ref 193. Copyright 2000 Macmillan Magazines Ltd.) A proposed pathway based on the X-ray structure of the photolyase.[196]

is generated in less than 10 ns (the actual number is limited by the experimental approach). Deprotonation of the $WH^{\bullet+}$ occurs in 300 ns, and the proton is transferred to buffer or water. The lifetime of the $WH^{\bullet+}$ (17 ms) is limited by the rate of proton loss relative to the rate of back-ET. While early time-resolved EPR experiments[199,200] suggested detection of a $WH^{\bullet+}$, later experiments suggested that the interpretation of the data was not unambiguous. While the visible spectrum of the $WH^{\bullet+}$ is consistent with model $WH^{\bullet+}$'s, the EPR data supporting this assignment need to be reexamined.

Insight into the mechanism of $FADH^{\bullet}$ reduction has been provided by a high-resolution X-ray structure[196] (Figure 15) and recent theoretical studies.[201] A model has been put forth that the $WH^{\bullet+}$ observed by visible spectroscopy is associated with W306 that is solvent-exposed. This model is supported by site-directed mutagenesis studies in which the W306F photolyase mutant is unable to reduce $FADH^{\bullet}$. The W306Y mutant, however, was also ineffective at reduction of the $FADH^{\bullet}$ for reasons that are unclear, given its oxidation potential and pK_a (-2 for $YH^{\bullet+}$). Two mechanisms are viable for formation of the $W306H^{\bullet+}$: one involves tunneling and the other involves hopping and a pathway involving amino acid radical intermediates.[196] In the latter case, formation of the $W306H^{\bullet+}$ has been proposed to proceed through oxidation and reduction of two additional Ws: W382 and W359. W382 is 3.9 Å from $FADH^{\bullet}$ and 5.2 Å from W359. W359 is 5.1 Å from W306. The intermediates in this ET process have not been spectroscopically detected but have been proposed to exist and to be $WH^{\bullet+}$s, as there are no proton acceptors supplied by amino acids within 5 Å of these tryptophans. The photolyase mutant, W382F, has been prepared and the quantum yield of photoreduction was found to be 2 times higher than that of the wild-type enzyme. This increase translates to a 2-fold increase in the rate of electron transfer.[198] Radical transport by hopping would predict that the rate constant should decrease upon mutation; thus, these mutation studies support a tunneling model. Direct photophysical interrogation of the W359F, W382F, or the corresponding Y mutants would establish that these residues are not involved in the photoreduction as intermediates.

Additional insight into photolyase activation has come from a comparison of the photolyase from *Anacystis nidulans* and *E. coli*. In *A. nidulans* photolyase,[203,204] the triad of Ws is conserved (W390, W367, and W314). The terminal hole is generated on Y468, however, which is 8.6 Å from W314 and is located on the surface of the protein. In the absence of exogenous reductants in this system, $FADH^{-}$ and $Y^{\bullet}$ are generated in <500 ns, and reverse ET regenerates $FADH^{\bullet}$ and Y. The $t_{1/2}$ of the $Y^{\bullet}$ is 73 ms. Interestingly, back-ET experiences an isotope effect ($t_{1/2}$ = 198 ms), though the basis for the increase in $Y^{\bullet}$ lifetime has not yet been determined.

The importance of the photoactivation process remains to be established, as the protein probably exists in the reduced form in vivo and is only oxidized as an artifact of isolation under aerobic conditions. Furthermore, the *E. coli* W306F photolyase that is inactive in photo-reactivation of the $FADH^{\bullet}$ in vitro has wild-type (wt) photolyase efficiency in DNA repair in vivo. The conservation of the three Ws in all DNA photolyases and similar conservation of Ws in photolyase-like blue-light receptors indicate that these aromatic residues are clearly very important in this class of proteins; however, the intermediacy of these residues as actual oxidized amino acid radicals in ET over 14 Å is still open to question. If they are involved in the ET reduction of $FADH^{\bullet}$, the photolyase system is the only system thus far shown to involve aromatic amino acid residues in an ET process (>10 Å).[193] However, this process may not be physiologically relevant.

Several important conclusions can be drawn from the studies on photolyase that are of direct importance for thinking about the PCET process in RNR (Figure 3). If intermediate amino acid radicals are involved in this process, then charge-compensating simultaneous proton transfer is not a prerequisite for intraprotein radical transfer in the photoactivation process. Clearly, the oxidation of W306 to the $W306H^{\bullet+}$, in the *E. coli* case, precedes loss of the proton. Theoretical studies indicate that, while internal W deprotonation would be favorable, the process is probably slow, as there are no proton acceptors in the vicinity of these residues.[193]

Second, the reversibility of the redox reaction between the FADH• and the $WH^{\bullet+}$ (*E. coli*) or Y• (*A. nidulans*) provides a model for the reversible Y•, S• transfer between R1 and R2 (Figure 3). The FADH• is stable, as is the Y•, although the triggering of hole migration (light vs binding of substrate and effector to R1) is clearly very different. The studies on photolyase demonstrate that holes in aromatic amino acids can be detected and suggest mechanisms by which the lifetimes of the holes can be extended to facilitate their detection. The rate of reverse ET in the *E. coli* photolyase system is reduced by deprotonation of the $WH^{\bullet+}$ in buffer at pH 7.4 and increased in the buffer of lower pH. This is an example of the interplay between pH, redox potentials, and ET rates, which is clearly important in RNR. In the case of the *A. nidulans* photolyase, Y• hole transfer in the reverse direction is slowed in D_2O.[204] The studies on photolyase further demonstrate the power of light-induced reactions in triggering rapid reactions required to detect intermediates generated in very rapid ET reactions.

2. The PCET of the Photosynthetic Reaction Center

Perhaps the best-studied PCET systems are the photosynthetic reaction center (RC) in *Rhodobacter sphaeroides* and *Rhodobacter capsulatus* (Figure 8).[205] The RC initiates light-induced ET from the primary donor species, the bacteriochlorophyll special pair, through a series of electron acceptors including bacteriochlorophyll, bacteriopheophytin, and ubiquinone (Q_A) to ultimately reduce the bound ubiquinone Q_B. The reduced Q_B (Q_BH_2) transfers its electrons to the cytochrome *bc*1 complex, pumping protons across the membrane. The oxidized bacteriochlorophyll dimer is then reduced by cytochrome *c*2, completing the reaction cycle. The RC is thus a light-driven quinone reductase involving two electron-transfer and two proton-transfer reactions (Figure 16). The availability of structures[206] of all of the components and some complexes of this system, a genetic system to make mutants, the ability to use rapid kinetics methods and light triggering, and the ability to replace the bound ubiquinone (Q_B) and Q_A with a variety of other small molecules with altered redox potentials have allowed much insight into the proton transfers coupled to ET as well as the protein dynamics. Many recent reviews on this well-characterized system are available.[205,207] We will briefly focus on the results, and their attendant methods to obtain the results, related to similar problems associated with the RNR system.

a. Docking between Two Proteins for Electron Transfer. A major problem encountered in most ET reactions between proteins is the nature and lifetime of the interaction. In many cases, evidence for protein−protein interactions under physiological conditions has been elusive. A similar problem exists with RNR: the interaction between R1 and R2 subunits is weak. The docking of cytochrome *c*2 with the RC typifies this problem (Figures 8 and 17).[208,209] The K_d is weak (0.3 μM at 10 mM ionic strength, pH 7.5, nonphysiological conditions), and in vitro the docking can be rate-limiting. If the complex is formed, then the ET is rate-limiting and independent of the concentration of cytochrome *c*2. The mechanism(s) of protein docking in this and many other systems is (are) still being extensively investigated, despite the availability of structures of the complexes. The inter-

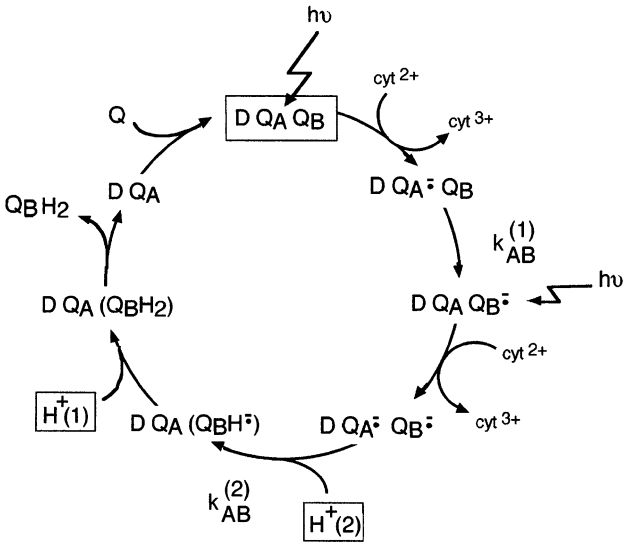

Figure 16. Quinone reduction cycle in bacterial RC. D is the primary electron donor. Note that $H^+(1)$ is the first proton delivered to E212 of the RC and required for the first ET to occur. It has been designated $H^+(1)$, although it is the second proton to be delivered to Q_B to produce Q_BH_2. The nomenclature in this figure, adapted from Okamura, Feher, and co-workers,[210,213] has been changed to be consistent with the equations in the text. The conformational changes discussed in the text are not indicated in this figure. (Reproduced with permission from ref 205. Copyright 2000 Elsevier.)

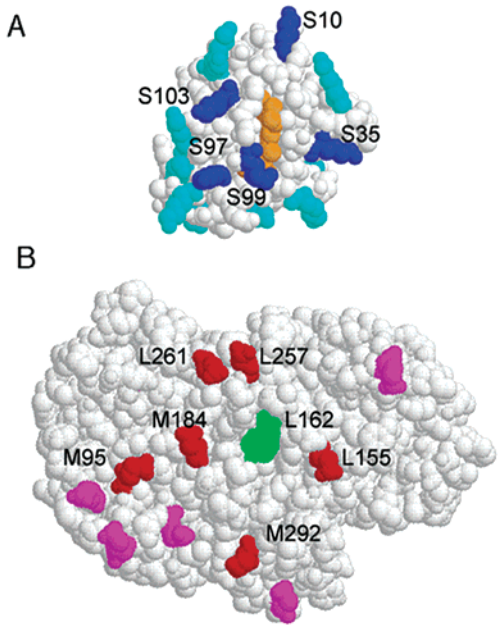

Figure 17. Views of the interaction surfaces of (A) cytochrome *c*2 from *R. sphaeroides* and (B) the RC from *R. sphaeroides*. The Lys residues on the cytochrome are shown in dark blue, and the acidic residues on the RC are shown in bright red. Additional charged residues are shown in light blue on the cytochrome and light red on the RC. The proposed ET contact groups, the heme (orange) on the cytochrome and the Y L162 (green), on RC are shown. (Reprinted with permission from ref 209. Copyright 2002 American Chemical Society.)

play between weak electrostatic interactions (due to desolvation penalties) in defining specificity, and the hydrophobic interactions in defining affinity are the issues in question. Weak interactions, in this case and in the case of R1 and R2, make study of their interactions a challenging experimental problem. Recent studies of the interaction of cytochrome *c*2 (reduced state) and RC (oxidized state) have revealed the initial importance of diffuse complementary potential energy surfaces in the docking interactions and not specific salt bridges (as may be the case in other systems),

$$\mathrm{cyt}^{2+} + \mathrm{RC}(\mathrm{D}^{+}\mathrm{Q}^{-}) \rightleftharpoons \mathrm{cyt}^{2+}{-}\mathrm{RC}(\mathrm{D}^{+}\mathrm{Q}^{-}) \xrightarrow{k_{ET}} \mathrm{cyt}^{3+}{-}\mathrm{RC}(\mathrm{DQ}^{-}) \quad (17)$$

These interactions facilitate optimal binding and a transition state for ET, and they may further help to nucleate specific hydrophobic interactions. Interactions identified by mutagenesis and ET measurements have recently been complemented by a structure of the complex (Figure 17).[208] The structure of cytochrome *c*2 from *R. sphaeroides* shows a solvent-exposed heme edge (orange) surrounded by positively charged lysine residues (dark blue). The surface of RC contains a solvent-exposed Y-L162 (green, L is the one of the subunits of the RC) located directly above the bacteriocholorphyll dimer surrounded by negatively charged glutamates and aspartates (bright red). Y-L162 has been shown to be a conduit for docking between the heme edge on cytochrome *c*2 and the RC.[209] These studies have also revealed, however, that Y-L162 is not essential in the ET process, providing an example that aromatics do not play an essential role in short-range ET processes. A similar electrostatic complementarity is not apparent on the proposed docking surfaces of R1 and R2 of RNRs.

b. Dissecting Electron Transfer and Proton Transfer. A second issue that has been investigated in detail is the mechanism of reduction of Q_B by Q_A (Figure 16) that can be subdivided into two sequential light-induced electron-transfer reactions.[210,211] The first ET produces a stable anionic semiquinone $Q_B^{\bullet -}$:

$$Q_A^{\bullet -}Q_B \xrightarrow{k_{AB}^1} Q_AQ_B^{\bullet -} \quad (18)$$

No protonation occurs in this step, but a protonation of E212 of the protein is thought to be important for the ET to occur. In addition, a slow conformational change is required to generate the state activated for ET, $[Q_A^{\bullet -}Q_B]^P$, followed by the rapid ET step,

$$Q_A^{\bullet -}\,Q_B \xrightarrow{k_c} [Q_A^{\bullet -}Q_B]^P \xrightarrow{\text{fast } k_{ET}} Q_AQ_B^{\bullet -} \quad (19)$$

The ability to replace the quinones in this system has facilitated studies on the importance of the driving force in the first ET step. In the *R. sphaeroides* system, the native Q_{10} that binds in the Q_A binding site has been replaced by a variety of quinones that span 150 mV in reduction potential. Using a variety of complementary methods, it has been shown[210] that the rate of ET from $Q_A^{\bullet -}$ to Q_B in this first ET step does not change with driving force. Furthermore, a strong temperature dependence on this process was observed, suggesting that a rate-limiting conformation change is required before ET. Conformational gating (and perhaps protonation, see below) and protein dynamics play an essential role in the first step of this reduction process. Since light provides the trigger for the first ET reaction, X-ray structures of the dark RC (DQ_AQ_B) and light-activated RC ($D^+Q_AQ_B^{\bullet -}$) have provided a possible explanation for the conformational change in this process. Figure 18 shows the region of Q_B binding and

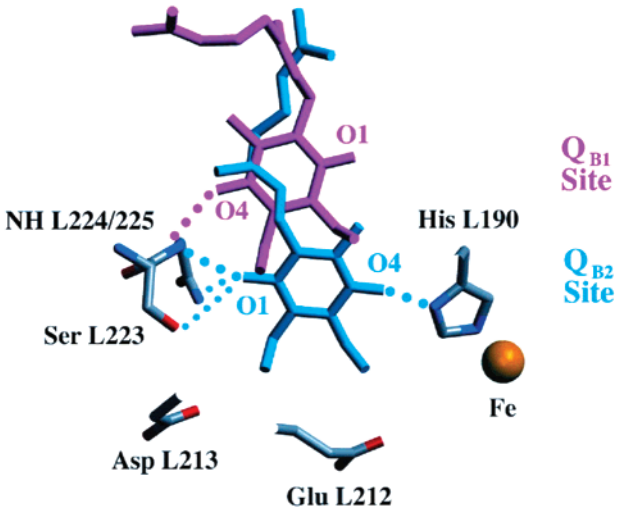

Figure 18. Comparison of the binding positions for Q_B determined from the light ($D^+Q_AQ_B^{\bullet -}$) and dark (DQ_AQ_B) X-ray crystal structures of the RC. Movement from an inactive-distal (purple) to an active-proximal (blue) binding site is proposed as the major structural change involved with the conformational gating of ET from $Q_A^{\bullet -}$ to Q_B. Hydrogen-bonding partners are connected by dotted lines.[205] (Reprinted with permission from ref 205. Copyright 2000 Elsevier.)

demonstrates a large difference in the positioning of this quinone between the two states. The evidence for the importance of E212 protonation in the first ET reaction was provided by measuring the decrease in k_{AB}^1 (see Figure 16) with increasing pH. These kinetic studies generated the hypothesis that E212 has a pK_a of 8.5 and must be protonated prior to ET. Both of the steps in eq 20 encompass the chemistry

$$Q_A^{\bullet -}Q_B\text{- -EL212CO}_2^{-} \overset{\text{fast } k_{H^+}}{\rightleftharpoons} Q_A^{\bullet -}Q_B\text{- -EL212CO}_2\text{H} \xrightarrow{\text{slow } k_c} Q_AQ_B^{\bullet -}\text{- -EL212CO}_2\text{H} \quad (20)$$

of eqs 18 and 19. The pK_a of E212 appears to be perturbed by 4 orders of magnitude. Thus, in addition to the conformational change involving Q_B accompanying the first ET, a change in protonation state of the protein, specifically at E212, is also important.[212] This proton-transfer reaction may be very different from the multitude of proton-transfer steps that might be expected in the RNR system (Figure 3). However, the studies of the RC re-emphasize the ability of proteins to dramatically perturb pK_as of

residues by changes in environment. The ability to determine pK_as of residues in the putative pathway in the RNR radical initiation process is thus particularly important.

Since the double reduction of Q_B takes place in two sequential light-induced ET reactions, the two ET steps and the two protonation steps can be dissected (Figure 16). Identification of the amino acid side chains involved in the protonation process is particularly challenging, but the availability of structure, mutant proteins, and a chemical rescue method has provided a detailed model for how the overall protonation process occurs.[211,213]

The first protonation of Q_B occurs during the second ET to Q_A,

$$Q_A^{\bullet -}Q_B^{\bullet -} + H^+ \underset{\text{fast}}{\overset{k_H^+}{\rightleftharpoons}} Q_A^{\bullet -}Q_BH^{\bullet} \xrightarrow[\text{slow}]{k_{ET}} Q_AQ_BH^- \xrightarrow{k_{int}} Q_AQ_BH_2 \quad (21)$$

GluH Glu$^-$

This protonation is unfavorable, and the $Q_BH^{\bullet}$ accepts a second electron from $Q_A^{\bullet -}$; this is the rate-determining step and is followed by a rapid proton transfer from E212. On the basis of structure and mutagenesis studies, the transfers of proton 1 (proton 1 has been defined as the one initially taken up by E212, although it is not the first proton transferred to $Q_B^{\bullet -}$) and proton 2 (the first proton provided $Q_B^{\bullet -}$) are thought to enter the active site through surface residues (H126, H128, and D124) and then involve D-M17, D-L210, and D-L213 (L and M are the subunits of the RC and D is aspartic acid, Figure 19).

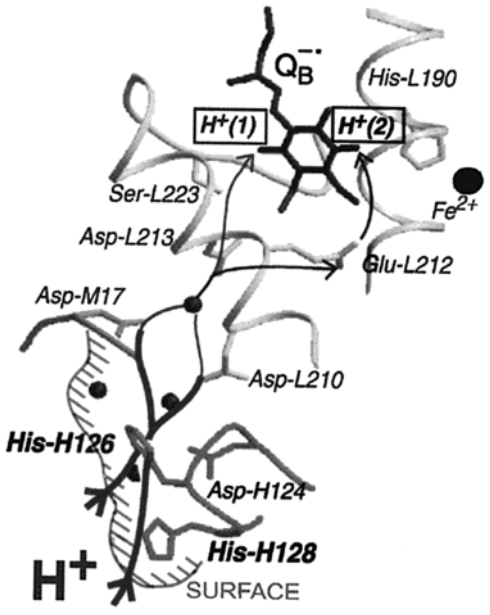

Figure 19. Part of the structure of the RC in the charge-separated state. Shown are the secondary quinone, Q_B, and the amino acid residues that are important for the transfer of $H^+(1)$ and $H^+(2)$ to Q_BH_2. Water molecules are indicated by small spheres. (Reprinted with permission from ref 205. Copyright 2000 Elsevier.)

At this point, the two proton pathways are proposed to partition, with proton 1 ultimately being transferred from E212H to the reduced Q_B to give Q_BH_2. The details of the overall reduction have been examined using site-directed mutants in which two surface histidines (H126 and 128) were replaced with alanines. Rates of proton uptake for the first and second proton in this mutant system were slowed by factors of 10 and 4, respectively. Evidence that the reduced rates are associated with reduced rate constants in proton transfer was provided by the pH dependence of each ET reaction.[211] Further support for this model was provided by chemical rescue experiments on the double (H → A) mutant RC. In these experiments, increasing concentrations of imidazole were added to the reaction in an effort to restore the rates observed with the wt-RC. In fact, the rescue experiments were successful. The studies with the double H → A mutants revealed that both the first and second ET rates were limited by proton uptake from solution. While alternative explanations for the observed results are possible, the imidazole rescue studies demonstrated that fast proton uptake could be restored with imidazole. These studies have provided much insight into the coupling of the ET and PT processes in this complex system. As summarized in Figure 19, and from additional studies summarized in an excellent review,[205] there appears to be a redundancy in the proton-transfer pathway (H126 or H128 and D-M17 or D-L210) for both protons. Closer to the quinone there appears to be an obligatory requirement of D-L213, S-L223, and E-L212. The studies on proton transfer in the RC demonstrate a number of principles that must be considered when thinking about the PCET process in RNR. First, as noted above, pK_as of groups involved in the proton transfer can be perturbed by 4 orders of magnitude. Second, it is difficult to perturb protonation steps such that large effects can be measured. In the case of the RC, rate differences of only 5−10 are observed. Thus, given that the stability of proteins is limited to physiological pH ranges (pH 6.5−9 in the case of RNR), the maximum differences in the case of RNR and deoxynucleotide reduction in a pH rate profile may be only a factor of 10−100. The complexity of the proton-transfer steps in RC suggests that alternative pathways may be prevalent in the RNR system as well. Exploring the reasonable possibilities requires excellent structural data.

C. Generality of Amino Acid Radical Intermediates in ET/PCET Reactions?

Studies from photolyase,[193,197,201] the photosynthetic reaction center,[205] and hole migration in DNA[114,122,136,156] provide a framework for thinking about RNRs. However, as outlined in the remainder of this review, RNRs present a unique problem in Y$^{\bullet}$-dependent and long-range PCET reactions. The Y$^{\bullet}$ oxidant of RNR resides in a hydrophobic pocket protected from the external environment and has a lifetime of several days.[214] Y$^{\bullet}$s in solution have lifetimes of milliseconds, and Y$^{\bullet}$s characterized in other protein systems function as transient intermediates (the PS II O_2-evolving manganese cluster, cyclooxygenases I and II, and the putative intermediate in cytochrome *c* oxidase).[5,215] The radical initiation in class I RNRs is long-range, >35 Å, in contrast with most biological systems, in which redox cofactors are separated by 10−14 Å.[104] The long-range ET and the

rate for nucleotide reduction require a pathway model involving aromatic amino acid radicals (Figure 3). While $WH^{\bullet+}$ has been implicated in diferric−$Y^{\bullet}$ cluster assembly in R2 (see section V.C), cytochrome *c* peroxidase, and photolyase, there are presently no other physiologically relevant examples that definitively establish the involvement of amino acid radicals in long-range PCET. The essential roles of RNRs in nucleic acid metabolism make the choice of such a radical initiation process baffling, given the potential for mistakes in both replication and repair. The remainder of the review will focus on class I RNRs: the evidence that the radical initiation is long-range and that a pathway involving aromatic amino acids is possible. A mechanism for regulation of this process to minimize radical damage is presented.

V. Establishing the Radical Pathway in RNR: Is ET or PCET Really Long-Range?

Insight into the radical initiation process of the class I RNRs has been provided by a comparison of the R1 structure with the structure of the class II RNR and the α2 subunit of the class III RNR. The similarities between these structures will be briefly summarized before focusing on the class I enzymes.

A. Insight into the Radical Initiation Process in R1: A Structural Comparison of the Three Classes of RNRs

As noted in section II, the three classes of RNRs differ in their quaternary structures, primary sequences, the source of reducing equivalents in the reduction process, and their metallo-cofactors (Figure 1, eq 1). The latter has provided the basis for class differentiation. The class II RNRs are found in both procaryotes and eucaryotes[216] and exist as either monomers (85 kDa, α)[217−219] or homodimers (α2).[220] They use the cobalt-containing cofactor adenosylcobalamin (AdoCbl) as their radical initiator. Class II RNRs, as with class I RNRs, also possess five cysteines essential for catalysis. The most detailed studies have been carried out on the *Lactobacillus leichmannii* enzyme that will serve as the prototype in subsequent discussions. Three cysteines are located in the active site. C408 is oxidized to a $S^{\bullet}$, the radical initiator. C119 and C419 are oxidized to a disulfide, providing the reducing equivalents to make the deoxynucleotide (Figure 2). Two additional cysteines are located at the C-terminus of the protein (C731 and C736) and re-reduce the active-site disulfide, required for multiple turnovers. *E. coli* thioredoxin can also reduce these external cysteines.

The class III RNRs are homodimers (α2). The active form of this subunit contains one stable glycyl radical ($G^{\bullet}$) per dimer that is essential for catalysis.[221−230] Generation of the $G^{\bullet}$ requires a second protein (β2) that is either an activating enzyme or a subunit. This protein contains one 4Fe4S cluster per monomer and binds *S*-adenosylmethionine (SAM). Both SAM and the iron cluster are required for $G^{\bullet}$ formation.[231−233] In the case of the *Lactobacillus lactis* RNR, the activating enzyme binds to α2 transiently to generate the $G^{\bullet}$ that can catalyze multiple turnovers of nucleotide to deoxynucleotide.[234] In the case of the *E. coli* class III RNR, the interaction between the α2 and β2 is very tight. In contrast to the class I and II RNRs, formate is used as a reductant (eq 1), and there are only two conserved cysteines in the active site.[226] Additional conserved cysteines play a role in $G^{\bullet}$ formation that is not yet clarified.[228]

Structures of the *L. leichmannii* class II RNR[235] and the T4 phage class III RNR[236] have recently been determined. Comparison of these structures with those of the class I R1 reveal that all three classes of RNRs possess very similar active-site architecture. The conserved active-site cysteines are found in a 10-stranded α,β barrel composed of five parallel and five antiparallel strands. In each case there is a finger loop in the middle of the barrel. At the tip of this loop is located the cysteine that becomes the putative $S^{\bullet}$. A superposition of 70 Cα atoms of the $(\alpha/\beta)_{10}$ barrel core structures gives a root-mean-square deviation between the class I and II RNRs of 1.0 Å and a root-mean-square deviation between the class II and III structures of 1.8 Å. The class I and II enzymes are much more similar to each other than either is to the class III RNR. All three RNRs initiate catalysis by 3′-hydrogen atom abstraction from the nucleotide substrate to form a 3′-nucleotide radical, which after water loss generates a 3′-ketodeoxynucleotide (Figure 2).[235,237] Although the reducing equivalents required for reduction are provided by cysteine oxidation in the class I and II RNRs and formate in the class III RNRs, similar mechanisms of reduction involving transient thiyl radicals can be postulated in all three systems.[6,7,230,238]

The similarities in the active-site architectures of the RNRs from each class confirmed expectations based on extensive biochemical and chemical experiments.[237,239] Unexpectedly, however, the structural comparison revealed that AdoCbl and the $G^{\bullet}$ (residue 580 in the T4 phage enzyme) in class II and III RNRs, respectively, were located at the C-terminus of their respective α subunits and in the same position as two absolutely conserved tyrosines Y730 and Y731 at the C-terminus of the class I R1 (Figure 20). Furthermore, the position of these radical initiators (AdoCbl, $G^{\bullet}$, and Y730/Y731) is conserved in three-dimensional space relative to the cysteine to be oxidized to the $S^{\bullet}$ (Figure 20). AdoCbl has been shown to generate a $S^{\bullet}$ via direct hydrogen atom abstraction,[240] and the $G^{\bullet}$ presumably generates $S^{\bullet}$ by direct hydrogen atom abstraction as well. The overlap of AdoCbl, $G^{\bullet}$, and the two Ys in R1, as will be discussed later, thus suggests the importance of hydrogen atom abstraction in $S^{\bullet}$ formation in the class I RNRs.

B. A Docking Model for R1−R2: A Proposed Pathway for Radical Initiation

In the class I RNRs, the radical initiator is the diiron−$Y^{\bullet}$ cofactor located on R2, while the active site for nucleotide reduction initiated by transient $S^{\bullet}$ formation is located on R1 (Figure 3).[15,18,241,242] A mechanism for this radical initiation, first proposed by Uhlin and Eklund, is based on a docking model generated from shape complementarity of the structures of the R1 and R2 subunits (Figure 21).[15] It was

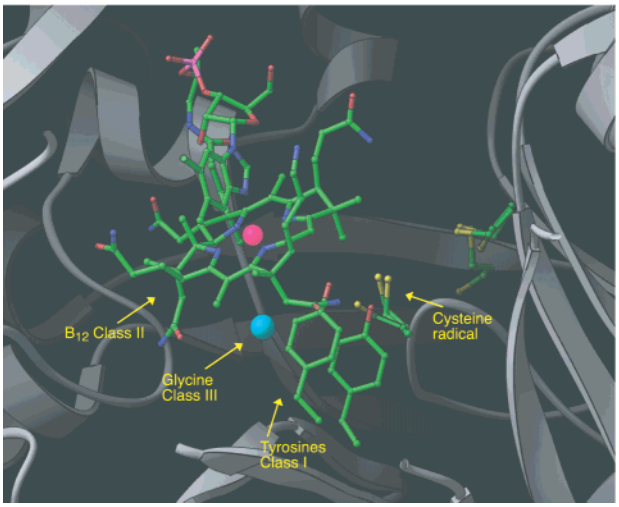

Figure 20. Commonality of the radical initiation ($S^{\bullet}$ formation) and active sites of the class I, II, and III RNRs, as presented in Sintchak et al.[235] Note the amazing spatial similarities in the location of the radical initiators AdoCbl, $G^{\bullet}$, and Y730. Note that, while the dimethylbenzimidazole ligand of AdoCbl is shown, the adenosyl axial ligand is not shown due to thermal lability in the structure. Since hydrogen atom abstraction to generate $S^{\bullet}$ has been demonstrated in the class II RNR and is strongly inferred from the chemistry and location of the $G^{\bullet}$ in the class III RNR,[236] one can infer that $S^{\bullet}$ formation by Y730 is likely to involve hydrogen atom transfer as well.[15,25]

proposed that these subunits formed a 1:1 complex and R1 straddles R2 in much the same way as a cowboy sits on a saddle.[243−246] The docking model requires a few additional comments. First, the C-terminal tail of R2 provides most of the binding energy for R1−R2 interactions. Removal of the C-terminus of R2 (6−20 amino acids, depending on the organism) inactivates reductase due to loss of subunit interactions. Furthermore, peptides with sequences identical to the C-terminii of the viral, bacterial, or mammalian R2s are sequence-specific competitive inhibitors of their R2s interaction with their own R1.[247−250] In both the *E. coli* and mouse RNRs,[251] the interactions between R1 and R2 are weak, on the order of 0.1−0.2 μM. Figure 21 shows the proposed docking model in two orientations and includes the conserved residues in R2 and R1 thought to be involved in the radical initiation process (Figures 3 and 22). The C-terminal regions (30−40 amino acids) of all R2 structures are thermally labile. In the *E. coli* R2, the last detectable amino acid is residue 340 of 375. The crystallization of R1 required the presence of a peptide (20 amino acids) identical to the C-terminus of R2. In the R1 structure, the peptide is shown in red and residues 360−375 are visible.[252−254] If one assumes that the peptide bound to R1 adopts a conformation similar to the one adopted by the C-terminus of R2 bound to R1, then one has a docking model in which only 19 amino acids (341−359) are missing. Residue 356, conserved in all R2s and thought to play an essential role in radical initiation, is located within this "invisible" region. This docking study results in a model cited above where the distance between the $Y^{\bullet}$ on R2 is >35 Å from the precursor to the $S^{\bullet}$ radical on R1.

Class I RNRs have turnover numbers for nucleotide reduction that vary between 2 and 10 s^{-1}. The ET theory described in eq 12 can be used to calculate a

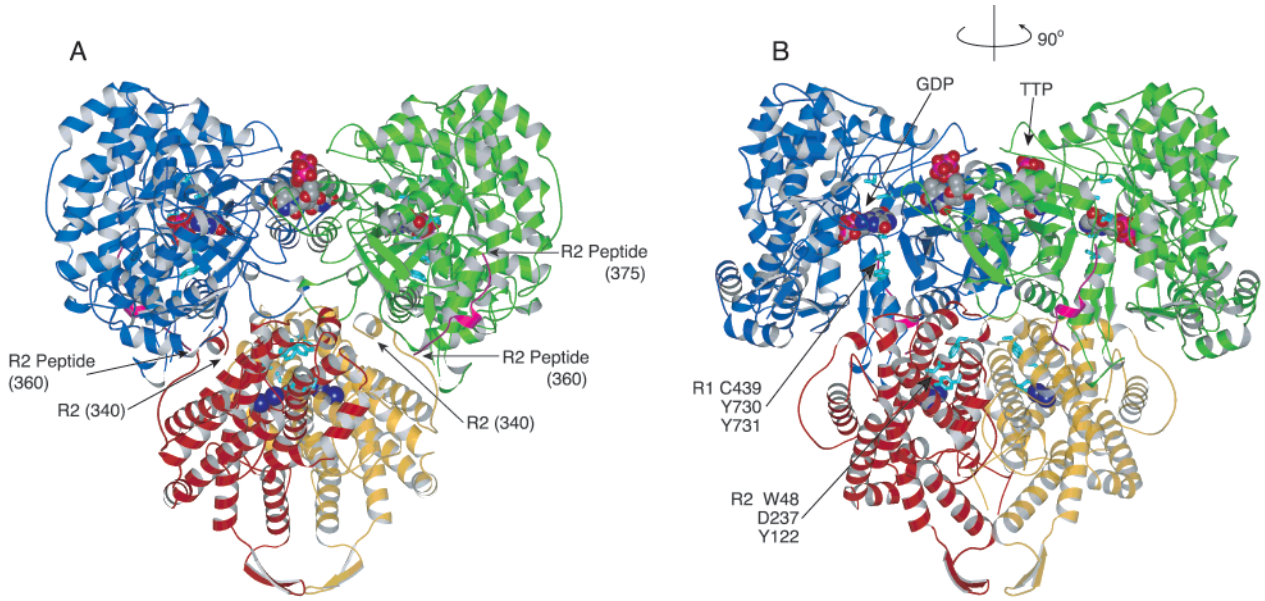

Figure 21. Docking model of the R1 (α2) and R2 (β2) subunits of *E. coli* RNR based on shape complementarity.[15,25] (A) The monomers of R1 are indicated in blue and green. Each monomer has substrate (GDP) and effector (TTP) in a CPK rendition. The TTPs are located at the subunit interface between the two R1 monomers at the tip of a four-helix bundle, two from each monomer. Also indicated in R1 are the three active-site cysteines (C439, C225, and C462) and two tyrosines (Y730 and Y731) thought to be involved in ET between R1 and R2. All of these residues are in cyan. R1 was crystallized with a peptide identical to the last 22 amino acids of R2. The C-terminal 15 residues of this peptide, 360−375 of R2, are shown in red. The monomers of R2 are indicated in red and gold. The two irons on each monomer are shown in blue balls. The residues thought to be involved in ET between R1 and R2 are shown in cyan (Y122, D237, and W48). In all structures of R2, the C-terminal (30−50) amino acids are thermally labile and hence are not observed. The last visible C-terminal amino acid of R2 from *E. coli*, residue 340, is labeled. (B) The model structure shown in (A) is rotated 90° around the 2-fold axis of symmetry shown. Structure A shows the surface complementarity and B shows the ET pathway.

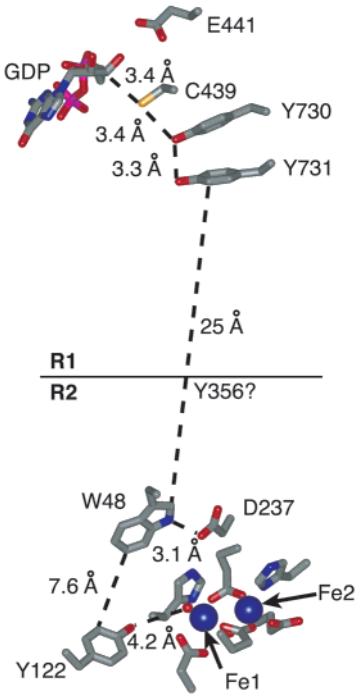

Figure 22. Using the model structure described in Figure 21, the conserved residues proposed to be involved in the ET between R1 and R2 are shown, as are the distances between these residues. The distance labeled 25 Å between Y731 on R1 and W48 on R2 is based on the docking model shown in Figure 21. Note a water (red dot) adjacent to Fe1.

turnover number for RNR if this step is rate-limiting. Assuming a 35-Å distance between the centers, an optimum driving force for cysteine oxidation, a tunneling model in which k_{ET} falls off exponentially with distance, and a β value of 1.1−1.4 Å^{-1}, the rate constant for nucleotide reduction would be 10^{-4}−10^{-9} s^{-1}. Nucleotide reduction would thus be limited by the ET process, and the turnover would be much less than that observed for the enzyme. Thus, the tunneling model, thought to accommodate most ET processes in biological systems,[104] does not account for the biochemistry of the class I RNRs. This calculation and the structures of R1 and R2 led Eklund, Sjöberg, Graslund, and their collaborators to a model in which amino acid radicals must be intermediates in the radical initiation process (Figures 3 and 22).[243−246] The amino acid residues depicted (Figures 21 and 22) are conserved in all R1 and R2 sequences thus far examined.

In addition to the distance of the ET, a second major problem is measurement of reduction potentials of the proposed amino acids (Y, W, and C) involved in the ET pathway (Table 2).[5,255] The pH

Table 2. Reduction Potential for Blocked Amino Acids

reaction	$E^{\circ\prime}$ (NHE)/V
RS$^{\bullet}$ → RSH	1.33[a]
RS$^{\bullet}$ → RS$^-$	0.77[b]
WH$^{\bullet+}$ → WH	1.15[c]
W$^{\bullet}$ → WH	0.9−1.05[d]
Y$^{\bullet}$ → YOH	0.83−0.94[e]
Y$^{\bullet}$ → YO$^-$	0.65[f]

[a] Reference 333. [b] Reference 334. [c] References 308, 309. [d] References 308, 309. [e] Reference 309. [f] Reference 255.

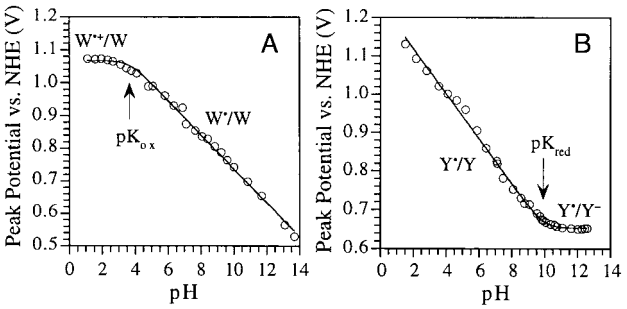

Figure 23. Differential pulse voltammetry has been used to measure the pH dependence of the reduction potential of N-acylated, C-esterified amino acids of W and Y.[255]

dependence of the redox potentials for Y and W is shown in Figure 23. A Y$^{\bullet}$ at pH 7 has a reduction potential of 0.84 V versus NHE and is not capable of oxidizing a cysteine (SH) to a S$^{\bullet}$ at pH 7.0 that has an reduction potential of 1.33 V. However, if the thiol of the cysteine is deprotonated, the reduction potential drops to 0.77 V, making the oxidation thermodynamically feasible.[256] The inability of a Y$^{\bullet}$ to oxidize a SH has assumed no perturbation of the pK_as or the redox potentials of the amino acids. If these assumptions are correct, then the model for ET in the radical initiation by class I RNRs must include coupling with proton(s) transfer or, alternatively, direct hydrogen atom(s) transfer. The validity of these assumptions needs to be examined, as pK_as of amino acid side chains in a variety of enzymatic systems, as noted in section IV.B.2, can be perturbed by up to 5 orders of magnitude, as can reduction potentials of a variety of cofactors.

Changes in the reduction potentials for Y, W, and C as a function of pH provide one mechanism by which Nature may be able to fine-tune an ET process. The ET could be coupled in a stepwise or a concerted fashion to proton or hydrogen atom transfer that can be modulated by substrate or, in the case of RNR, substrate and allosteric effectors. For example, a protonated tryptophan cation radical (WH$^{\bullet+}$) is a more potent oxidant than a tryptophan radical (W$^{\bullet}$) at pH 7 ($E^{\circ\prime}$ = 1.15 vs 0.89 V). If the environment of the protein can enforce protonation of this oxidized amino acid (pK_a of 4.5), then oxidation of Y to Y$^{\bullet}$ is facilitated.

Let us examine the proposed pathway for radical initiation. The proposal of Sjöberg, Graslund, and their collaborators[15,243−246] has been that there are 10 essential residues on the pathway shown for the *E. coli* RNR:

$$\text{Y122} \rightarrow \text{D84} \rightarrow \text{Fe1} \rightarrow \text{H118} \rightarrow \text{D237} \rightarrow \text{W48} \rightarrow \text{Y356} \rightarrow \text{Y731} \rightarrow \text{Y730} \rightarrow \text{C439} \quad (22)$$

The Y122$^{\bullet}$ is proposed to be reduced by hydrogen atom transfer that occurs by an unspecified mechanism through this pathway to oxidize W48.[11,239−242] From the R2 structure, a directly coordinated hydrogen-atom-transfer pathway between Y122 and C439 is not feasible. Such a pathway would require transfer of a proton or hydrogen atom from W48 to D237 and subsequently H118. Hydrogen atom transfer of H118 would require dissociation of this residue from Fe1 (see Figure 22). One example of this type of

histidine displacement in diiron proteins, ruberythrin, has recently been reported;[257] however, no evidence for histidine dissociation in R2 presently exists.

A more reasonable model for communication between W48 and Y122 would involve ET by tunneling with a separate protonation step. Several groups have suggested the importance of water bound to Fe1 as the source of the "H•" (see Figure 22).[258,259] The transfer of a H• from an Fe^{3+}-bound water is chemically unlikely, considering the redox potential and given that there is no evidence for changes in the redox state of Fe1 during the nucleotide reduction process. However, the water on Fe1 could be the source of the proton delivered to the Y, once the Y• is reduced to the phenolate. In this model, the Fe1 in the diiron core would transiently be in a hydroxide-ligated state, in contrast with a water-ligated state in the resting protein.[26,28] The available structures of NrdB and NrdF and the available spectroscopic information on intermediate X in diiron cluster assembly, discussed below, suggest that this option is chemically viable.[10,260] Furthermore, the ability of the W48 to communicate with Y122 by a proton-coupled ET process in which the two steps are not directly coupled, also outlined below, has ample precedent in the chemistry of the diiron−Y• cofactor assembly.[11,261]

The connectivity between W48 and C439 has also been proposed to occur via a series of direct hydrogen atom transfers.[244] The caveat is that Y356 is located in the C-terminus of R2 that, as noted in Figure 21, is not visible in the structure of any R2. There is a large structural void of 25 Å between W48 of R2 and Y731 of R1 (Figure 22).[244,258] If Y356 is located midway between W48 and Y731, then ET can occur rapidly. The long distance in the present model, however, would make hydrogen atom transfer between these residues less likely without large conformational reorganization during the radical initiation process. However, the hydrogen-atom-transfer model for radical initiation between Y731 and C439 in R1 is structurally and chemically appealing (section V.A). This coupling within R1, as will be discussed later, is also supported by biochemical experiments. Uhlin and Eklund were the first to point out the unusual configuration of Y731 and Y730 relative to C439 (Figures 21 and 22).[15] These Ys are absolutely conserved in all class I RNRs and, as discussed previously in comparison of the structures of the three classes of RNRs, are likely players in the radical initiation process. Theoretical calculations on radical initiation between Y731 → Y730 → C439 at the DFT-B3LYP level suggest that a hydrogen atom transfer between Y731 and Y730 has a barrier of 4.9 kcal mol^{-1}, while that between Y730 and C439 has a barrier of 8.1 kcal mol^{-1}.[258] The communication between Y731 and W48 was also suggested to have a "low" energy barrier, but calculations were not possible because of the absence of structural information on Y356 relative to W48 on R2 and Y731 on R1.

Examination of the structure of R1 suggests that an alternative mechanism for deprotonation of C439 should be considered. E441 is 4.7 Å from C439 SH (Figure 2) and could potentially function as a general base catalyst to generate a thiolate in the radical initiation process. The pK_as of C439 and E441 are obviously mismatched for such a function, and the orientation of the glutamate relative to this cysteine in the available structure would need to be altered. To date, no high-resolution structure of any substrate bound to the active site of any R1 in the presence of effector has been obtained, and some surprises might result. Site-directed mutagenesis studies, however, reveal that E441Q R1 is still capable of 3′-hydrogen atom abstraction from nucleotide.[13,262,263] E441 is therefore unlikely to function in thiolate formation.

C. Radical Initiation Process in R2: Insight from Studies of Diiron–Y• Cluster Assembly

An interesting unresolved issue of RNR chemistry involves the mechanism by which the diiron−Y• cofactor is generated in vivo from apo R2.[1,10] Cofactor assembly requires Fe^{2+} binding and a four-electron reduction of O_2 to H_2O. Studies of the stoichiometry of the reaction reveal that three of the electrons required for O_2 reduction are provided by Y122 and two Fe^{2+}'s and that the fourth electron is provided by an external reducing equivalent (eq 23).[11,264−266] In

$$H^+ + R2{-}Y122 + 3Fe^{2+} + O_2 \rightarrow Fe^{3+}{-}O{-}Fe^{3+} + R2{-}Y122^{\bullet} + Fe^{3+} + H_2O \quad (23)$$

vitro, the reductant can be supplied by additional Fe^{2+} or buffer. In vivo, the source of the reductant has not yet been identified. While the assembly of the diiron−Y• cluster in the *E. coli* RNR appears not to be linked to nucleotide reduction—that is, R1 is not required—this assembly does require the interaction of R2 with an iron delivery system, either a protein chaperone or a small iron chelator and a protein such as a ferredoxin or a flavodoxin to deliver the reducing equivalent. Our present working hypothesis is that the ET pathway in the assembly process is shared with part of the ET pathway in the nucleotide reduction process, Y122 → W48 → Y356, and that W48 is the key modulator of both processes. In the case of diiron−Y• assembly, W48 is a key player for the one-electron chemistry required for cofactor assembly and distinguishes this chemistry from the two-electron chemistry observed with methane monooxygenase that has a similar diiron cluster. In the nucleotide reduction process, we believe W48 and the proton sink within its vicinity (D237) allow reversible ET between Y122 and W48. We favor the congruence of the ET pathways (Y122 → W48 → Y356), despite the observations that the Y356F and Y356A mutants of R2 are "inactive" (discussed in detail below) with respect to nucleotide reduction yet are as active and efficient as wt-R2 in the in vitro assembly of the active diiron−Y• cofactor.[11,246,250,261,267,268] Our in vitro studies on the early steps in diiron cluster assembly have been hampered by our inability to load iron onto R2 and deliver the reducing equivalent in a controlled fashion. These difficulties presumably are not encountered in vivo.[10,261] Our current model is that in vivo, the C-terminal tail housing Y356 adopts a defined conformation upon interaction with the protein(s) in the

cell involved in the biosynthesis of the diiron cluster in R2 in much the same way this tail is envisioned to become structured upon interaction with R1 in the nucleotide reduction process. We believe, therefore, that several experiments investigating the formation of the active diiron−Y• cofactor that have established mechanisms of communication between Y122 and W48 in R2 are relevant to the nucleotide reduction process.[11,261,267]

The most thoughtful overview of the mechanism of cluster assembly is provided in recent papers by Bollinger and co-workers.[269,270] The model, based on extensive time-resolved experiments from a number of laboratories and structures of the diferrous and diferric resting states of R2 (Figure 24), is shown in

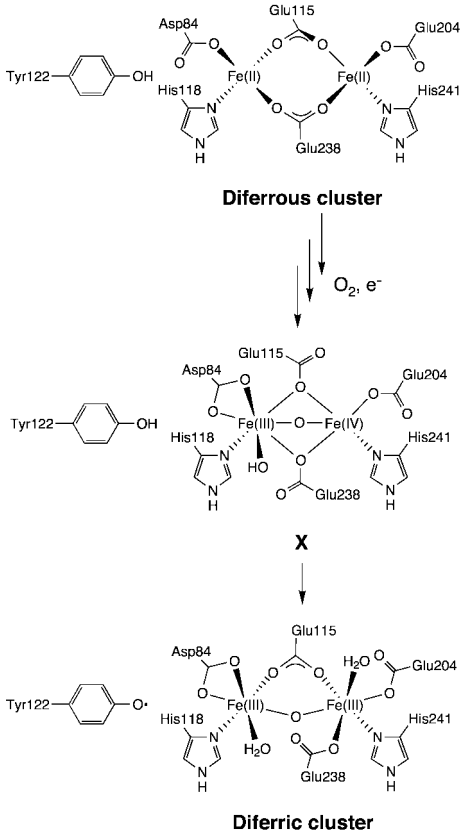

Figure 24. Mechanism of assembly of the diferric−Y• cofactor of R2 based on time-resolved physical methods and X-ray crystallography of diferrous cluster of R2[27] and diferric cluster of R2 with its reduced Y•.[28] The diferrous cluster shows Fe1 and Fe2, and each is four-coordinate. The spectroscopy, however, strongly suggests that one iron is four-coordinate and one is five-coordinate.[338] The structure of X is unknown, but the present formulation is based on ENDOR, ESR, and EXAFS spectroscopies of this intermediate.[10]

Figure 25.[1,10,11] The pertinent experiments, briefly discussed below, establish that a transient W48H•+ (Figure 26) and an Fe^{3+}/Fe^{4+} intermediate (designated X, Figures 24 and 25) are formed during diiron−Y• assembly.[11,267,271−275] When the required reducing equivalent is readily available, intermediate X is thought to oxidize Y122 to the Y•, and the W48H•+ is thought to be rapidly reduced by the external reductant from the surface of the protein (pathway A, Figure 25). However, when the required

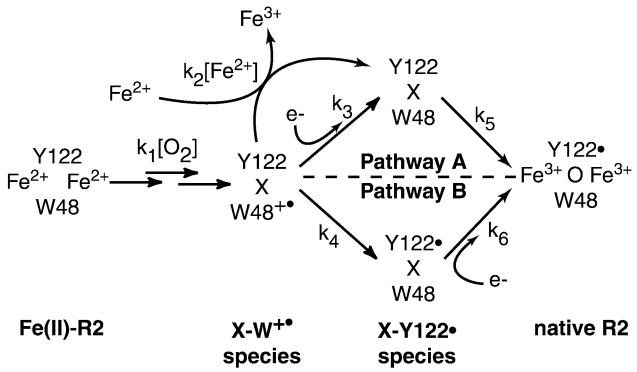

Figure 25. Kinetic mechanism of assembly of the diiron−Y• cluster modified from the studies of Bollinger et al.[11,261,267,271] Pathway A is thought to be the physiologically relevant mechanism in which X generates the diferric−Y• cluster. Pathway B occurs when the extra reducing equivalent is not readily available and the W48H•+ generates the Y•.

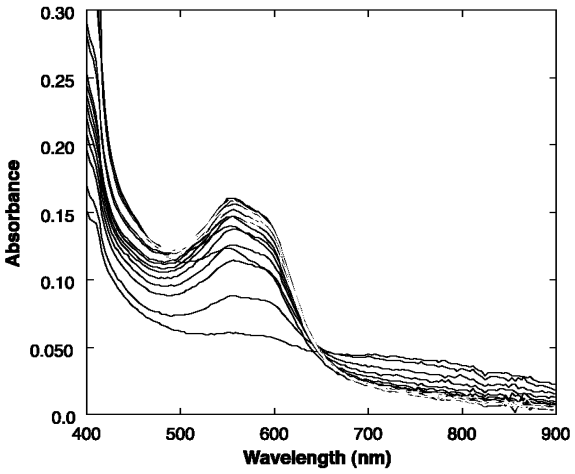

Figure 26. Spectrum of the WH•+ generated in the diiron−Y• cofactor assembly in *E. coli* R2. Note that the assignment of the transient at 560 nm as a W48H•+ is based on studies on model small molecules and peptides and a similar assignment for a WH•+ in cytochrome *c* peroxidase based on ENDOR experiments.

reducing equivalent for cofactor assembly is absent (pathway B, Figure 25), the W48H•+ can oxidize Y122 to Y122• directly, generating an intermediate containing both X and Y•.[261,267,271] The rate constants for Y122 oxidation are 0.85 and 6.2 s^{-1} through pathways A and B, respectively. Reduction of X to the diferric cluster is slow by pathway B (0.6 s^{-1}) and hence not thought to be of physiological importance.[261] However, the redox-active communication between Y122 and W48 is established. This interaction is essential in the back-PCET process in nucleotide reduction.

The potential importance of W48 and of a W48H•+ was first pointed out by Nordlund and Eklund.[28,29] They proposed that the Fe1 → H118 → D237 → W48 pathway in R2 could be mechanistically important in cofactor assembly and nucleotide reduction, based on the structurally analogous and spectroscopically well-characterized Fe(heme) → H → D → W ET pathway in cytochrome *c* peroxidase (Figure 27).[276,277] In peroxidase, incubation of the heme Fe^{3+} with hydrogen peroxide results in formation of an intermediate,

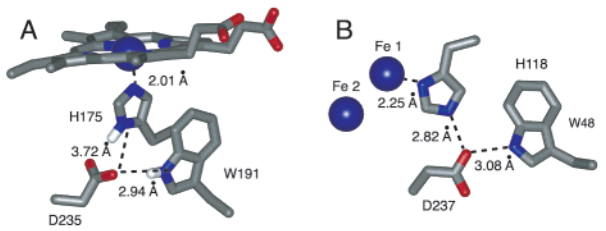

Figure 27. Comparison of the residues involved in assembly of the diiron cluster in R2 (A) relative to the pathway for reduction of the ferryl porphyrin $W^{\bullet+}$ in cytochrome *c* peroxidase (B).[276] Adapted from the proposal originally made by Nordlund and Eklund.[28] Note the W → D → H → Fe commonality.

now known to be a ferryl porphyrin−$WH^{\bullet+}$. The protonated state of the oxidized tryptophan is unusual in that the pK_a of such a species in water is 4.5. The activated species is subsequently reduced by ET from cytochrome *c*, generating the ferryl porphyrin. The ferryl porphyrin−$WH^{\bullet+}$ intermediate was detected by stopped-flow visible spectroscopy and by EPR and ENDOR spectroscopies. Its characterization by ENDOR spectroscopy ultimately led to its identification.[277] EPR studies have established the presence of the $W48H^{\bullet+}$ in cofactor assembly in R2.[261,270] The protonation state, however, is inferred from the absorption spectrum and not from ENDOR analysis. In the case of cytochrome *c* peroxidase, the kinetic competence of the $W191H^{\bullet+}$ has been established. In the R2 cluster, the presence of intermediate X (Figures 24 and 25) precludes a direct comparison of the re-oxidation of Y122 in this process with its re-oxidation in the back-PCET step of nucleotide reduction. Thus, the chemical competence of the $W48H^{\bullet+}$ in the reduction process is established, but the kinetic competence cannot be established from these experiments.

An incompletely understood mechanistic issue in cluster assembly is the mechanism by which intermediate X oxidizes Y122 (Figures 24 and 25). A number of options are possible and depend on the location of Fe^{3+} and Fe^{4+} in intermediate X (Figure 24). If Fe^{3+} is adjacent to Y122, then the most reasonable mechanism for its oxidation involves ET to generate the diferric cluster, followed by rapid deprotonation (pK_a of −2) of the $YH^{\bullet+}$. If the Fe^{4+} is adjacent to Y122, then hydrogen atom abstraction is possible. A commonality of the mechanism of cluster assembly and radical initiation for nucleotide reduction would favor a mechanism involving ET followed by H^+ transfer, because in the radical initiation of nucleotide reduction no high-valent iron intermediates are likely involved. One possible structure for intermediate X in cluster assembly places an Fe^{3+}-bound disordered hydroxide adjacent to Y122. This hydroxide could become protonated during the oxidation of Y122 to the $Y^{\bullet}$ and generate the water-bound state of the resting diferric cluster (Figure 24). The identity of Fe1 as an Fe^{3+} in intermediate X was first proposed by Bollinger from Mössbauer titration experiments (Fe2 and Fe1 bind with different affinities to R2[278,279]) and a structure of mouse R2 crystallized at pH 4.7, in which a single iron was bound at the Fe2 position.[260,273,280] Additional studies are required to demonstrate, however, under neutral conditions, that the tightly bound iron is still Fe2. Regardless of the detailed mechanism of Y122 oxidation, kinetic and spectroscopic experiments in conjunction with the structure demonstrate that W48 of R2 can oxidize Y122.

The radical initiation in the class I RNRs is unique relative to most biological ET processes, not only because of the distance but also because the reaction is reversible, with a stable hole residing on Y122. As outlined below, in contrast to the simplified model of radical initiation by hydrogen atom transfers, multiple mechanisms involving superexchange and hole hopping, similar to the multiple mechanisms proposed for charge migration in DNA, are probably required for the communication between the two subunits of RNR.[243−246,281]

D. Testing Models for Radical Initiation: Support for Long-Distance Radical Transfer

As noted above, there is no structure of the R1−R2 complex. Therefore, the possibility needs to be considered that a large conformational change can accompany subunit, effector, and substrate interactions, reducing the distance required for radical initiation. A conformational change placing Y122 of R2 closer to C439 of R1 could nullify the requirement for intermediates in the ET process. The most compelling arguments against large conformational reorganization come from a comparison of the structures of the three classes of RNRs (Figure 20)[235] and the many structures of R2. Within R1, a PCET pathway covering 7 Å and involving Y731 → Y730 → C439 is a very reasonable model (Figure 22). The distance relationship within R2 between Y122, the iron cluster, and W48 is established not only by structure but also by analysis of the exchange-coupled EPR spectra of intermediates observed in cofactor assembly.[282] Distances required to simulate the exchange-coupled intermediates agree with the X-ray data that suggest that the edge of W48 can be as close as 7.6 Å to the Y122.[282] The missing connection between R1 and R2 is the C-terminal tail of R2 that includes the conserved Y356 (Figures 21 and 22) with a distance of 25 Å. Placement of Y356 midway between W48 and Y731, as noted above, allows for rapid ET.

Direct evidence for radical transfer from the $Y^{\bullet}$ on R2 to the active site of R1 has been provided by studies with two mechanism-based inhibitors of RNR: 2′-azido-2′-deoxynucleoside-5′-diphosphate (N_3NDP) and 2′-vinylfluorocytidine-5′-diphosphate (VFCDP) (Figure 28).[283,284] In the case of both of these mechanism-based inhibitors,[285] their incubation with R1 and R2 leads to reduction of the $Y122^{\bullet}$, RNR inactivation, and formation of a new radical located in the active site of R1.[286−288] In the case of the N_3NDP, the new radical is nitrogen-centered ($N^{\bullet}$) and is derived from the azide moiety of N_3UDP (N_3CDP, N_3ADP) after loss of nitrogen gas. The $N^{\bullet}$ is covalently attached to C225 located in the active site of R1 (Figure 28A).[289,290] In the case of N_3UDP, deuteration of the 3′-hydrogen of the nucleotide analog exhibits an isotope effect on rate of the $Y^{\bullet}$ loss. Thus, a direct coupling of radical initiation and chemistry on the nucleotide is established. In the case of VFCDP, $Y^{\bullet}$ loss occurs concomitant with formation of an allylic

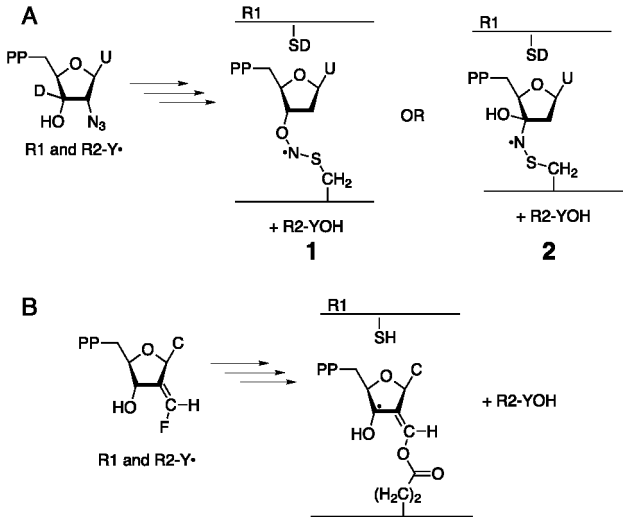

Figure 28. Inactivation of *E. coli* RNR by mechanism-based inhibitors. (A) For inhibitor, 2′-azido-2′-deoxyuridine-5′-diphosphate, the Y• on R2 disappears concomitant with formation of a nitrogen-centered radical (N•) covalently bound to C225 and nucleotide on R1. ESEEM and EPR spectroscopic methods suggest that the structure of the N• is either 1 or 2.[283] (B) For inhibitor, 2′-fluoromethylene-2′-deoxycytidine 5′-diphosphate, the Y• on R2 disappears concomitant with formation of a new allylic radical covalently attached to E441 in the active site of R1.[339]

nucleotide radical, covalently attached to E441 in the active site of R1 (Figure 28B).[284] These studies demonstrate that long-range ET does occur. Pulsed electron−electron double-resonance spectroscopy, a method that can measure weak dipolar interactions over 15−50 Å, or similar methods are required to establish the actual distance.

E. Is ET or PCET Conformationally Gated?

As noted in the Introduction, RNRs control the specificity and activity of the reduction of all nucleotides in vivo and thus are regulated in a complex and incompletely understood fashion.[3] One mechanism of regulation involves dNTPs and ATP binding to sites in R1 removed from the active site.[291,292] At least two and possibly three allosteric binding sites have been implicated.[24] The importance of conformational gating, binding of ligands that lead to conformational changes that trigger ET, is now documented in a number of systems and needs to be addressed in RNR.[70] Specifically, radical initiation over 35 Å should occur only when the substrate and/or an allosteric effector are positioned on the R1 subunit ready for reduction. To study ET, one must understand which step or steps are rate-limiting in the class I RNRs. If ET were not rate-limiting, then one would need to perturb the system to make ET rate-limiting so that its kinetics could be studied. Despite extensive studies on the ET process in class I RNRs,[243−246] the rate-determining step has not been established. The similarities in the structures and chemistry of the class I and II RNRs suggest that some insight into rate-limiting steps might be obtained by a comparison of the two systems. However, bear in mind that, in the class II RNR, the AdoCbl is 7 Å from the cysteine to be oxidized, whereas in the class I RNR, the distance is proposed to be >35 Å.

The class II RNR from *L. leichmannii* is a monomer. Mechanistic studies on this enzyme are thus devoid of problems associated with understanding subunit interactions. The *L. leichmannii* RNR uses nucleoside triphosphate substrates and has a turnover number of 2 s^{-1}.[293] The mechanism of this RNR is the best characterized to date, based on a variety of pre-steady-state experiments. The radical initiation process involves carbon−cobalt bond homolysis, concomitant with S• formation, and occurs with k_{app} = 250 s^{-1} (Figure 29).[294] The radical initiation step

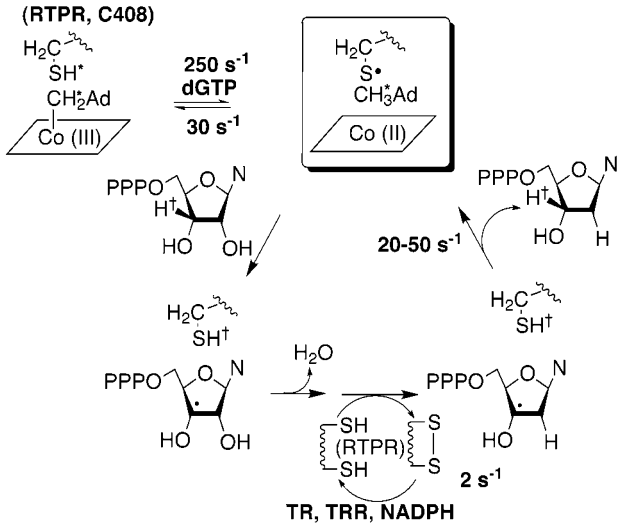

Figure 29. Overview of the kinetic mechanism of AdoCbl-dependent RNR based on pre-steady-state kinetics experiments.[6]

involves direct hydrogen atom abstraction.[294−297] The existence of the exchange-coupled thiyl radical and cob(II)alamin is supported by EPR analysis and by stopped-flow experiments carried out with [5′-^{2}H]-AdoCbl in D_2O. In the latter case, the amount of the exchange-coupled radical intermediate (S• and cob(II)alamin) is increased by a factor of 2 relative to similar experiments carried out with AdoCbl in H_2O. The unusual fractionation factor (0.5) associated with SH groups strongly supports the involvement of a cysteinyl radical in this intermediate. The ^{2}H would rather reside on the carbon of 5′-deoxyadenosine than on the S of cysteine.[298] The rate constant for dNTP formation in the first turnover, measured by rapid chemical quench experiments, is 20 s^{-1} for CTP as substrate and 50 s^{-1} for ATP as substrate.[294] The apparent rate constant during the first turnover for re-formation of the carbon−cobalt bond is 30 s^{-1} with ATP as substrate. Studies have further revealed that the carbon−cobalt bond is re-formed on every turnover and that, in fact, a single AdoCbl can serve as cofactor to more than one enzyme. Unlike most B12-requiring enzymes, AdoCbl binding to RNR is weak. The rate-determining step of this class II RNR is either re-reduction of the disulfide, a conformation change, or a conformational change accompanying re-reduction of the disulfide. An additional observation pertinent to conformational gating by allosteric effectors is that binding of dGTP to the enzyme in the absence of its substrate ATP can promotes homolysis of the carbon−cobalt bond (k_{app} = 50 s^{-1}). Substrate binding enhances the rate by at least 5-fold.

The class I RNR from *E. coli* has an active-site architecture remarkably similar to that of the class II RNR, with a similar catalytic apparatus.[235,237] Furthermore, the turnover number of class I RNRs, 2−10 s^{-1} depending on the substrate/effector composition, is very similar to the turnover number of the *Lactobacillus* RNR. A mechanistic model for the *E. coli* RNR is shown in Figure 30, based on pre-steady-state experiments. These experiments on the class I RNR are considerably more complex than those on the class II RNR due to the required weak interaction between R1 and R2 (K_d = 0.1−0.2 μM).[249] The results from pre-steady-state experiments have limited the mechanistic options.[299]

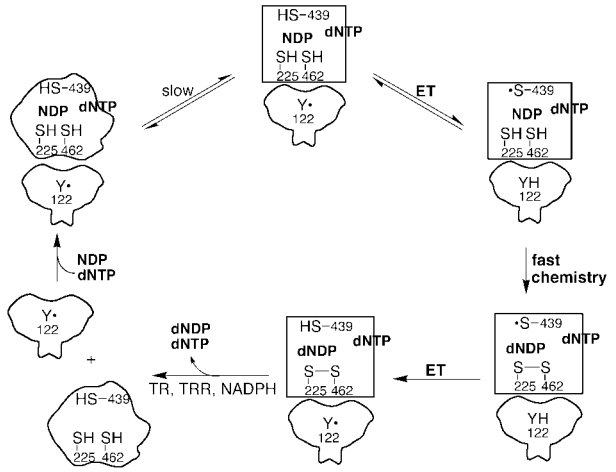

Figure 30. Postulated kinetic mechanism of the class I RNR based on pre-steady-state kinetics experiments.[299] For simplicity, R1 and R2, each homodimers, are indicated as a single protein. The conformational change for R1 is indicated by conversion of circle-like shape to a square. The numbering of residues is based on *E. coli* R1−R2.

A key to unraveling the rate-determining step or steps in the *E. coli* class I RNR is the observation from pre-steady-state studies that, regardless of the experimental conditions, the Y•, which has a sharp absorption feature at 410 nm with an ϵ = 1800 M^{-1} cm^{-1}, is not lost under any conditions of turnover in which the substrate, effector, or pH is varied.[299,300] The mechanistic model requires that the Y• is reduced and re-oxidized. The simplest way to rationalize these observations, given that the Y• is essential for catalysis (Figure 30), is that the rate-determining step is a physical step occurring prior to the radical initiation step. The chemistry of nucleotide reduction involving Y• reduction and re-oxidation must occur rapidly relative to the physical step(s). Thus, in contrast to the class II RNR, the radical initiation step is completely masked or gated by conformational change(s) or proton-gated conformational change(s) that triggers the ET process. This conformational change could involve binding of substrate, allosteric effectors, or both.

Additional evidence to support this model comes from a comparison of the rate of dNDP formation in the pre-steady state (protein concentrations of 3 μM, physiological conditions), the rate of disulfide formation in the pre-steady state, and the rate of dNDP formation in the steady state (0.1 μM, normal assay conditions).[299,301] The k_{obs} in all cases is the same under the same conditions and varies between 2 and 10 s^{-1}, depending on the substrate and effector. (In the absence of effector, the turnover number is 2 s^{-1}.) Our kinetic model of this reaction requires that Y• reduction, chemistry, and YH re-oxidation occur with rate constants of $>10^3$, >200, and $>10^3$ s^{-1}, respectively. If our kinetic model is correct, it suggests that reduction in the "rate constant" for chemistry by a factor of 5 (from 500 to 100 s^{-1}) should allow disappearance and reappearance of the Y• to be detected. One method to perturb the rate of chemistry is to use [3′-^{2}H]-nucleoside diphosphates (Figure 2A). In the steady state, with [3′-^{2}H]-UDP and [3′-^{2}H]-ADP as substrates, only V/K isotope effects (≤3) have been observed. In the pre-steady state, using [3′-^{2}H]-UDP, no change in the Y• signature was detected (though the rates of dUDP formation have not yet been measured). Only with mechanism-based inhibitors, which partition irreversibly from the normal catalytic pathway, can Y• loss be detected and correlated with 3′ carbon−hydrogen bond cleavage of the nucleotide analog.[285] The model that best accommodates the steady-state and pre-steady-state results is that the rate-limiting step in the *E. coli* RNR is a slow conformational change preceding PCET. This conclusion has important implications in the design of experiments to study the radical initiation process.

For the sake of completeness, examination of nucleotide reduction under physiological concentrations (1−3 μM range) of R1, R2, and thioredoxin (Tr) requires multiple rate-limiting steps in the reduction process. Re-reduction of the disulfide of R1, which probably requires dissociation of R2 from R1 and association of R1 with reduced thioredoxin, can also be partially rate-limiting, as in the case of the class II RNR.[299] However, even if re-reduction becomes partially rate-limiting, the rate of ET is still governed by the conformational switch prior to the chemistry.

Recent studies modeled after those carried out with the class II RNR suggest that the chain length of the radical reaction for the class I RNR is 1, that is, the Y• is reduced and re-oxidized on each turnover.[299] The studies involved assaying R1 in the presence of excess R2 and assaying R2 in the presence of excess R1. The turnover number in the latter case is 1.4−2 times higher than the turnover number in the former case. The simplest interpretation of these data is that R2 can turn over more than one R1 and that the Y• is reduced and oxidized during every turnover. These results suggest that R2 may interact transiently with R1 and perhaps provide a reasonable explanation for the inability to obtain a structure of the R1−R2 complex.

F. Site-Directed Mutagenesis Studies in R1 and R2

The mechanism of radical initiation has been studied in the laboratories of Sjöberg, Graslund, and Thelander.[243−246] The major tool has been site-directed mutagenesis. More recent in vivo complementation studies are consistent with the mutagenesis results.[302] Mutants of every residue in the putative pathway (Figure 22) have been generated (Table 3).

Table 3. Activity of Mutants on the Putative PCET Pathway in *E. coli* and Mouse R2

protein	iron/ R2	Y•s/R2	SA (nmol/ min mg)	N• formation[c] (s^{-1})	Y• loss[c] (s^{-1})
E coli[a]					
wt-R2	2.9	0.8	5000	0.68	0.64
D237E	2.7	1.0	340 (7%)	0.084	0.044
D237N	4.4	0.6 (unstable)	13 (0.3%)		
wt-R1			1650		
Y730F			26 (1.6%)		no loss
Y731F			26 (1.6%)		no loss
mouse[b]					
wt-R2	2.2	0.5−0.8	337		
W103F[d]			3.0 (0.9%)[e]		
W103Y[d]			1.9 (0.55%)[e]		
D266A[f]			0.5 (0.15%)[e]		
wt-R1			228		
Y370F[g]			0.7 (0.31%)[h]		
Y370W[g]			3.7 (1.6%)[h]		

[a] References 243, 244. [b] References 245, 246. [c] wt or mutant RNRs were incubated with N_3UDP, and N• formation and Y• loss were monitored (Figure 28). [d] W48 in *E. coli* numbering. [e] Calculated from Table 3 of ref 245 using the lowest protein concentration. [f] D237 in *E coli* numbering. [g] Y356 in *E. coli* numbering. [h] Calculated from Table 1 of ref 246 using the lowest protein concentration.

A number of these mutants (Y730F, Y731F R1, and D237E R2) has also been examined crystallographically. A technical problem associated with mutant protein production has complicated the interpretation of the results from these studies. Since RNR is an essential protein, expression of either the mutant R1s or R2s has thus far always been carried out in a system that contains contaminating wt-R1 and R2 from the expression host. The amount of this wt protein, in our hands, can vary from 1.5 to 8%, depending on the level of overexpression of the mutant protein. In addition, since both R1 and R2 are dimers, heterodimers between mutant and wt proteins are always present. Thus, with several exceptions, which will be discussed later, when mutant proteins are described as being inactive, they possess activity from 1 to 2% of that of the wt protein, presumably due to wt contamination. A good lower limit of detection of activity, therefore, in most mutants studied has not been set. An additional problem associated with the mutagenesis of the aromatic amino acids in the PCET pathway (Figure 22) is that there are no natural amino acids that can maintain the putative H-bonding network. This network may be important in a hydrogen-atom-transfer mechanism, in conformational gating in the PCET pathway, or in modulation of intermediate amino acid redox potentials. With these caveats, studies on these mutants have demonstrated the importance of these residues in maintaining RNR activity.

Particularly informative are the Y730 and Y731-R1 mutants. Sjöberg has replaced these Ys with F's and has crystallized the mutant proteins.[244] Difference density maps with the wt-R1 structure have shown that that F substitutions do not perturb the structure. The "absence" of activity for Y730F and Y731F R1 mutants (Table 3) has been interpreted to support the importance of hydrogen atom transfer in the radical initiation. Using partially deuterated-R1, EPR methods were undertaken to look for generation of a transient 2,3,5,6-deutero-Y• on R1 by reduction of Y122• on R2. The deuteration would alter the EPR hyperfine interactions of any Y•s generated in R1 and would make them distinct from Y122• on R2. No changes in the EPR spectrum of the Y122• were observed, supporting their conclusion that the Y-to-F mutants are inactive and that ET was not triggered. The conclusion from these mutagenesis and structural studies, in conjunction with the absolute conservation of these residues (>40 sequences), is that Y730 and Y731 play a key role in radical initiation.

It should be pointed out that recent theoretical studies[303] measuring self-exchange between phenols and phenol radicals have suggested that this process involves PCET and not hydrogen atom transfer. PCET implies that the proton and the electron are transferred to different orbitals. The favored transition state for the self-exchange reaction is very different, however, from the structure of the Y731−Y730−C439 triad in R1. The mechanistic differentiation between a concerted and stepwise process (PCET and hydrogen atom transfer) is challenging and may not be resolvable in such a complex protein as RNR.

The structural comparison of the three classes of RNRs further implicates a hydrogen atom abstraction mechanism for S• formation within R1 involving Y730 and suggests one solution to the thermodynamically unfavorable oxidation of a cysteine (SH) by a Y• (Table 2). One might have expected with Y731F-R1 that if the pathway between Y122 and C439 involved only ET, tunneling between the hole in Y356-R2 and Y730 in R1 (16 Å) could occur at a rate fast enough to account for enzyme turnover. The generated Y730• could then abstract a hydrogen atom from C439 and initiate nucleotide reduction. Alternatively, if radical generation within this triad occurs through a hydrogen atom abstraction mechanism, then Y730F-R1 would be expected to be completely inactive, since removal of a hydrogen atom from C439 by Y731• is physically impossible and Y731• would be unable to oxidize C439 via an ET process. Thus, lack of dNDP formation in Y731F and Y730F R1 mutants supports the H-atom-transfer model between Y731, Y730, and C439.

Two key issues in this model for radical initiation between Y731 and C439 are essential to understand. The first is thermodynamic: based on reduction potentials measured in model systems (Table 2), the Y122•-mediated oxidation of C439 is uphill and likely coupled to a hydrogen atom removal. The reduction potentials most likely will be modulated by the locations of protons within the Y371−Y730−C439 triad and influenced by substrate and effector. Second, many of the thermodynamically "uphill" steps in the nucleotide reduction process can be driven to the right by coupling of an unfavorable reaction to a rapid irreversible step (Figure 31). According to the model chemistry on which our mechanism is based, the rapid irreversible step in nucleotide reduction is proposed to be loss of water on cleavage of the 2′-carbon−hydroxyl bond.[6] Thus, the protein's ability to alter reduction potentials by proton gating and the ability of 3′-radical nucleotide to rapidly lose water are two essential features of the nucleotide reduction process.

Figure 31. Nucleotide reduction on R1 is proposed to involve reversible PCET between Y122• on R2 and C439 on R1. Y122• is a stable radical ($t_{1/2}$ = 4 days). The reduction potentials for formation of the amino acid radical intermediates in this process are unknown. The scheme is based on reduction potentials in model systems reported in Table 2. The hypothesis is that the radical initiation can be tuned by the pH dependence of the reduction potentials. Generation of the C439• on R1 is proposed to initiate 3′-hydrogen atom abstraction from the NDP substrate, which may also be uphill. However, the hallmark of RNR chemistry is coupling of an uphill process to a rapid irreversible step—loss of water from the 2′ position of the nucleotide. The Y122• is then regenerated on each turnover.

In contrast to the results with mutants in the R1 part of the ET pathway, two mutants of the PCET pathway in R2 are active in dNDP formation, one from *E. coli* and one from mouse.[243,246] The best characterized is *E. coli* D237E-R2.[243] A structure of this mutant has been solved and is very similar to the wt enzyme (Figures 22 and 32). This mutant R2

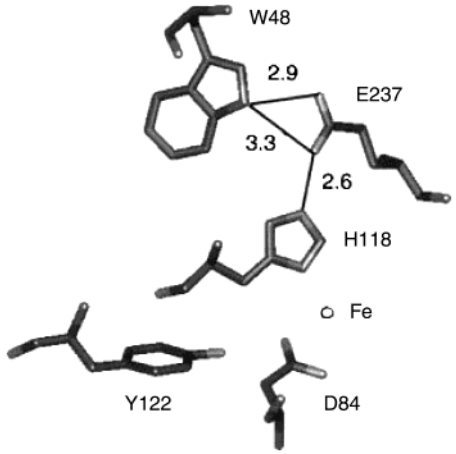

Figure 32. Structure of D237E-R2, the best-characterized mutant in the *E. coli* putative ET pathway that still appears to make deoxynucleotides. (Adapted from ref 243.)

can generate dNDP at 7% the rate of the wt-R2. To ensure that the activity was associated with D237E-R2 and not contaminating wt-R2, the enzyme was incubated with N_3CDP, which is known to destroy the Y• and generate a N-centered radical in the active site of R1 (Figure 28). Loss of the Y• and formation of N• occurred with this mutant. However, no spin quantitation of either radical was reported. While it seems unlikely that contaminating wt-R2 could be 7% of the R2 isolated, the very slow rate constants observed for Y• loss, and hence the low radical concentrations observed, make this a possibility. Taken at face value, these data support the importance of an acidic residue in position 237 of R2 that can become transiently protonated.

In our opinion, the most informative mechanistic results in this set of experiments (D237X-R2s) were those from the studies on the D237N-R2 mutant. The activity of this mutant was reported to be 0.3% that of the wt enzyme, presumably due to contaminating wt-R2. Thus, despite maintaining the H-bonding network, no nucleotide reduction above background was observed. We postulate that the position of the proton between W48 and D237 plays a key role in tuning the oxidation potential of W48. One possible scenario is that a proton transfer between $W48H^{\bullet+}$ and D237 is coupled to the ET between Y122• and W48. In this model, the Y122 is reduced directly by tunneling of an electron from W48. The source of proton to generate the Y122 phenol could be the water bound to Fe1 (Figure 24). The oxidation potential of the W48 could be modulated by transfer of a proton to D237, leaving a W48•. This radical could oxidize Y356 (Figure 22) concomitant (or sequentially) with W48• protonation. This model predicts that if these steps are rate-determining, then a solvent isotope effect would be observed on this reaction. The D237N mutant would be unable to facilitate this oxidation, and hence the mutant might be expected to be inactive. Unfortunately, D237N-R2 did not crystallize, and hence an unanticipated structure could also explain these results. An altered conformation was the hypothesis favored by Ekberg et al. for the inactivity of this mutant.[243]

Similar studies using site-directed mutants have been carried out to characterize S• formation in the mouse RNR.[246] The diiron−Y• is much less stable in the mouse R2 (called M2) than in the bacterial RNRs, and the R2 is inhomogeneous due to proteolysis. Variable radical and iron content of R2 and loss of both over short incubation times makes interpretation of the mutant studies difficult, as the turnover numbers are very low relative to those of the *E. coli* RNR. Mutants of all the amino acids in the putative ET pathway have been generated in mouse R1 and R2 as well. They are also "inactive" (see Table 3), except for Y370W (*E. coli* Y356 equivalent), which loses its radical and exhibits 1.6 % wt activity. However, a second mutant, D266A (*E. coli* E237 equivalent), is claimed to be inactive, even though dCDP was apparently detected. This claim is difficult to interpret. The mouse protein is expressed in *E. coli*, and since the *E. coli* subunits cannot complement the mouse subunits, the activity cannot be associated with *E. coli* R2 contamination. A much lower limit of detection for the mouse RNR mutants is theoretically accessible, in comparison with the *E. coli* system. However, as noted above, the cofactor is unstable. One interpretation of the Y370W R2 results is that the ET is triggered but partitions between turnover and loss of the radical from the normal pathway due to the mutation. Efforts to detect radical intermediates were unsuccessful. The mutagenesis experiments on *E. coli* and mouse RNRs reinforce the importance of these residues that are absolutely conserved in the nucleotide reduction process.

G. New Methods To Study Radical Initiation in RNR

Whereas these mutagenesis studies have established that the proteins are "inactive", they have not

Table 4. C-Terminal Tails of R2 Are Unique and Peptides Are Potent Inhibitors of R1 Interaction with R2

protein	C-terminal peptide	
E. coli R2[a]	EVEVSSYLVGQIDSEVDTDDLSNFQL	K_i (μM)
	[1−37]	18.3
	[1−30]	21.5
	[1−20]	20.0
	[1−19]	40.0
	[1−8]	370
	[12−20]	4000
mouse R2[b]	EKRVGEYQRMGVMSNSTENSFTLDADF	IC_{50} (μM)
	Ac-[1−9]	10.0
	Ac-[1−6]	>400
herpes viral R2[c]	ECRSTSECRSTSYAGAVVNDL	IC50 (μM)
	[1−15]	42
	[1−12]	29
	[1−9]	36−60
	[1−7]	283

[a] Reference 249. [b] Reference 248. [c] References 335, 336.

shown the existence of amino acid radical intermediates along the proposed pathway. Therefore, we are taking three alternative approaches to examine the mechanism of radical initiation in RNR. Two of the approaches make use of unnatural amino acids, and the third approach uses a peptide in place of the C-terminus of R2 and light to trigger PCET on the submicrosecond time scale. Each method will be discussed in turn.

1. Semisynthesis of R2 Using Intein Technology and Unnatural Amino Acids

The first method to replace natural amino acids with unnatural amino acids involves semisynthesis of the R2 subunit. This method has targeted Y356, important in radical initiation by sequence conservation and mutagenesis studies.[268] Y356 is located in the disordered C-terminus of *E. coli* R2 (Figures 21 and 22), suggesting that ligation of a peptide containing this residue would be possible without protein denaturation.[249,250,304] Extensive studies on the importance of the C-terminal tails of viral,[247,252] *E. coli*,[249] and mouse R2s[248,305] have revealed that each tail of the homodimer binds independently to R1 and is largely responsible for the interaction of R2 with R1. Peptides (Table 4), ranging in size from 9 to 37 amino acids, with sequences identical to the C-terminus of R2 in each specific organism are competitive inhibitors of R2 binding to the corresponding R1. We have recently succeeded in synthesizing R2 using residues 1−353, made by recombinant DNA technology, and residues 354−375, made synthetically with a peptide synthesizer.[306] Using this methodology, Y356 can be replaced by any unnatural amino acid to investigate the role of this residue in the PCET process or its site of interaction with R1 and R2 through photoaffinity labeling. The semisynthesis uses intein chemistry (Figure 33), developed by New England Biolabs.[307] The method is based on self-splicing proteins observed in a number of biological systems and produces R2 (1−353) with an intein and a chitin-binding domain fused at the C-terminus of the construct. The chitin-binding domain facilitates its purification. The purified construct is then

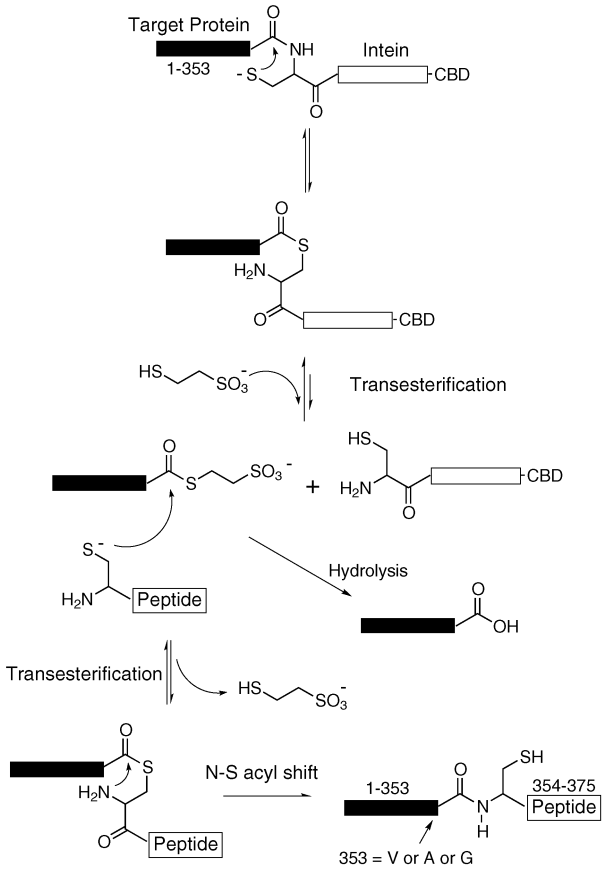

Figure 33. Strategy for the preparation of semisynthetic R2 generated using intein technology.

treated with a small organic thiol, and the intein and chitin-binding domain are removed. The R2 (1−353)-thioester is now reacted with an N-terminal cysteine-containing peptide (354−375) made synthetically. Thiotransesterification and an acyl shift from the thioester to the amine result in full-length R2. The optimum site of new peptide bond formation was determined by a variety of site-directed mutagenesis experiments and R2 sequence alignments.

The unnatural amino acids chosen to replace Y356 are shown in Figure 34. The 3-nitrotyrosinate (pK_a

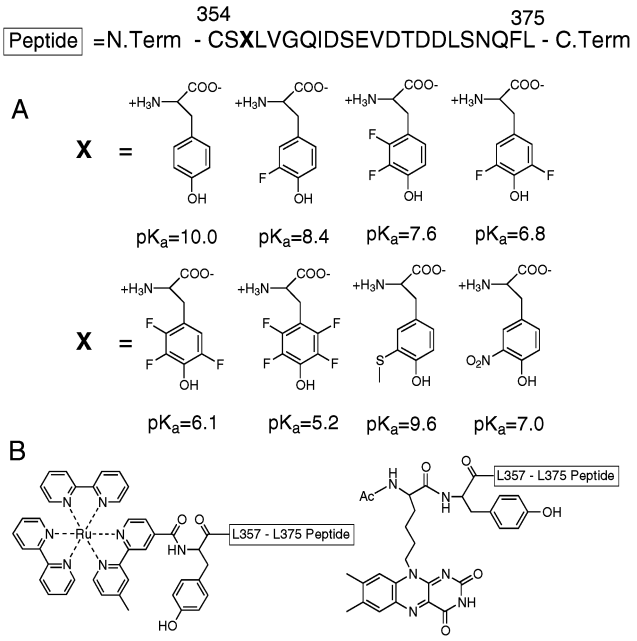

Figure 34. (A) Peptide used for making R2 prepared semisynthetically (Figure 33). X is a variety of tyrosine analogs. The pK_as of each of these tyrosines is also shown. (B) Peptide with modified tyrosine derivatives (a tethered $Ru(bpy)_3^{2+}$ and a flavin used to generate a transient Y•, as described in the text).

= 7.2) was chosen as it is more difficult to oxidize than tyrosinate by 0.3 V,[308,309] and it maintains the hydrogen-bonding network postulated to gate ET and/or modulate the redox potential. The hypothesis is that the 3-nitrotyrosine would block the radical initiation pathway, allowing equilibration of the hole between Y122• and W48 to Y122 and $W48H^{\bullet+}$ or W48•, if the proton is transferred to D237 (Figure 22). A transient visible absorption feature or EPR feature associated with the $W48H^{\bullet+}$ (Figure 26) or W48• could, therefore, be detected, depending on the K_{eq}. Tyrosine analogs with redox potentials lower than that of tyrosinate, such as 3-thiomethyltyrosine, were chosen as radical traps in much the same way as 8-oxoguanine[310] or 3-methylindole[156] was used in DNA hole migration studies (see section III.D.3). Radical species could potentially be detected by transient visible or EPR spectroscopy.[5] A variety of fluorinated tyrosines have also been prepared.[311] The pK_as of these compounds vary between 5.2 and 10, and the reduction potentials for the 3-F- and 2,3-diF-tyrosine are not substantially different from that of tyrosine at pH 7. Furthermore, the reduction potentials can be modulated by pH within the physiological range. Studies with these analogs could define the importance of pK_a, reduction potential, and proton-gated conformational change in the radical initiation if ET becomes the rate-determining step. These fluorinated tyrosines[312] will provide a direct test of the hydrogen-atom-transfer mechanism.[243−245]

While we can measure the pK_as of these tyrosine derivatives (Figure 34) and their reduction potentials[255] in solution, both of these parameters can be perturbed by the protein environment. The magnitude of the perturbation is important for the correct interpretation of the studies with the mutant proteins. Limited information is available about the reduction potentials of amino acid radicals known to be involved in catalysis.[5] The work of Tommos, Dutton, and their colleagues in protein maquettes[255] and the Gray laboratory using azurin as a model system[313] will provide this essential information.

There are several shortcomings to the use of unnatural amino acids at Y356. One is that the location of Y356 relative to its two redox-active partners (W48-R2 and Y731-R1) has not been established. In the absence of structure, however, photoaffinity labels in position 356 in the C-terminal peptide or semisynthetic R2 will provide the desired information. A second shortcoming is that this method is only readily amenable to proteins in which the residues at the C-terminus or N-terminus are of interest, unless the protein can be renatured. The benefits of this method are that one can minimally perturb a system in a chemically informative fashion. One can also obtain the large amounts of protein required for analysis by biophysical methods.

2. Use of Unnatural Amino Acids in Vivo with Orthologous tRNA/tRNA Synthetase Pairs

A second approach to generate mutant RNRs with unnatural amino acids is potentially much more versatile. Recently, Schultz and his colleagues developed a method to generate an orthologous pair of macromolecules (tRNA/tRNA synthetase) that specifically recognize a unique unnatural amino acid.[314−316] The genes for this orthologous pair of molecules are placed in *E. coli* that is then grown on medium containing the unnatural amino acid that is recognized by the tRNA synthetase. The tRNA synthetase then charges the unique tRNA with this unnatural amino acid, and the *E. coli* translation apparatus does the rest. This method requires that the amino acid is readily taken up into the cell and that the ribosome machinery and proteins such as EF-Tu in *E. coli* are capable of interacting with the charged tRNA. The success of this method has recently been reported using the methyl ether of tyrosine, 4-azidophenylalanine, and a benzophenone amino acid.[316,317] This method will allow us to examine other tyrosines in the PCET pathway, specifically Y730 and Y731 in R1. The shortcomings of the method are that each amino acid substitution requires evolution of a new set of genes for the orthologous tRNA/tRNA synthetase pair. Furthermore, the bacteria must be able to take up the amino acid into the cell, and the amino acid must not be toxic. The benefits are that the cell does the work to generate the protein with a single targeted replacement with an unnatural amino acid. In contrast to the in vitro experiments using a similar approach that are often limited by the quantity of protein obtained, much larger amounts of protein can be obtained when the protein of interest can be expressed in vivo.

3. Generation of Amino Acid Radicals on Fast Time Scales

The third method to investigate radical initiation involves making a small-molecule radical initiator for the class I RNR which functions in the same way that

AdoCbl functions in the class II RNR. This method takes advantage of the fact that peptides to the C-terminus of R2 (Figure 34, Table 4) are competitive inhibitors of R2 and R1 interaction, with K_is of 10−20 μM.[249] As noted above, two peptides can bind to R1 in a non-cooperative fashion. Peptides such as those described in Figure 34B have been synthesized by attaching a flavin, benzophenone, or Ru and, more recently, Re compounds to the N-terminus of the peptide adjacent to Y356. These peptides, in the presence of light, should be capable of generating a transient Y356$^{\bullet}$. The lifetime of the radical generator differs with the attachment. If the peptide is appropriately bound to R1, then in the presence of substrate and allosteric effector, one might be able to start the ET pathway at Y356, bypassing the rest of R2. The power of this approach is apparent from the photoactivation of photolyase described in section IV.B.1.

VI. Summary: ET in Biological Systems and the Uniqueness of RNRs

Most ET reactions in biology occur over distances of 10−15 Å by tunneling mechanisms. ET analyzed in small proteins, in which a redox cofactor is appended at a specific position of known distance from a second redox cofactor and characterized structurally, has allowed determination of generic λ and β values.[81,101,104,318] These model systems are unencumbered by conformational changes that often mask the redox reactions associated with more complex proteins. Also, minimal flexibility in varying the driving force of the reaction in these complex proteins to study ET makes determination of λ difficult. In numerous systems involved in ET, the X-ray structures have revealed the presence of oxidizable aromatic amino acids between the redox-active cofactors, suggesting that aromatic residues might play a role in the ET process. Mutation of these aromatic residues in systems where ET is rate-limiting, however, has had minimal effects (2- to 4-fold) on the observed rate constants.[319−322] Intramolecular transfer in azurins, in which a tryptophan was inserted into a putative ET pathway between the copper and a disulfide, where ET was induced by pulse radiolysis, resulted in an increase in the rate constant for ET of only 7-fold.[323] Thus, the general consensus has been that aromatic amino acid radicals are not intermediates in these "short"-distance ET processes. The protein environment clearly affects ET, as reflected in the extensive studies from the Gray and Winkler group. The role of aromatic amino acids is presently the focus of much attention and may provide an explanation for the discrepancy between calculated and observed rates of ET in a number of systems.[313] Model systems in which high-resolution structures are available and amino acid side chains and their environments can be varied in a systematic fashion are essential to developing a realistic model for RNR. New methods to trigger the "instantaneous" generation of Y and W radicals by light-mediated processes is also important in defining optical and EPR signatures of these species as a function of environment.[324,325]

RNR stands out as a unique system in which very long-range hole migration appears to be required for activity. While the long distance between Y122$^{\bullet}$ on R2 and the putative S$^{\bullet}$ on R1 must be verified by experimental approaches, the available data support this long-range hole migration, and thus amino acid radicals are required to play a role as intermediates in a discrete pathway. In no system thus far, either DNA or proteins, have transient intermediates been detected between donor and acceptor. Placing thermodynamic holes in the pathway in DNA and in RNR has blocked ET, and new technologies to place unnatural amino acids into proteins hold promise for buildup and detection of oxidized amino acids in much the same way that this has recently been carried out with an indole derivative in DNA.[156] The stability of the Y122$^{\bullet}$ and the triggering of the nucleotide reduction by binding of substrate and effector ensures that this remarkable radical initiation does not result in protein self-inactivation. The choice of this radical initiation from a chemical perspective is baffling. The availability of new experimental approaches, and the important insight from model systems, should allow the mechanism of radical initiation in the class I RNRs to be elucidated in the not-too-distant future.

VII. Acknowledgments

This work was supported by National Institutes of Health GM 29595 (J.S.) and GM 47274 (D.G.N.). We thank all of our co-workers who have worked on this project over the years.

VIII. References

(1) Eklund, H.; Uhlin, U.; Farnegardh, M.; Logan, D. T.; Nordlund, P. *Prog. Biophys. Mol. Biol.* **2001**, *77*, 177.
(2) Jordan, A.; Reichard, P. *Annu. Rev. Biochem.* **1998**, *67*, 71.
(3) Thelander, L.; Reichard, P. *Annu. Rev. Biochem.* **1979**, *48*, 133.
(4) Zhou, B. B. S.; Elledge, S. J. *Nature* **2000**, *408*, 433.
(5) Stubbe, J.; van der Donk, W. A. *Chem. Rev.* **1998**, *98*, 705.
(6) Licht, S.; Stubbe, J. In *Comprehensive Natural Products Chemistry*; Barton, S. D., Nakanishi, K., Meth-Cohn, O., Poulter, C. D., Eds.; Elsevier Science: New York, 1999; Vol. 5, p 163.
(7) Eklund, H.; Fontecave, M. *Struct. Fold. Des.* **1999**, *7*, R257.
(8) Reichard, P. *Annu. Rev. Biochem.* **1995**, *64*, 1.
(9) Reichard, P. *Trends Biochem. Sci.* **1997**, *22*, 81.
(10) Stubbe, J.; Riggs-Gelasco, P. *Trends Biochem. Sci.* **1998**, *23*, 438.
(11) Bollinger, J. M.; Edmondson, D. E.; Huynh, B. H.; Filley, J.; Norton, J. R.; Stubbe, J. *Science* **1991**, *253*, 292.
(12) Gerfen, G. J.; Bellew, B. F.; Un, S.; Bollinger, J. M., Jr.; Stubbe, J.; Griffin, R. G.; Singel, D. J. *J. Am. Chem. Soc.* **1993**, *115*, 6420.
(13) Lawrence, C. C.; Bennati, M.; Obias, H. V.; Bar, G.; Griffin, R. G.; Stubbe, J. *Proc. Natl. Acad. Sci. U.S.A.* **1999**, *96*, 8979.
(14) Sahlin, M.; Sjoberg, B. M. *Subcell. Biochem.* **2000**, *35*, 405.
(15) Uhlin, U.; Eklund, H. *Nature* **1994**, *370*, 533.
(16) Lin, A. N.; Ashley, G. W.; Stubbe, J. *Biochemistry* **1987**, *26*, 6905.
(17) Mao, S. S.; Johnston, M. I.; Bollinger, J. M.; Stubbe, J. *Proc. Natl. Acad. Sci. U.S.A.* **1989**, *86*, 1485.
(18) Mao, S. S.; Holler, T. P.; Yu, G. X.; Bollinger, J. M., Jr.; Booker, S.; Johnston, M. I.; Stubbe, J. *Biochemistry* **1992**, *31*, 9733.
(19) Aberg, A.; Hahne, S.; Karlsson, M.; Larsson, A.; Ormo, M.; Ahgren, A.; Sjoberg, B. M. *J. Biol. Chem.* **1989**, *264*, 12249.
(20) Sjoberg, B. M.; Reichard, P.; Graslund, A.; Ehrenberg, A. *J. Biol. Chem.* **1978**, *253*, 6863.
(21) Filatov, D.; Ingemarson, R.; Johansson, E.; Rova, U.; Thelander, L. *Biochem. Soc. Trans.* **1995**, *23*, 903.
(22) Eriksson, S.; Thelander, L. *Ciba Found. Symp.* **1978**, 165.
(23) Thelander, M.; Graslund, A.; Thelander, L. *J. Biol. Chem.* **1985**, *260*, 2737.
(24) Scott, C. P.; Kashlan, O. B.; Lear, J. D.; Cooperman, B. S. *Biochemistry* **2001**, *40*, 1651.
(25) Uhlin, U.; Eklund, H. *J. Mol. Biol.* **1996**, *262*, 358.
(26) Eriksson, M.; Jordan, A.; Eklund, H. *Biochemistry* **1998**, *37*, 13359.

(27) Logan, D. T.; Su, X. D.; Aberg, A.; Regnstrom, K.; Hajdu, J.; Eklund, H.; Nordlund, P. *Structure* **1996**, *4*, 1053.
(28) Nordlund, P.; Eklund, H. *J. Mol. Biol.* **1993**, *232*, 123.
(29) Nordlund, P.; Sjoberg, B. M.; Eklund, H. *Nature* **1990**, *345*, 593.
(30) Nielsen, B. B.; Kauppi, B.; Thelander, M.; Thelander, L.; Larsen, I. K.; Eklund, H. *FEBS Lett.* **1995**, *373*, 310.
(31) Voegtli, W. C.; Ge, J.; Perlstein, D. L.; Stubbe, J.; Rosenzweig, A. C. *Proc. Natl. Acad. Sci. U.S.A.* **2001**, *98*, 10073.
(32) Marcus, R. A. *J. Chem. Phys.* **1956**, *24*, 966.
(33) Marcus, R. A.; Eyring, H. *Annu. Rev. Phys. Chem.* **1964**, *15*, 155.
(34) Marcus, R. A.; Sutin, N. *Biochim. Biophys. Acta* **1985**, *811*, 265.
(35) Marcus, R. A. *Angew. Chem., Int. Ed. Engl.* **1993**, *32*, 1111.
(36) Marcus, R. A. *Rev. Mod. Phys.* **1993**, *65*, 599.
(37) Marcus, R. A. *Adv. Chem. Phys.* **1999**, *106*, 1.
(38) Wasielewski, M. R., personal communication.
(39) Mussell, R. D.; Nocera, D. G. *J. Am. Chem. Soc.* **1988**, *110*, 2764.
(40) Mussell, R. D.; Nocera, D. G. *Inorg. Chem.* **1990**, *29*, 3711.
(41) Mussell, R. D.; Nocera, D. G. *J. Phys. Chem.* **1991**, *95*, 6919.
(42) Marcus, R. A.; Siders, P. *J. Phys. Chem.* **1982**, *86*, 622.
(43) McCleskey, T. M.; Winkler, J. R.; Gray, H. B. *J. Am. Chem. Soc.* **1992**, *114*, 6935.
(44) Burshtein, A. I. *Adv. Chem. Phys.* **2001**, *114*, 419.
(45) Turró, C.; Zaleski, J. M.; Karabatsos, Y. M.; Nocera, D. G. *J. Am. Chem. Soc.* **1996**, *118*, 6060.
(46) Creutz, C.; Sutin, N. *Proc. Natl. Acad. Sci. U.S.A.* **1973**, *70*, 1701.
(47) Grimes, C. J.; Piszkiewicz, D.; Fleischer, E. B. *Proc. Natl. Acad. Sci. U.S.A.* **1974**, *71*, 1408.
(48) Holwerda, R. A.; Wherland, S.; Gray, H. B. *Annu. Rev. Biophys. Bioeng.* **1976**, *5*, 363.
(49) Rawlings, J.; Wherland, S.; Gray, H. B. *J. Am. Chem. Soc.* **1976**, *98*, 2177.
(50) Wood, F. E.; Cusanovich, M. A. *Bioinorg. Chem.* **1975**, *4*, 337.
(51) Wherland, S.; Gray, H. B. *Proc. Natl. Acad. Sci. U.S.A.* **1976**, *73*, 2950.
(52) Cummins, D.; Gray, H. B. *J. Am. Chem. Soc.* **1977**, *99*, 5158.
(53) Wherland, S.; Pecht, I. *Biochemistry* **1978**, *17*, 2585.
(54) Mauk, A. G.; Coyle, C. L.; Bordignon, E.; Gray, H. B. *J. Am. Chem. Soc.* **1979**, *101*, 5054.
(55) Nocera, D. G.; Winkler, J. R.; Yocom, K. M.; Bordignon, E.; Gray, H. B. *J. Am. Chem. Soc.* **1984**, *106*, 5145.
(56) Winkler, J. R.; Nocera, D. G.; Yocom, K. M.; Bordignon, E.; Gray, H. B. *J. Am. Chem. Soc.* **1982**, *104*, 5798.
(57) Crane, B. R.; Di Bilio, A. J.; Winkler, J. R.; Gray, H. B. *J. Am. Chem. Soc.* **2001**, *123*, 11623.
(58) Mines, G. A.; Ramirez, B. E.; Gray, H. B.; Winkler, J. R. In *Photochemistry and radiation chemistry: complementary methods for the study of electron transfer*; Wishart, J. F., Nocera, D. G., Eds.; ACS Advances in Chemistry Series 254; American Chemical Society: Washington, DC, 1998; p 51.
(59) Farver, O.; Pecht, I. *Biophys. Chem.* **1994**, *50*, 203.
(60) Gray, H. B. *Chem. Soc. Rev.* **1986**, *15*, 17.
(61) Farver, O.; Pecht, I. *Mol. Cryst. Liq. Cryst.* **1991**, *194*, 215.
(62) Gray, H. B.; Winkler, J. R. In *Electron Transfer in Chemistry*; Balzani, V., Ed.; Wiley-VCH: Weinheim, Germany, 2001; Vol. 3.1.1, p 3.
(63) Wright, J. L.; Wang, K.; Geren, L.; Saunders: A. J.; Pielak, G. J.; Durham, B.; Millett, F. In *Photochemistry and radiation chemistry: complementary methods for the study of electron transfer*; Wishart, J. F., Nocera, D. G., Eds.; ACS Advances in Chemistry Series 254; American Chemical Society: Washington, DC, 1998; p 99.
(64) Gray, H. B.; Winkler, J. R. *Annu. Rev. Biochem.* **1996**, *65*, 537.
(65) Winkler, J. R.; Gray, H. B. *Chem. Rev.* **1992**, *92*, 369.
(66) Chang, I.-J.; Gray, H. B.; Winkler, J. R. *J. Am. Chem. Soc.* **1991**, *113*, 7056.
(67) Bjerrum, M. J.; Casimiro, D. R.; Chang, I. J.; Di Bilio, A. J.; Gray, H. B.; Hill, M. G.; Langen, R.; Mines, G. A.; Skov, L. K.; et al. *J. Bioenerg. Biomembr.* **1995**, *27*, 295.
(68) Tollin, G. In *Electron Transfer in Chemistry*; Balzani, V., Ed.; Wiley-VCH: Weinheim, Germany, 2001; Vol. 4.1.5, p 202.
(69) Sun, D.; Davidson, V. L. *Prog. React. Kinet. Mech.* **2002**, *27*, 209.
(70) Davidson, V. L. *Acc. Chem. Res.* **2000**, *33*, 87.
(71) Wang, K.; Zhen, Y.; Sadoski, R.; Grinnell, S.; Geren, L.; Ferguson-Miller, S.; Durham, B.; Millett, F. *J. Biol. Chem.* **1999**, *274*, 38042.
(72) Nocek, J. M.; Zhou, J. S.; Forest, S. D.; Priyadarshy, S.; Beratan, D. N.; Onuchic, J. N.; Hoffman, B. M. *Chem. Rev.* **1996**, *96*, 2459.
(73) Millett, F. S. *J. Bioenerg. Biomembr.* **1995**, *27*, 261.
(74) McLendon, G.; Hake, R. *Chem. Rev.* **1992**, *92*, 481.
(75) Tezcan, F. A.; Crane, B. R.; Winkler, J. R.; Gray, H. B. *Proc. Natl. Acad. Sci. U.S.A.* **2001**, *98*, 5002.
(76) Millett, F.; Durham, B. *Biochemistry* **2002**, *41*, 11315.
(77) Gunner, M. R.; Robertson, D. E.; Dutton, P. L. *J. Phys. Chem.* **1986**, *90*, 3783.
(78) Gunner, M. R.; Dutton, P. L. *J. Am. Chem. Soc.* **1989**, *111*, 3400.
(79) Williams, R. J. P. *Inorg. Chim. Acta Rev.* **1971**, *5*, 137.
(80) Vallee, B. L.; Williams, R. J. P. *Proc. Natl. Acad. Sci. U.S.A.* **1968**, *59*, 498.
(81) Gray, H. B.; Winkler, J. R.; Wiedenfeld, D. *Coord. Chem. Rev.* **2000**, *200*, 875.
(82) Winkler, J. R.; Wittung-Stafshede, P.; Leckner, J.; Malmstrom, B. G.; Gray, H. B. *Proc. Natl. Acad. Sci. U.S.A.* **1997**, *94*, 4246.
(83) Machczynski, M. C.; Gray, H. B.; Richards, J. H. *J. Inorg. Biochem.* **2002**, *88*, 375.
(84) Malmström, B. G. In *Oxidases and Related Redox Systems*; King, T. E., Masin, H. S., Morrison, M., Eds.; Wiley: New York, 1964; p 207.
(85) Williams, R. J. P. *J. Solid State Chem.* **1999**, *145*, 488.
(86) Sun, D.; Chen, Z.-w.; Mathews, F. S.; Davidson, V. L. *Biochemistry* **2002**, *41*, 13926.
(87) Roth, J. P.; Klinman, J. P. *Proc. Natl. Acad. Sci. U.S.A.* **2003**, *100*, 62.
(88) Merzbacher, E. *Quantum Mechanics*, 2nd ed.; Wiley: New York, 1961.
(89) Hopfield, J. J. *Proc. Natl. Acad. Sci. U.S.A.* **1974**, *71*, 3640.
(90) Levich, V. G. *Adv. Electrochem. Electrochem. Eng.* **1966**, *4*, 249.
(91) McConnell, H. M. *J. Chem. Phys.* **1961**, *35*, 508.
(92) Beratan, D. N.; Onuchic, J. N.; Hopfield, J. J. *J. Chem. Phys.* **1987**, *86*, 4488.
(93) Kuki, A.; Wolynes, P. G. *Science* **1987**, *236*, 1647.
(94) Beratan, D. N.; Onuchic, J. N.; Winkler, J. R.; Gray, H. B. *Science* **1992**, *258*, 1740.
(95) Onuchic, J. N.; Beratan, D. N.; Winkler, J. R.; Gray, H. B. *Annu. Rev. Biophys. Biomol. Struct.* **1992**, *21*, 3640.
(96) Beratan, D. N.; Betts, J. N.; Onuchic, J. N. *Science* **1991**, *252*, 1285.
(97) Betts, J. N.; Beratan, D. N.; Onuchic, J. N. *J. Am. Chem. Soc.* **1992**, *114*, 4043.
(98) Skourtis, S. S.; Beratan, D. N. *Adv. Chem. Phys.* **1999**, *106*, 377.
(99) Moser, C. C.; Keske, J. M.; Warncke, K.; Farid, R. S.; Dutton, P. L. *Nature* **1992**, *355*, 796.
(100) Farid, R. S.; Moser, C. C.; Dutton, P. L. *Curr. Opin. Struct. Biol.* **1993**, *3*, 225.
(101) Winkler, J. R. *Curr. Opin. Chem. Biol.* **2000**, *4*, 192.
(102) Jones, M. L.; Kurnikov, I. V.; Beratan, D. N. *J. Phys. Chem. A* **2002**, *106*, 2002.
(103) Regan, J. J.; Onuchic, J. N. *Adv. Chem. Phys.* **1999**, *107*, 497.
(104) Page, C. C.; Moser, C. C.; Chen, X.; Dutton, P. L. *Nature* **1999**, *402*, 47.
(105) Williams, R. J. P. *J. Biol. Inorg. Chem.* **1997**, *2*, 373.
(106) Boon, E. M.; Barton, J. K. *Curr. Opin. Struct. Biol.* **2002**, *12*, 320.
(107) Treadway, C. R.; Hill, M. G.; Barton, J. K. *Chem. Phys.* **2002**, *281*, 409.
(108) Nunez, M. E.; Barton, J. K. *Curr. Opin. Chem. Biol.* **2000**, *4*, 199.
(109) Brun, A. M.; Harriman, A. *J. Am. Chem. Soc.* **1992**, *114*, 3656.
(110) Meade, T. J.; Kayyem, J. F. *Angew. Chem., Int. Ed. Engl.* **1995**, *34*, 352.
(111) Grinstaff, M. W. *Angew. Chem., Int. Ed. Engl.* **1999**, *38*, 3629.
(112) Giese, B. *Annu. Rev. Biochem.* **2002**, *71*, 51.
(113) Giese, B. *Curr. Opin. Chem. Biol.* **2002**, *6*, 612.
(114) Giese, B. *Acc. Chem. Res.* **2000**, *33*, 631.
(115) Lewis, F. D. In *Electron Transfer in Chemistry*; Balzani, V., Ed.; Wiley-VCH: Weinheim, Germany, 2001; Vol. 3.1.5, p 105.
(116) Lewis, F. D.; Letsinger, R. L.; Wasielewski, M. R. *Acc. Chem. Res.* **2001**, *34*, 159.
(117) Lewis, F. D.; Liu, X.; Liu, J.; Hayes, R. T.; Wasielewski, M. R. *J. Am. Chem. Soc.* **2000**, *122*, 12037.
(118) Sugiyama, H.; Saito, I. *J. Am. Chem. Soc.* **1996**, *118*, 7063.
(119) Conwell, E. M.; Basko, D. M. *J. Am. Chem. Soc.* **2001**, *123*, 11441.
(120) Yoshioka, Y.; Kitagawa, Y.; Takano, Y.; Yamaguchi, K.; Nakamura, T.; Saito, I. *J. Am. Chem. Soc.* **1999**, *121*, 8712.
(121) Kim, N. S.; Zhu, Q.; LeBreton, P. R. *J. Am. Chem. Soc.* **1999**, *121*, 11516.
(122) Schuster, G. B. *Acc. Chem. Res.* **2000**, *33*, 253.
(123) Murphy, C. J.; Arkin, M. R.; Jenkins, Y.; Ghatlia, N. D.; Bossmann, S. H.; Turro, N. J.; Barton, J. K. *Science* **1993**, *262*, 1025.
(124) Purugganan, M. D.; Kumar, C. V.; Turro, N. J.; Barton, J. K. *Science* **1988**, *241*, 1645.
(125) Nunez, M. E.; Hall, D. B.; Barton, J. K. *Chem. Biol.* **1999**, *6*, 85.
(126) Hall, D. B.; Holmlin, R. E.; Barton, J. K. *Nature* **1996**, *382*, 731.
(127) Kelley, S. O.; Barton, J. K. *Science* **1999**, *283*, 375.
(128) Turro, N. J.; Barton, J. K. *J. Biol. Inorg. Chem.* **1998**, *3*, 201.
(129) Beratan, D. N.; Priyadarshy, S.; Risser, S. M. *Chem. Biol.* **1997**, *4*, 3.
(130) Lewis, F. D.; Liu, J.; Weigel, W.; Rettig, W.; Kurnikov, I. V.; Beratan, D. N. *Proc. Natl. Acad. Sci. U.S.A.* **2002**, *99*, 12536.
(131) Lewis, F. D.; Wu, T.; Liu, X.; Letsinger, R. L.; Greenfield, S. R.; Miller, S. E.; Wasielewski, M. R. *J. Am. Chem. Soc.* **2000**, *122*, 2889.
(132) Priyadarshy, S.; Risser, S. M.; Beratan, D. N. *J. Phys. Chem.* **1996**, *100*, 17678.
(133) Meggers, E.; Michel-Beyerle, M. E.; Giese, B. *J. Am. Chem. Soc.* **1998**, *120*, 12950.

(134) Nakatani, K.; Dohno, C.; Saito, I. *J. Am. Chem. Soc.* **1999**, *121*, 10854.
(135) Bixon, M.; Giese, B.; Wessely, S.; Langenbacher, T.; Michel-Beyerle, M. E.; Jortner, J. *Proc. Natl. Acad. Sci. U.S.A.* **1999**, *96*, 11713.
(136) Giese, B.; Amaudrut, J.; Kohler, A.-K.; Spormann, M.; Wessely, S. *Nature* **2001**, *412*, 318.
(137) Henderson, P. T.; Jones, D.; Hampikian, G.; Kan, Y.; Schuster, G. B. *Proc. Natl. Acad. Sci. U.S.A.* **1999**, *96*, 8353.
(138) Jortner, J.; Bixon, M.; Langenbacher, T.; Michel-Beyerle, M. E. *Proc. Natl. Acad. Sci. U.S.A.* **1998**, *95*, 12759.
(139) Bixon, M.; Jortner, J. *J. Am. Chem. Soc.* **2001**, *123*, 12556.
(140) Bixon, M.; Jortner, J. *Chem. Phys.* **2002**, *281*, 393.
(141) Giese, B.; Spichty, M. *Chem. Phys. Chem.* **2000**, *1*, 195.
(142) Wan, C.; Fiebig, T.; Schiemann, O.; Barton, J. K.; Zewail, A. H. *Proc. Natl. Acad. Sci. U.S.A.* **2000**, *97*, 14052.
(143) Wan, C.; Fiebig, T.; Kelley, S. O.; Treadway, C. R.; Barton, J. K.; Zewail, A. H. *Proc. Natl. Acad. Sci. U.S.A.* **1999**, *96*, 6014.
(144) Tierney, M. T.; Sykora, M.; Khan, S. I.; Grinstaff, M. W. *J. Phys. Chem. B* **2000**, *104*, 7574.
(145) Lewis, F. D.; Wu, T.; Zhang, Y.; Letsinger, R. L.; Greenfield, S. R.; Wasielewski, M. R. *Science* **1997**, *277*, 673.
(146) Lewis, F. D.; Liu, X.; Liu, J.; Miller, S. E.; Hayes, R. T.; Wasielewski, M. R. *Nature* **2000**, *406*, 51.
(147) Lewis, F. D.; Zuo, X.; Liu, J.; Hayes, R. T.; Wasielewski, M. R. *J. Am. Chem. Soc.* **2002**, *124*, 4568.
(148) Lewis, F. D.; Liu, J.; Liu, X.; Zuo, X.; Hayes, R. T.; Wasielewski, M. R. *Angew. Chem., Int. Ed.* **2002**, *41*, 1026.
(149) Lewis, F. D.; Liu, X.; Miller, S. E.; Wasielewski, M. R. *J. Am. Chem. Soc.* **1999**, *121*, 9746.
(150) Lewis, F. D.; Liu, X.; Miller, S. E.; Hayes, R. T.; Wasielewski, M. R. *J. Am. Chem. Soc.* **2002**, *124*, 14020.
(151) Lewis, F. D.; Kalgutkar, R. S.; Wu, Y.; Liu, X.; Liu, J.; Hayes, R. T.; Miller, S. E.; Wasielewski, M. R. *J. Am. Chem. Soc.* **2000**, *122*, 12346.
(152) Lewis, F. D.; Liu, X.; Miller, S. E.; Hayes, R. T.; Wasielewski, M. R. *J. Am. Chem. Soc.* **2002**, *124*, 11280.
(153) Lewis, F. D.; Liu, X.; Wu, Y.; Miller, S. E.; Wasielewski, M. R.; Letsinger, R. L.; Sanishvili, R.; Joachimiak, A.; Tereshko, V.; Egli, M. *J. Am. Chem. Soc.* **1999**, *121*, 9905.
(154) Lewis, F. D.; Wu, Y.; Hayes, R. T.; Wasielewski, M. R. *Angew. Chem., Int. Ed.* **2002**, *41*, 3485.
(155) Schiemann, O.; Turro, N. J.; Barton, J. K. *J. Phys. Chem. B* **2000**, *104*, 7214.
(156) Pascaly, M.; Yoo, J.; Barton, J. K. *J. Am. Chem. Soc.* **2002**, *124*, 9083.
(157) Friis, E. P.; Andersen, J. E. T.; Kharkats, Y. I.; Kuznetsov, A. M.; Nichols, R. J.; Zhang, J. D.; Ulstrup, J. *Proc. Natl. Acad. Sci. U.S.A.* **1999**, *96*, 1379.
(158) Volk, M.; Aumeier, G.; Langenbacher, T.; Feick, R.; Ogrodnik, A.; Michel-Beyerle, M.-E. *J. Phys. Chem. B* **1998**, *102*, 735.
(159) Chang, C. J.; Brown, J. D. K.; Chang, M. C. Y.; Baker, E. A.; Nocera, D. G. In *Electron Transfer in Chemistry*; Balzani, V., Ed.; Wiley-VCH: Weinheim, Germany, 2001; Vol. 3.2.4, p 409.
(160) Cukier, R. I.; Nocera, D. G. *Annu. Rev. Phys. Chem.* **1998**, *49*, 337.
(161) Turró, C.; Chang, C. K.; Leroi, G. E.; Cukier, R. I.; Nocera, D. G. *J. Am. Chem. Soc.* **1992**, *114*, 4013.
(162) Zhao, X. G.; Cukier, R. I. *J. Phys. Chem.* **1995**, *99*, 945.
(163) Cukier, R. I. *J. Phys. Chem.* **1994**, *98*, 2377.
(164) Sessler, J. L.; Wang, B.; Springs, S. L.; Brown, C. T. In *Comprehensive Supramolecular Chemistry*; Murakami, Y., Ed.; Pergamon Press: Oxford, 1996; Vol. 4, p 311.
(165) Sessler, J. L.; Sathiosatham, M.; Brown, C. T.; Rhodes, T. A.; Wiederrecht, G. *J. Am. Chem. Soc.* **2001**, *123*, 3655.
(166) Berg, A.; Shuali, Z.; Asano-Someda, M.; Levanon, H.; Fuhs, M.; Moebius, K.; Wang, R.; Brown, C.; Sessler, J. L. *J. Am. Chem. Soc.* **1999**, *121*, 7433.
(167) Ward, M. D. *Chem. Soc. Rev.* **1997**, *26*, 365.
(168) Berman, A.; Izraeli, E. S.; Levanon, H.; Wang, B.; Sessler, J. L. *J. Am. Chem. Soc.* **1995**, *117*, 8252.
(169) Sessler, J. L.; Wang, B.; Harriman, A. *J. Am. Chem. Soc.* **1995**, *117*, 704.
(170) Shafirovich, V. Y.; Courtney, S. H.; Ya, N.; Geacintov, N. E. *J. Am. Chem. Soc.* **1995**, *117*, 4920.
(171) Sessler, J. L.; Wang, B.; Harriman, A. *J. Am. Chem. Soc.* **1993**, *115*, 10418.
(172) Harriman, A.; Kubo, Y.; Sessler, J. L. *J. Am. Chem. Soc.* **1992**, *114*, 388.
(173) Ghaddar, T. H.; Castner, E. W.; Isied, S. S. *J. Am. Chem. Soc.* **2000**, *122*, 1233.
(174) Yeh, C.-Y.; Miller, S. E.; Carpenter, S. D.; Nocera, D. G. *Inorg. Chem.* **2001**, *40*, 3643.
(175) Roberts, J. A.; Kirby, J. P.; Wall, S. T.; Nocera, D. G. *Inorg. Chim. Acta* **1997**, *263*, 395.
(176) Deng, Y.; Roberts, J. A.; Peng, S.-M.; Chang, C. K.; Nocera, D. G. *Angew. Chem., Int. Ed. Engl.* **1997**, *36*, 2124.
(177) Kirby, J. P.; van Dantzig, N. A.; Chang, C. K.; Nocera, D. G. *Tetrahedron Lett.* **1995**, *36*, 3477.
(178) Roberts, J. A.; Kirby, J. P.; Nocera, D. G. *J. Am. Chem. Soc.* **1995**, *117*, 8051.
(179) Kirby, J. P.; Roberts, J. A.; Nocera, D. G. *J. Am. Chem. Soc.* **1997**, *119*, 9230.
(180) Hammes-Schiffer, S. *Chem. Phys. Chem.* **2002**, *3*, 33.
(181) Hammes-Schiffer, S. In *Electron Transfer in Chemistry*; Balzani, V., Ed.; Wiley-VCH: Weinheim, Germany, 2001; Vol. 1.1.5, p 189.
(182) Rostov, I.; Hammes-Schiffer, S. *J. Chem. Phys.* **2001**, *115*, 285.
(183) Jang, S.; Cao, J. *J. Chem. Phys.* **2001**, *114*, 9959.
(184) Iordanova, N.; Decornez, H.; Hammes-Schiffer, S. *J. Am. Chem. Soc.* **2001**, *123*, 3723.
(185) Shin, S.; Cho, S. I. *Chem. Phys.* **2000**, *259*, 27.
(186) Decornez, H.; Hammes-Schiffer, S. *J. Phys. Chem. A* **2000**, *104*, 9370.
(187) Soudackov, A.; Hammes-Schiffer, S. *J. Am. Chem. Soc.* **1999**, *121*, 10598.
(188) Fang, J.-Y.; Hammes-Schiffer, S. *J. Chem. Phys.* **1997**, *106*, 8442.
(189) Fang, J.-Y.; Hammes-Schiffer, S. *J. Chem. Phys.* **1997**, *107*, 5727.
(190) Cukier, R. I. *J. Phys. Chem.* **1996**, *100*, 15428.
(191) Cukier, R. I. *J. Phys. Chem. B* **2002**, *106*, 1746.
(192) Soudackov, A.; Hammes-Schiffer, S. *J. Chem. Phys.* **2000**, *113*, 2385.
(193) Aubert, C.; Vos, M. H.; Mathis, P.; Eker, A. P.; Brettel, K. *Nature* **2000**, *405*, 586.
(194) Carell, T.; Burgdorf, L. T.; Kundu, L. M.; Cichon, M. *Curr. Opin. Chem. Biol.* **2001**, *5*, 491.
(195) Sancar, A. *Annu. Rev. Biochem.* **2000**, *69*, 31.
(196) Park, H. W.; Kim, S. T.; Sancar, A.; Deisenhofer, J. *Science* **1995**, *268*, 1866.
(197) Li, Y. F.; Heelis, P. F.; Sancar, A. *Biochemistry* **1991**, *30*, 6322.
(198) Sancar, A. *Chem. Rev.* **2003**, *103*, 2203 (in this issue).
(199) Kim, S. T.; Sancar, A.; Essenmacher, C.; Babcock, G. T. *Proc. Natl. Acad. Sci. U.S.A.* **1993**, *90*, 8023.
(200) Gindt, Y. M.; Vollenbroek, E.; Westphal, K.; Sackett, H.; Sancar, A.; Babcock, G. T. *Biochemistry* **1999**, *38*, 3857.
(201) Popovic, D. M.; Zmiric, A.; Zaric, S. D.; Knapp, E.-W. *J. Am. Chem. Soc.* **2002**, *124*, 3775.
(202) Cheung, M. S.; Daizadeh, I.; Stuchebrukhov, A. A.; Heelis, P. F. *Biophys. J.* **1999**, *76*, 1241.
(203) Aubert, C.; Brettel, K.; Mathis, P.; Eker, A. P.; Boussac, A. *J. Am. Chem. Soc.* **1999**, *121*, 8659.
(204) Aubert, C.; Mathis, P.; Eker, A. P.; Brettel, K. *Proc. Natl. Acad. Sci. U.S.A.* **1999**, *96*, 5423.
(205) Okamura, M. Y.; Paddock, M. L.; Graige, M. S.; Feher, G. *Biochim. Biophys. Acta* **2000**, *1458*, 148.
(206) Stowell, M. H. B.; McPhillips, T. M.; Rees, D. C.; Solitis, S. M.; Abresch, E.; Feher, G. *Science* **1997**, *276*, 812.
(207) Heathcote, P.; Fyfe, P. K.; Jones, M. R. *Trends Biochem. Sci.* **2002**, *27*, 79.
(208) Axelrod, H. L.; Abresch, E. C.; Okamura, M. Y.; Yeh, A. P.; Rees, D. C.; Feher, G. *J. Mol. Biol.* **2002**, *319*, 501.
(209) Tetreault, M.; Cusanovich, M.; Meyer, T.; Axelrod, H.; Okamura, M. Y. *Biochemistry* **2002**, *41*, 5807.
(210) Graige, M. S.; Feher, G.; Okamura, M. Y. *Proc. Natl. Acad. Sci. U.S.A.* **1998**, *95*, 11679.
(211) Adelroth, P.; Paddock, M. L.; Tehrani, A.; Beatty, J. T.; Feher, G.; Okamura, M. Y. *Biochemistry* **2001**, *40*, 14538.
(212) Mezzetti, A.; Nabedryk, E.; Breton, J.; Okamura, M. Y.; Paddock, M. L.; Giacometti, G.; Leibl, W. *Biochim. Biophys. Acta* **2002**, *1553*, 320.
(213) Adelroth, P.; Paddock, M. L.; Sagle, L. B.; Feher, G.; Okamura, M. Y. *Proc. Natl. Acad. Sci. U.S.A.* **2000**, *97*, 13086.
(214) Ormo, M.; Regnstrom, K.; Wang, Z.; Que, L., Jr.; Sahlin, M.; Sjoberg, B. M. *J. Biol. Chem.* **1995**, *270*, 6570.
(215) Pesavento, R. P.; van der Donk, W. A. *Adv. Protein Chem.* **2001**, *58*, 317.
(216) Gleason, F. K.; Olszewski, N. E. *J. Bacteriol.* **2002**, *184*, 6544.
(217) Blakley, R. L. *J. Biol. Chem.* **1965**, *240*, 2173.
(218) Panagou, D.; Orr, M. D.; Dunstone, J. R.; Blakley, R. L. *Biochemistry* **1972**, *11*, 2378.
(219) Vitols, E.; Hogenkamp, H. P. C.; Brownson, C.; Blakley, R. L.; Connellan, J. *Biochem. J.* **1967**, *104*, 58.
(220) Eliasson, R.; Pontis, E.; Jordan, A.; Reichard, P. *J. Biol. Chem.* **1999**, *274*, 7182.
(221) Ollagnier, S.; Mulliez, E.; Gaillard, J.; Eliasson, R.; Fontecave, M.; Reichard, P. *J. Biol. Chem.* **1996**, *271*, 9410.
(222) Sun, X. Y.; Eliasson, R.; Pontis, E.; Andersson, J.; Buist, G.; Sjoberg, B. M.; Reichard, P. *J. Biol. Chem.* **1995**, *270*, 2443.
(223) Sun, X. Y.; Ollagnier, S.; Schmidt, P. P.; Atta, M.; Mulliez, E.; Lepape, L.; Eliasson, R.; Graslund, A.; Fontecave, M.; Reichard, P.; Sjoberg, B. M. *J. Biol. Chem.* **1996**, *271*, 6827.
(224) Eliasson, R.; Pontis, E.; Sun, X.; Reichard, P. *J. Biol. Chem.* **1994**, *269*, 26052.
(225) Reichard, P. *J. Biol. Chem.* **1993**, *268*, 8383.
(226) Mulliez, E.; Ollagnier, S.; Fontecave, M.; Eliasson, R.; Reichard, P. *Proc. Natl. Acad. Sci. U.S.A.* **1995**, *92*, 8759.
(227) Young, P.; Andersson, J.; Sahlin, M.; Sjoberg, B. M. *J. Biol. Chem.* **1996**, *271*, 20770.

(228) Andersson, J.; Westman, M.; Sahlin, M.; Sjoberg, B. M. *J. Biol. Chem.* **2000**, *275*, 19449.
(229) Larsson, K. M.; Andersson, J.; Sjoberg, B.-M.; Nordlund, P.; Logan, D. T. *Structure* **2001**, *9*, 739.
(230) Fontecave, M.; Mulliez, E.; Logan, D. T. *Prog. Nucleic Acid Res. Mol. Biol.* **2002**, *72*, 95.
(231) Ollagnier, S.; Mulliez, E.; Schmidt, P. P.; Eliasson, R.; Gaillard, J.; Deronzier, C.; Bergman, T.; Graslund, A.; Reichard, P.; Fontecave, M. *J. Biol. Chem.* **1997**, *272*, 24216.
(232) Tamarit, J.; Mulliez, E.; Meier, C.; Trautwein, A.; Fontecave, M. *J. Biol. Chem.* **1999**, *274*, 31291.
(233) Padovani, D.; Thomas, F.; Trautwein, A. X.; Mulliez, E.; Fontecave, M. *Biochemistry* **2001**, *40*, 6713.
(234) Torrents, E.; Eliasson, R.; Wolpher, H.; Graslund, A.; Reichard, P. *J. Biol. Chem.* **2001**, *276*, 33488.
(235) Sintchak, M. D.; Arjara, G.; Kellogg, B. A.; Stubbe, J.; Drennan, C. L. *Nat. Struct. Biol.* **2002**, *9*, 293.
(236) Logan, D. T.; Andersson, J.; Sjoberg, B. M.; Nordlund, P. *Science* **1999**, *283*, 1499.
(237) Stubbe, J. *Proc. Natl. Acad. Sci. U.S.A.* **1998**, *95*, 2723.
(238) Stubbe, J.; Ge, J.; Yee, C. S. *Trends Biochem. Sci.* **2001**, *26*, 93.
(239) Stubbe, J. *Adv. Enzymol. Relat. Areas Mol. Biol.* **1990**, *63*, 349.
(240) Licht, S. S.; Booker, S.; Stubbe, J. *Biochemistry* **1999**, *38*, 1221.
(241) Stubbe, J. *J. Biol. Chem.* **1990**, *265*, 5329.
(242) Mao, S. S.; Yu, G. X.; Chalfoun, D.; Stubbe, J. *Biochemistry* **1992**, *31*, 9752.
(243) Ekberg, M.; Potsch, S.; Sandin, E.; Thunnissen, M.; Nordlund, P.; Sahlin, M.; Sjoberg, B. M. *J. Biol. Chem.* **1998**, *273*, 21003.
(244) Ekberg, M.; Sahlin, M.; Eriksson, M.; Sjoberg, B. M. *J. Biol. Chem.* **1996**, *271*, 20655.
(245) Rova, U.; Goodtzova, K.; Ingemarson, R.; Behravan, G.; Graslund, A.; Thelander, L. *Biochemistry* **1995**, *34*, 4267.
(246) Rova, U.; Adrait, A.; Potsch, S.; Graslund, A.; Thelander, L. *J. Biol. Chem.* **1999**, *274*, 23746.
(247) Dutia, B. M.; Frame, M. C.; Subak-Sharpe, J. H.; Clark, W. N.; Marsden, H. S. *Nature* **1986**, *321*, 439.
(248) Fisher, A.; Yang, F. D.; Rubin, H.; Cooperman, B. S. *J. Med. Chem.* **1993**, *36*, 3859.
(249) Climent, I.; Sjoberg, B. M.; Huang, C. Y. *Biochemistry* **1991**, *30*, 5164.
(250) Climent, I.; Sjoberg, B. M.; Huang, C. Y. *Biochemistry* **1992**, *31*, 4801.
(251) Lycksell, P. O.; Ingemarson, R.; Davis, R.; Graslund, A.; Thelander, L. *Biochemistry* **1994**, *33*, 2838.
(252) Moss, N.; Beaulieu, P.; Duceppe, J. S.; Ferland, J. M.; Gauthier, J.; Ghiro, E.; Goulet, S.; Grenier, L.; Llinasbrunet, M.; Plante, R.; Wernic, D.; Deziel, R. *J. Med. Chem.* **1995**, *38*, 3617.
(253) Moss, N.; Beaulieu, P.; Duceppe, J. S.; Ferland, J. M.; Garneau, M.; Gauthier, J.; Ghiro, E.; Goulet, S.; Guse, I.; Jaramillo, J.; LlinasBrunet, M.; Malenfant, E.; Plante, R.; Poirier, M.; Soucy, F.; Wernic, D.; Yoakim, C.; Deziel, R. *J. Med. Chem.* **1996**, *39*, 4173.
(254) Lycksell, P. O.; Sahlin, M. *FEBS Lett.* **1995**, *368*, 441.
(255) Tommos, C.; Skalicky, J. J.; Pilloud, D. L.; Wand, A. J.; Dutton, P. L. *Biochemistry* **1999**, *38*, 9495.
(256) Stubbe, J. *Nature* **1994**, *370*, 502.
(257) Jin, S.; Kurtz, D. M., Jr.; Liu, Z. J.; Rose, J.; Wang, B. C. *J. Am. Chem. Soc.* **2002**, *124*, 9845.
(258) Siegbahn, P. E. M.; Eriksson, L.; Himo, F.; Pavlov, M. *J. Phys. Chem. B* **1998**, *102*, 10622.
(259) Schmidt, P. P.; Rova, U.; Katterle, B.; Thelander, L.; Graslund, A. *J. Biol. Chem.* **1998**, *273*, 21463.
(260) Willems, J. P.; Lee, H. I.; Burdi, D.; Doan, P. E.; Stubbe, J.; Hoffman, B. M. *J. Am. Chem. Soc.* **1997**, *119*, 9816.
(261) Baldwin, J.; Krebs, C.; Ley, B. A.; Edmondson, D. E.; Huynh, B. H.; Bollinger, J. M., Jr. *J. Am. Chem. Soc.* **2000**, *122*, 12195.
(262) van der Donk, W. A.; Yu, G. X.; Silva, D. J.; Stubbe, J. *Biochemistry* **1996**, *35*, 8381.
(263) Persson, A. L.; Sahlin, M.; Sjoberg, B. M. *J. Biol. Chem.* **1998**, *273*, 31016.
(264) Ochiai, E.; Mann, G. J.; Graslund, A.; Thelander, L. *J. Biol. Chem.* **1990**, *265*, 15758.
(265) Atkin, C. L.; Thelander, L.; Reichard, P.; Lang, G. *J. Biol. Chem.* **1973**, *248*, 7464.
(266) Elgren, T. E.; Lynch, J. B.; Juarez-Garcia, C.; Munck, E.; Sjoberg, B. M.; Que, L., Jr. *J. Biol. Chem.* **1991**, *266*, 19265.
(267) Bollinger, J. M.; Tong, W. H.; Ravi, N.; Huynh, B. H.; Edmondson, D. E.; Stubbe, J. *J. Am. Chem. Soc.* **1994**, *116*, 8024.
(268) Tong, W.; Burdi, D.; Riggs-Gelasco, P.; Chen, S.; Edmondson, D.; Huynh, B. H.; Stubbe, J.; Han, S.; Arvai, A.; Tainer, J. *Biochemistry* **1998**, *37*, 5840.
(269) Baldwin, J.; Voegtli, W. C.; Khidekel, N.; Moenne-Loccoz, P.; Krebs, C.; Pereira, A. S.; Ley, B. A.; Huynh, B. H.; Loehr, T. M.; Riggs-Gelasco, P. J.; Rosenzweig, A. C.; Bollinger, J. M., Jr. *J. Am. Chem. Soc.* **2001**, *123*, 7017.
(270) Krebs, C.; Chen, S.; Baldwin, J.; Ley, B. A.; Patel, U.; Edmondson, D. E.; Huynh, B. H.; Bollinger, J. M. *J. Am. Chem. Soc.* **2000**, *122*, 12207.
(271) Bollinger, J. M.; Tong, W. H.; Ravi, N.; Huynh, B. H.; Edmonson, D. E.; Stubbe, J. *J. Am. Chem. Soc.* **1994**, *116*, 8015.
(272) Burdi, D.; Sturgeon, B. E.; Tong, W. H.; Stubbe, J. A.; Hoffman, B. M. *J. Am. Chem. Soc.* **1996**, *118*, 281.
(273) Burdi, D.; Willems, J. P.; Riggs-Gelasco, P.; Antholine, W. E.; Stubbe, J.; Hoffman, B. M. *J. Am. Chem. Soc.* **1998**, *120*, 12910.
(274) Riggs-Gelasco, P. J.; Shu, L. J.; Chen, S. X.; Burdi, D.; Huynh, B. H.; Que, L.; Stubbe, J. *J. Am. Chem. Soc.* **1998**, *120*, 849.
(275) Sturgeon, B. E.; Burdi, D.; Chen, S. X.; Huynh, B. H.; Edmondson, D. E.; Stubbe, J.; Hoffman, B. M. *J. Am. Chem. Soc.* **1996**, *118*, 7551.
(276) Finzel, B. C.; Poulos, T. L.; Kraut, J. *J. Biol. Chem.* **1984**, *259*, 13027.
(277) Huyett, J. E.; Doan, P. E.; Gurbiel, R.; Houseman, A. L. P.; Sivaraja, M.; Goodin, D. B.; Hoffman, B. M. *J. Am. Chem. Soc.* **1995**, *117*, 9033.
(278) Umback, N. J.; Norton, J. R. *Biochemistry.* **2002**, 3984.
(279) Yang, Y. S.; Baldwin, J.; Ley, B. A.; Bollinger, J. M.; Solomon, E. I. *J. Am. Chem. Soc.* **2000**, *122*, 8495.
(280) Bollinger, J. M.; Chen, S. X.; Parkin, S. E.; Mangravite, L. M.; Ley, B. A.; Edmondson, D. E.; Huynh, B. H. *J. Am. Chem. Soc.* **1997**, *119*, 5976.
(281) Rebeil, R.; Nicholson, W. L. *Proc. Natl. Acad. Sci. U.S.A.* **2001**, *98*, 9038.
(282) Krebs, C.; Chen, S. X.; Baldwin, J.; Ley, B. A.; Patel, U.; Edmondson, D. E.; Huynh, B. H.; Bollinger, J. M. *J. Am. Chem. Soc.* **2000**, *122*, 12207.
(283) van der Donk, W. A.; Stubbe, J.; Gerfen, G. J.; Bellew, B. F.; Griffin, R. G. *J. Am. Chem. Soc.* **1995**, *117*, 8908.
(284) van der Donk, W. A.; Gerfen, G. J.; Stubbe, J. *J. Am. Chem. Soc.* **1998**, *120*, 4252.
(285) Stubbe, J.; van der Donk, W. A. *Chem. Biol.* **1995**, *2*, 793.
(286) Ator, M.; Salowe, S. P.; Stubbe, J.; Emptage, M. H.; Robins, M. J. *J. Am. Chem. Soc.* **1984**, *106*, 1886.
(287) Sjoberg, B. M.; Graslund, A.; Eckstein, F. *J. Biol. Chem.* **1983**, *258*, 8060.
(288) Thelander, L.; Larsson, B. *J. Biol. Chem.* **1976**, *251*, 1398.
(289) Salowe, S. P.; Ator, M. A.; Stubbe, J. *Biochemistry* **1987**, *26*, 3408.
(290) Salowe, S.; Bollinger, J. M., Jr.; Ator, M.; Stubbe, J.; McCraken, J.; Peisach, J.; Samano, M. C.; Robins, M. J. *Biochemistry* **1993**, *32*, 12749.
(291) Brown, N. C.; Reichard, P. *J. Mol. Biol.* **1969**, *46*, 39.
(292) Brown, N. C.; Reichard, P. *J. Mol. Biol.* **1969**, *46*, 25.
(293) Blakley, R. L. *Methods Enzymol.* **1978**, *51*, 246.
(294) Licht, S. S.; Lawrence, C. C.; Stubbe, J. *J. Am. Chem. Soc.* **1999**, *121*, 7463.
(295) Tamao, Y.; Blakley, R. L. *Biochemistry* **1973**, *12*, 24.
(296) Orme-Johnson, W. H.; Beinert, H.; Blakley, R. L. *J. Biol. Chem.* **1974**, *249*, 2338.
(297) Licht, S.; Gerfen, G. J.; Stubbe, J. *Science* **1996**, *271*, 477.
(298) Buckel, W.; Golding, B. T. *Chem. Soc. Rev.* **1996**, 329.
(299) Ge, J.; Stubbe, J. *Biochemistry* 2002, submitted for publication.
(300) Ator, M. A. Ph.D. Thesis, University of Wisconsin, Madison, WI, 1984.
(301) Erickson, H. K. *Biochemistry* **2000**, *39*, 9241.
(302) Ekberg, M.; Birgander, P.; Sjöberg, B.-M. *J. Bacteriol.* **2003**, *185*, 1167.
(303) Mayer, J.; Hrovat, D.; Thomas, J.; Borden, W. *J. Am. Chem. Soc.* **2002**, *124*, 11142.
(304) Sjoberg, B. M.; Karlsson, M.; Jornvall, H. *J. Biol. Chem.* **1987**, *262*, 9736.
(305) Fisher, A.; Laub, P. B.; Cooperman, B. S. *Nat. Struct. Biol.* **1995**, *2*, 951.
(306) Yee, C. S.; Gie, J.; Chang, M. C. Y.; Nocera, D. G.; Stubbe, J. *Abstracts of Papers*, 225th ACS National Meeting, New Orleans, LA, March 23−27, 2003; American Chemical Society: Washington, DC, 2003.
(307) Xu, M. Q.; Evans, T. C., Jr. *Methods Enzymol.* **2001**, *24*, 257.
(308) DeFilippis, M. R.; Murthy, C. P.; Broitman, F.; Weinraub, D.; Faraggi, M.; Klapper, M. H. *J. Phys. Chem.* **1991**, *95*, 3416.
(309) DeFilippis, M. R.; Murthy, C. P.; Faraggi, M.; Klapper, M. H. *Biochemistry* **1989**, *28*, 4847.
(310) Stemp, E. D. A.; Arkin, M. R.; Barton, J. K. *J. Am. Chem. Soc.* **1997**, *119*, 2921.
(311) Kim, K.; Cole, P. A. *J. Am. Chem. Soc.* **1998**, *120*, 6851.
(312) Chen, H. L.; Phillips, R. S. *Biochemistry* **1993**, *32*, 11591.
(313) Di Bilio, A. J.; Crane, B. R.; Wehbi, W. A.; Kiser, C. N.; Abu-Omar, M. M.; Carlos, R. M.; Richards, J. H.; Winkler, J. R.; Gray, H. B. *J. Am. Chem. Soc.* **2001**, *123*, 3181.
(314) Chin, J. W.; Martin, A. B.; King, D. S.; Wang, L.; Schultz, P. G. *Proc. Natl. Acad. Sci. U.S.A.* **2002**, *99*, 11020.
(315) Chin, J. W.; Santoro, S. W.; Martin, A. B.; King, D. S.; Wang, L.; Schultz, P. G. *J. Am. Chem. Soc.* **2002**, *124*, 9026.
(316) Wang, L.; Schultz, P. G. *Chem. Commun.* **2002**, 1.
(317) Wang, L.; Brock, A.; Herberich, B.; Schultz, P. G. *Science* **2001**, *292*, 498.
(318) Gray, H. B.; Winkler, J. R. *FASEB J.* **1997**, *11*, P62.
(319) Davidson, V. L.; Jones, L. H.; Graichen, M. E.; Zhu, Z. *Biochim. Biophys. Acta* **2000**, *1457*, 27.

(320) Dohse, B.; Mathis, P.; Wachtveitl, J.; Laussermair, E.; Iwata, S.; Michel, H.; Oesterhelt, D. *Biochemistry* **1995**, *34*, 11335.
(321) Illerhaus, J.; Altschmied, L.; Reichert, J.; Zak, E.; Herrmann, R. G.; Haehnel, W. *J. Biol. Chem.* **2000**, *275*, 17590.
(322) Witt, H.; Malatesta, F.; Nicoletti, F.; Brunori, M.; Ludwig, B. *J. Biol. Chem.* **1998**, *273*, 5132.
(323) Farver, O.; Skov, L. K.; Young, S.; Bonander, N.; Karlsson, B. G.; Vanngard, T.; Pecht, I. *J. Am. Chem. Soc.* **1997**, *119*, 5453.
(324) Burdi, D.; Aveline, B. M.; Wood, P. D.; Stubbe, J.; Redmond, R. W. *J. Am. Chem. Soc.* **1997**, *119*, 6457.
(325) Chang, M. C. Y.; Miller, S. E.; Carpenter, S. D.; Stubbe, J.; Nocera, D. G. *J. Org. Chem.* **2002**, *67*, 6820.
(326) Andrew, S. M.; Thomasson, K. A.; Northrup, S. H. *J. Am. Chem. Soc.* **1993**, *115*, 5516.
(327) Mines, G. A.; Bjerrum, M. J.; Hill, M. G.; Casimiro, D. R.; Chang, I. J.; Winkler, J. R.; Gray, H. B. *J. Am. Chem. Soc.* **1996**, *118*, 1961.
(328) Di Bilio, A. J.; Hill, M. G.; Bonander, N.; Karlsson, B. G.; Villahermosa, R. M.; Malmstroem, B. G.; Winkler, J. R.; Gray, H. B. *J. Am. Chem. Soc.* **1997**, *119*, 9921.
(329) Skov, L. K.; Pascher, T.; Winkler, J. R.; Gray, H. B. *J. Am. Chem. Soc.* **1998**, *120*, 1102.
(330) Di Bilio, A. J.; Dennison, C.; Gray, H. B.; Ramirez, B. E.; Sykes, A. G.; Winkler, J. R. *J. Am. Chem. Soc.* **1998**, *120*, 7551.
(331) Babini, E.; Bertini, I.; Borsari, M.; Capozzi, F.; Luchinat, C.; Zhang, X.; Moura, G. L. C.; Kurnikov, I. V.; Beratan, D. N.; Ponce, A.; Di Bilio, A. J.; Winkler, J. R.; Gray, H. B. *J. Am. Chem. Soc.* **2000**, *122*, 4532.
(332) McLendon, G.; Miller, J. R. *J. Am. Chem. Soc.* **1985**, *107*, 7811.
(333) Surdhar, P. S.; Armstrong, D. A. *J. Phys. Chem.* **1987**, *91*, 6532.
(334) Armstrong, D. A. In *Sulfur-Centered Reactive Intermediates in Chemistry and Biology*; Chatgilialoglu, C., Asmus, K.-D., Eds.; Plenum Press: New York, 1990; p 121.
(335) Gaudreau, P.; Michaud, J.; Cohen, E. A.; Langelier, Y.; Brazeau, P. *J. Biol. Chem.* **1987**, *262*, 12413.
(336) Gaudreau, P.; Paradis, H.; Langelier, Y.; Brazeau, P. *J. Med. Chem.* **1990**, *33*, 723.
(337) Kelley, S. O.; Holmlin, R. E.; Stemp, E. D.; Barton, J. K. *J. Am. Chem. Soc.* **1997**, *119*, 9861.
(338) Pulver, S. C.; Tong, W.; Bollinger, J. M., Jr.; Stubbe, J.; Solomon, E. I. *J. Am. Chem. Soc.* **1995**, *117*, 12664.
(339) Gerfen, G. J.; van der Donk, W. A.; Yu, G. X.; McCarthy, J. R.; Jarvi, E. T.; Matthews, D. P.; Farrar, C.; Griffin, R. G.; Stubbe, J. *J. Am. Chem. Soc.* **1998**, *120*, 3823.

CR020421U